Department of Physics and Astronomy

University of Heidelberg

Master thesis

in Physics

submitted by

Ruben Schupp

born in Ehringshausen

Year of submission 2016

Determination of beam properties of highly-charged ions extracted from TITAN's electron beam ion trap

This Master thesis has been written by Ruben Schupp

at

TRIUMF

under the supervision of

Priv.-Doz. Dr. José Crespo

and

Prof. Dr. Jens Dilling

High precision mass measurements of unstable isotopes are important for many physical applications, especially in nuclear physics. To measure these masses, the setup of TRIUMF's Ion Trap for Atomic and Nuclear Science (TITAN) at the Canadian Accelerator facility TRIUMF makes use of a Penning Trap. Masses of unstable isotopes with half-lives down to 8 ms have been determined with a precision of up to 1×10^{-8}.

However, for applications in nuclear particle physics, even higher precisions are needed. But the measurement precision with Penning traps is limited due to the short half-lives and/or the low production yields of the measured isotopes. To overcome these limitations, an Electron Beam Ion Trap (EBIT) charge breeder is used at TRIUMF's Ion Trap for Atomic and Nuclear Science (TITAN), to create Highly Charged Ions (HCIs) for the purpose of Penning trap mass spectrometry. With the higher charge state of the isotope, a precision gain of more than one order of magnitude or alternatively a significant reduction in measurement time can be achieved.

The achievable precision, however, is limited by the quality of the ion beam used for Penning trap mass measurements. Due to the effects of charge breeding, the beam properties - quantifiable by the transversal emittance and longitudinal energy spread - are increased and reducing the gain in measurement precision. Therefore, it is important for TITAN to measure and optimize the beam properties of HCIs extracted from the TITAN EBIT. For this reason, an Allison emittance meter as well as a Retarding field analyzer were designed and built in the scope of this work, to measure the transversal emittance and the longitudinal energy spread, respectively.

After the successful commissioning of the detectors, the properties of extracted beams were measured to be $\epsilon_{\mathrm{rms}} = 5.27(73)\,\pi\,\mathrm{mm\,mrad}$ for the emittance and $\Delta E_{\mathrm{beam}} = 19.7(21)\,\mathrm{eV/q}$ for the longitudinal energy spread, using ^{85}Rb of charge state 13+. In order to do precision mass measurements with HCIs, these values need to be reduced optimizing the charge breeding and extraction process. Further, it was found that the energy spread is dominated by the extraction mechanism of the ions, not by the used charge breeding mechanism. The detectors, as well as the measured values, are an important step towards high precision mass measurements of HCIs at TITAN.

Hochpräzisions-Massenmessungen von instabilen Isotopen sind von Bedeutung für eine Vielzahl von physikalischen Anwendungen und von besonderem Interesse in der Kernphysik. Um solche Massen zu messen, wird am TRIUMF's Ion Trap for Atomic and Nuclear Science (TITAN) Experiment eine Penningfalle verwendet. Mit dieser wurden bereits Massen von instabilen Isotopen mit Halbwertzeiten von 8 ms und Genauigkeiten von 1×10^{-8} gemessen.

Für Anwendungen in der Kernphysik sind jedoch Messungen mit noch größerer Genauigkeit von Nöten. Allerdings ist die Messgenauigkeit mit Penningfallen aufgrund der kurzen Halbwertzeiten und der kleinen Produktionsmenge der Isotope begrenzt. Um diese Begrenzungen zu überwinden, wurde eine Electron Beam Ion Trap (EBIT) im TITAN Experiment installiert, welche die einfach geladene Ionen zu hoch geladenen Ionen (HCIs) „brütet". Mit Hilfe des höheren Ladungszustandes des Ions kann die Messgenauigkeit mit der Penningfalle um mehr als eine Größenordnung gesteigert werden.

Die dabei erreichbare Genauigkeit ist jedoch durch die Qualität des Ionenstrahls begrenzt. Aufgrund des Ladungsbrütens verschlechtert sich die Qualität des Ionenstrahls – gemessen in transversaler Emittanz und longitudinaler Energieunschärfe – und der Zugewinn in Messgenauigkeit ist reduziert. Aus diesem Grund ist es für das TITAN Experiment wichtig die Strahleigenschaften von aus der TIAN EBIT extrahierten HCIs zu messen. Dafür wurde in dieser Arbeit ein Allison Emittanz Meter, sowie ein Retarding Field Analyzer (RFA) gebaut, um die transversale Emittanz, sowie die longitudinale Energieunschärfe der extrahierten HCIs zu messen.

Nach der erfolgreichen Inbetriebnahme der Detektoren, wurden die Strahleigenschaften gemessen und eine transversale Emittanz von $\epsilon_{\mathrm{rms}} = 5.27(73)$ π mm mrad, sowie eine longitudinale Energieunschärfe von $\Delta E_{\mathrm{beam}} = 19.7(21)$ eV/q gemessen. Für die Messungen wurde $^{85}\mathrm{Rb}^{13+}$ verwendet. Des Weiterem wurde gezeigt, dass die Strahlqualität ausschlaggebend vom Extraktionsprozess und nicht dem Prozess des Ladungsbrütens limitiert ist. Um das Ziel von Massenmessungen mit hoher Genauigkeit zu erreichen, müssen die gemessenen Werte durch weitere optimierung des Extraktionsprozesses aus der EBIT reduziert werden. Dafür können die beiden Detektoren benutzt werden und sind deswegen ein wichtiger Schritt für hoch genaue Massenmessungen von HCIs am TITAN Experiment.

Contents

1 Motivation for high precision mass measurements

Contents

The atomic mass is a fundamental property and provides insight into many fields of science, including chemistry, astronomy and physics. In the latter, high precision atomic mass measurements provide a versatile tool to a better understanding of how matter is built up a fundamental question in the field of physics.

In 1912 Sir Joseph John Thomson discovered, by means of atomic mass measurements, that elements exist with various numbers of neutrons - the isotopes [1]. With further improvements in mass measurement accuracy, it was observed in 1920 that the isotopes' masses do not differ by the mass of exactly one nucleon, as expected. This difference in mass, known as mass defect, was the first evidence for the existence of a nuclear binding energy and could be explained by the connection between energy and mass, given by Einstein's relation $E = mc^2$ [2].

Today, atomic mass measurements provide, among others, contributions to a new definition of the kilogram, tests of Quantum Electro Dynamic (QED) or tests of the weak interaction in the Standard Model of physics.

When measuring atomic masses, Penning traps, invented by H. G. Dehmelt [3], provide what is up to date the highest mass measurement precision ($\delta m/m$). By storing the ions in a superposition of a static electric and magnetic field, they can be exposed to quantum manipulation techniques, which lead to very accurate and precise measurements. In order to make the neutral atoms available to storage and manipulation via electromagnetic fields, they need to be ionized and Singly Charged Ions (SCIs) are typically used. Results from such trapping methods reach high precisions of $\Delta m/m \approx 1 \times 10^{-14}$ [4] nowadays.

1.1 Importance of mass measurements for nuclear and particle physics

The atomic mass as a fundamental property provides insight into a variety of problems in nuclear and particle physics. For example, it is needed for nuclear mass models (see Section 1.1.1).
Since the atomic binding energy is orders of magnitude smaller than the nuclear binding energy and well understood, atomic mass measurements reveal the mass of the nucleus. The latter then provides insight into the nuclear binding energy$B(Z, N)$ of the nucleus via

$$B(Z,N) = \left[Nm_{\mathrm{n}} + Zm_{\mathrm{p}} - M(Z,N)\right] c^2 \tag{1.1}$$

defined as difference in mass of the sum of all nucleons (N neutrons with mass m_{n} and P protons with mass m_{p}) and the total nuclear mass $M(Z, N)$ [5].
Since the nuclear binding energy represents all interactions in the many body system of the nucleus, it is used to gain information about the nuclear forces.
Another important application of mass measurements is the determination of Q-values which are needed for nuclear astrophysics or particle physics (see Sections 1.1.3 and 1.1.4). The Q-values are a defined as the amount of energy which is released in a nuclear reaction and are measured by the difference in mass between the product and the educt of the reaction

$$Q = (m_{\mathrm{product}} - m_{\mathrm{educt}})c^2. \tag{1.2}$$

Further, nuclear shell structure can be investigated with the help of two-neutron and two-proton separation energies $S_{2\mathrm{N}}, S_{2\mathrm{P}}$ (see Section 1.1.2).
To see, why atomic mass measurements of highest precision $\delta m/m \leq 10^{-7}$ are so important for nuclear physics, some of the applications will be further explained in more detail.

1.1.1 Nuclear mass models

To gain a better understanding of the nucleus and the relevant forces, various models [6, 7, 8] describe and predict the masses of all existing isotopes. To determine free parameters of the respective models, one typically fits certain measured isotope masses to predictions. Currently, most models provide a description of all known masses, especially

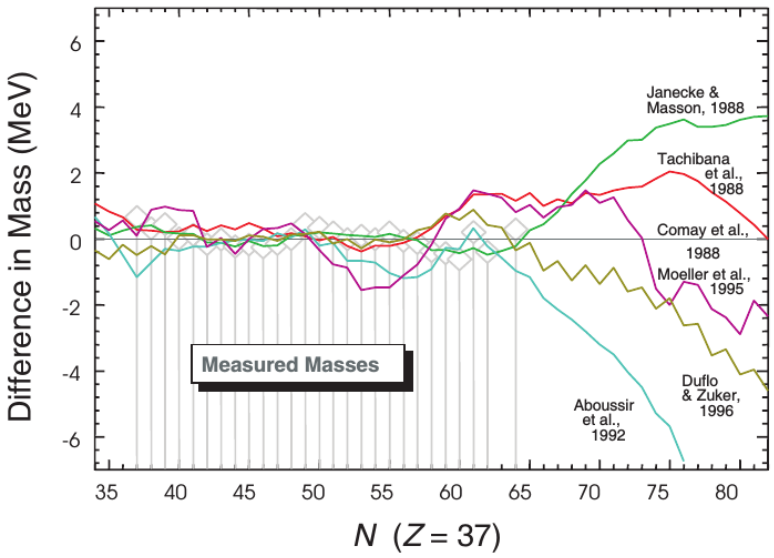

Figure 1.1: Deviation of measured masses of different rubidium isotopes and by various models predicted values. Model and measurement are in good agreement where the masses are known. However, the predictions for unknown masses vary vastly. Taken from [10]

good agreement is found for masses close to stability. However, the models deviate drastically among themselves for unstable isotopes of yet unknown mass (see Figure 1.1), clearly indicating yet unconsidered or unknown science.

To improve the models and make them less dependent on fitted parameters but also to improve our understanding of nuclei, mass measurements of unmeasured rare unstable nuclei are needed [2]. However, these isotopes can provide a challenge for mass measurements due to short half-lives $t_{1/2} \leq 10\,\text{ms}$ [9] and/or low production yields of 10 ions/s and less.

1.1.2 Shell structure investigations

Using nuclear mass measurements, nuclear forces as well as nuclear structure can be investigated [5]. An important tool do this is the two-neutron separation energy

$$S_{2\text{N}}(N,Z) = B(N,Z) - B(N-2,Z) \tag{1.3}$$

which requires the knowledge of two nuclei which differ by two neutrons. Alternatively, mass models can be used to predict the masses. Plotted against the respective neutron number of an isotopic chain, sudden drops in the two-neutron numbers become visible

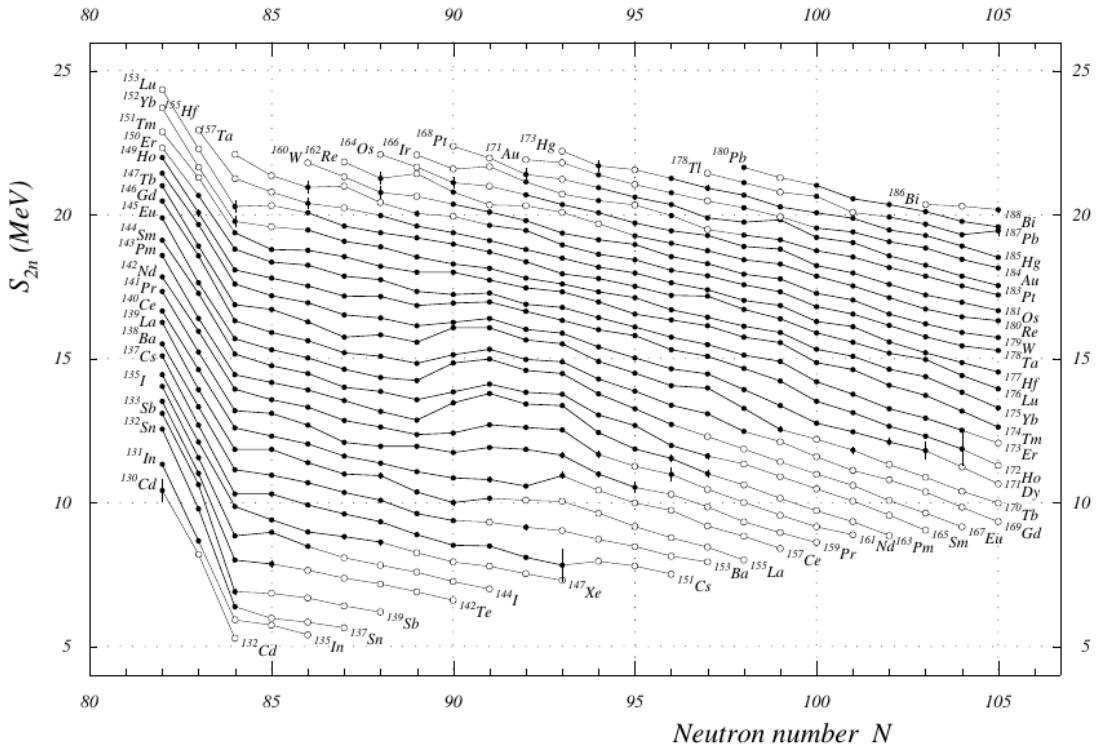

Figure 1.2: The $N = 82$ nuclear neutron-shell closure is clearly visible due to the sudden drop in the two neutron separation energy S_{2n}. Taken from [11]

(Figure 1.2).

These drops in the two neutron separation energy show that more energy is needed to remove a nucleon from the nucleus. Therefore they indicate a more stable configuration of the respective nucleus which is caused by a closure of the neutron shell. Therefore, two neutron separation energies are an important tool to investigate nuclear shell structure.

1.1.3 Nuclear astrophysics and abundance calculations

A key question in nuclear astrophysics is the understanding of the various mechanisms for nuclear synthesis in stellar environments [12, 13]. The understanding of nuclear reactions is important since they play a role for the production of all elements heavier than $A \geq 7$. To describe their production, the mass, half-life and cross-section values of unstable nuclei are needed. Among those, the nuclear mass plays a fundamental role since it contains information about the binding in the nuclei and is therefore important in the understanding of nuclear reaction rates for stellar processes [2]. In this context, the most important production mechanisms are the s- (slow neutron capture), r- (rapid neutron

capture), and rp- (rapid neutron capture) processes [2]. With the understanding of these reactions and their rates, the calculation of abundance distributions of the elements created after the big bang becomes possible which is another fundamental interest in the field.

1.1.4 Charged vector current hypothesis

An important matter of investigation in nuclear particle physics is the unitarity of the Cabibbo–Kobayashi–Maskawa (CKM) matrix in the Standard Model of physics.
The CKM matrix [14, 15] is the connection between the strong and weak flavor eigenstates of quarks

$$\begin{pmatrix} d_\mathrm{w} \\ s_\mathrm{w} \\ b_\mathrm{w} \end{pmatrix} = \begin{pmatrix} V_\mathrm{ud} & V_\mathrm{us} & V_\mathrm{ub} \\ V_\mathrm{cd} & V_\mathrm{cs} & V_\mathrm{cb} \\ V_\mathrm{td} & V_\mathrm{ts} & V_\mathrm{tb} \end{pmatrix} \begin{pmatrix} d_\mathrm{s} \\ s_\mathrm{s} \\ b_\mathrm{s} \end{pmatrix} \tag{1.4}$$

and describes the oscillation of quarks into other quark families. Here u, d, t, b, s, c represent the up, down, top, bottom, strange and charm quarks and the absolute squared of the matrix elements predict the probability of oscillation into the quark family in question. Since the CKM matrix describes the oscillation into different families and assuming conservation of the number of quarks, the sum over one row or column of the matrix must equal one [16]. If this is not the case, it could indicate physics beyond the Standard Model. For the most stringent test so far, the first row of the matrix is used in the following way:

$$|V_\mathrm{ud}|^2 + |V_\mathrm{us}|^2 + |V_\mathrm{ub}|^2 = 1 \tag{1.5}$$

where, V_ud provides the biggest contribution with approximately 95 %. While V_us and V_ub are determined by experiments in particle physics, V_ud can be determined by means of nuclear physics via super-allowed Fermi β-decays between zero-plus states in nuclei ($0^+ \rightarrow 0^+$). These transitions are almost independent of nuclear structure. Under the assumption of the Conserved Vector–Current (CVC) hypothesis, the product of the phase space integral f and the partial half life t of the decay provides access to V_ud via [17]

$$ft = \frac{K}{G_\nu^2 |M_\mathrm{F}|^2} = \frac{K}{|M_\mathrm{F}|^2 G_\mathrm{F}^2 |V_\mathrm{ud}|^2} \tag{1.6}$$

with the constant K, Fermi matrix element M_F of the transition and the vector coupling

constant G_ν. The latter, $G_\nu = G_\mathrm{F} V_\mathrm{ud}$, can be expressed as a product of V_ud and the Fermi weak coupling constant G_F. This is well known from the decay of the muon [1]. Experimentally, the half-life of the decay as well as the branching ratio must be measured to determine the partial half-life t. Further, the Q-value of the decay needs to be measured to determine the phase space integral f. Since f is proportional to Q^5, mass values of high precision $\delta m/m \geq 1 \times 10^{-8}$ and better are needed. Therefore, unitarity tests are a prime example of the importance of high precision mass measurement of isotopes.

1.2 Motivation for this work

For the above mentioned applications, often masses of nuclei far away from stability are needed. Moreover, depending on the application, relative mass measurement precisions must be reached to gain new knowledge [18]:

- nuclear structure, $\delta m/m \approx 10^{-7}$
- nuclear astrophysics, $\delta m/m \approx 10^{-7}$ to 10^{-8}
- test of fundamental symmetries, neutrino physics, $\delta m/m \approx 10^{-8}$ to 10^{-9}

With the use of Penning trap mass measurements, those accuracies are typically reached for stable atoms. However, measurements of unstable nuclei impose more limits on the precision. For example, the measurement duration is limited by their half life $t_{1/2}$. Moreover, the overall sensitivity of the experiment must be as high as possible to obtain measurements of atoms with low production yields of often only several atoms per second. Due to these reasons, mass measurements of unstable isotopes are limited in their precision (see Chapter 2). One way to overcome these limitations is the use of ions of higher charge states. An Electron Beam Ion Trap (EBIT) charge breeder [19, 20, 21] was installed at TRIUMF's Ion Trap for Atomic and Nuclear Science (TITAN) [22, 23] to change the charge state from singly charged to highly charged ions. Because of the increased charge of the ion, a potential precision gain of more than one order of magnitude is possible using Penning traps in combination with the Time-of-Flight Ion Cyclotron Resonance (TOF-ICR) mass measurement method [24] (see Chapter 2.1.1).
However, because of the ionization method used for charge breeding, the spread in the kinetic energy of the ions increases. Further, due to the extraction mechanism in the EBIT to produce a bunched beam for efficient capturing in the Penning Trap, even more energy spread is introduced.

Consequently, a significant reduction of the expected precision gain occurs, and ion losses can happen (see Chapter 2). Hence, the energy spread of Highly Charged Ions (HCIs) created in an EBIT must be reduced prior to their mass measurement.
For this purpose, a Cooler Penning Trap (CPET) has been developed at TITAN. It is important to minimize the temperature increase during charge breeding. Further, a low energy spread reduces ion losses for trapping in CPET and also for direct injection into the Measurement Penning Trap (MPET).
To improve the properties of the extracted beam, the parameters of the charge breeding process in the EBIT need to be understood and parameters of the ion extraction need to be studied (see Chapter 3). Therefore, an Allison emittance meter as well as a Retarding Field Analyzer (RFA) were designed and built within this work to measure the beam properties of beam extracted from the TITAN EBIT (see Chapter 5). With these devices the beam properties of HCIs ejected from the TITAN EBIT were measured for the first time (see Chapter 6). Additionally, different extraction parameters of HCI from the EBIT onto the beam properties were investigated.

2 The effect of beam properties and HCI in Penning trap mass measurements

Contents

Penning traps currently provide the highest-precision in atomic mass measurements [2]. However, the mass measurement precision of radioactive isotopes is limited by the production yields of down to 10^2 pps from the beam facility and isotope half lives of several milliseconds. Even though, precisions of up to 10^{-8} can be achieved at TRIUMF's Ion Trap for Atomic and Nuclear Science, higher precisions are needed to investigate fundamental symmetries.

Using Highly Charged Ions (HCIs) in Penning trap mass measurements, the problems can be overcome and an increase in precision can be achieved. However, the attainable precision gain is limited, due to the increased energy spread after charge breeding. In order to understand how the use of HCI increases the precision in the measurement, Penning Trap mass spectrometry will be explained in this chapter. Further, properties of ion beams are defined and quantitative measures are given. With this knowledge, the effect of HCIs and beam properties in high precision Penning trap mass measurements is investigated.

2.1 Mass measurements in Penning traps

Penning traps store ions in a superposition of static electric and magnetic fields. In this well defined environment, the ions become accessible for high precision measurements.
Axially, a charged particle is confined by an electric quadrupole field. The field is commonly produced using hyperbolically shaped electrodes. However, due to Gauss' law ($\nabla E = 0$), electrostatical confinement of charged particles is only possible in one direction. For this reason, a magnetic field provides radial confinement of the charged particle in a Penning trap.
The motion of a stored ion in the trap can be calculated and described by three eigen-motions (see Figure 2.1) and their corresponding eigen-frequencies.
The first is called axial frequency and describes the ion's oscillation in axial trap direction z

$$\omega_z = \sqrt{\frac{q \cdot U_{DC}}{m d_0^2}}. \tag{2.1}$$

It is dependent on the applied DC voltage U_{DC}, used for production of the quadrupole field, and further depends on the characteristic trap diameter $d_0^2 = \frac{1}{2}(z_0^2 + r_0^2)$ (see Figure 2.2).
Radially, the ion has two eigen-frequencies. The so-called modified cyclotron frequency ω_+ and the magnetron frequency ω_-

$$\omega_\pm = \frac{\omega_c}{2} \pm \sqrt{\frac{\omega_c}{4} - \frac{\omega_z}{2}}. \tag{2.2}$$

Penning trap mass measurements are carried out via precise frequency measurements [2] and precisions on the order of 10^{-14} are achieved [4]. The translation from mass to a frequency determination becomes possible due to the ions cyclotron frequency ω_c which

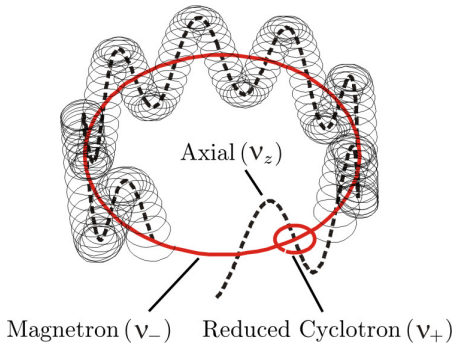

Figure 2.1: Eigen-motion of a stored ion in a Penning trap.

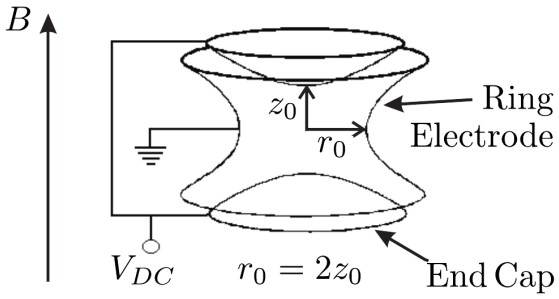

Figure 2.2: Schematic representation and dimensions of a parabolic shaped Penning Trap. Taken from [9]

is unique for each mass m

$$\omega_c = \frac{q}{m} \cdot B, \tag{2.3}$$

where q is the charge state of the ion and B the magnetic field strength.
To precisely measure the cyclotron frequency, different methods, including Fourier Transform Ion Cyclotron Resonance (FT-ICR) or TOF-ICR, can be used [25]. Since only TOF-ICR is used at TITAN, it is discussed in the following.

2.1.1 Determination of mass and cyclotron frequency using the TOF-ICR method

The mass of the ion is determined by measuring the cyclotron frequency ω_c. This can be achieved by applying an external electric quadrupole field of radio-frequency ω_{rf}, to couple the magnetron and reduced cyclotron motion of the ion.
If the applied frequency matches the ion's cyclotron frequency ($\omega_{rf} = \omega_c$), the ion is periodically converted between the two motions (see Figure 2.3). However, a full conversion only occurs for ions which are initially prepared in a pure magnetron motion. During a full conversion, the radius of the initial magnetron and final reduced cyclotron motion is the same. In other cases, the conversion is incomplete.
Since the reduced cyclotron frequency is typically much higher than the magnetron frequency ($\omega_+ >> \omega_-$), the ion gains kinetic energy during the process. However, if the frequency is not matched, the conversion is not complete and the ion gains less energy. Consequently, the cyclotron frequency can be determined by measuring the energy as a function of the applied radio-frequency (see Figure 2.4).
To measure the radial energy of an ion with a converted motion, it ejected from the Penning trap and the Time-of-Flight (TOF) from the trap to an ion detector is measured.

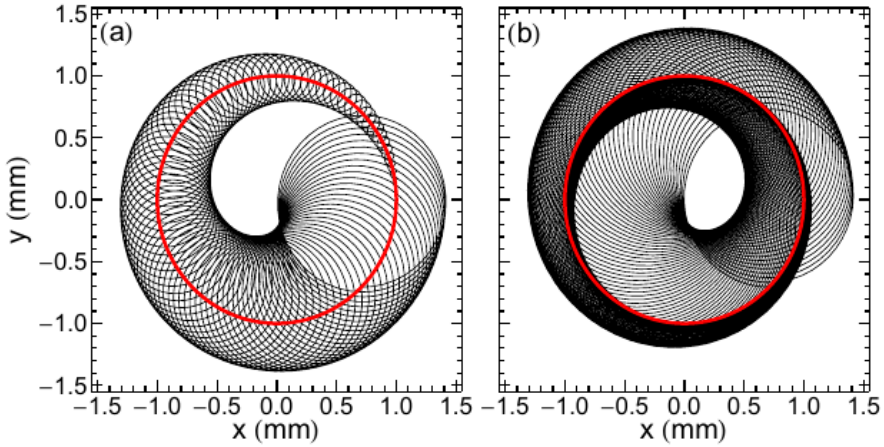

Figure 2.3: Conversion from a pure magnetron to a pure modified cyclotron motion (a) and back (b), using a quadrupolar excitation with frequency $\omega_{\mathrm{rf}} = \omega_{\mathrm{c}}$. The red line represents a magnetron motion with 1 mm radius. Taken from [26]

While leaving the trap, the ion experiences a high magnetic field gradient (see Figure 2.5). This gradient, in combination with the magnetic moment μ of the ion, generated by the circulating charge of the stored ion, results in a force in axial direction. For higher radial energy E_{r} of the trapped ion, the force increases while the TOF shortens.
The cyclotron frequency is then extracted from the TOF resonance which is described by [2]

$$T_{\mathrm{tof}}(\omega_{\mathrm{RF}}) = \int_{z_1}^{z_2} \sqrt{\frac{m/2}{E_0 - qU(z) - \mu(\omega_{\mathrm{RF}})B(z)}}\,dz \tag{2.4}$$

Here, E_0 denotes the axial energy of the ion before being released from the trap. $U(z)$ and $B(z)$ are the electric potential and the magnetic field on the flight path, respectively. The mass of the ion of interest is determined by measuring its cyclotron frequency and the cyclotron frequency of a reference ion ω_{ref} with well-known mass. Combining equation (2.3) for both ions, the mass of interest can be calculated

$$m = (m_{\mathrm{ion,ref}} + q \cdot m_{\mathrm{e}} - E_{\mathrm{B,ref}}) \cdot \frac{\omega_{\mathrm{ref}}}{q_{\mathrm{ref}}} \cdot \frac{q}{\omega} + q \cdot m_{\mathrm{e}} - E_{\mathrm{B}}. \tag{2.5}$$

To obtain the mass of the neutral atom, the masses in equation (2.5) are corrected for the missing electrons m_{e} and the binding energies $E_{\mathrm{B}}, E_{\mathrm{B,ref}}$.

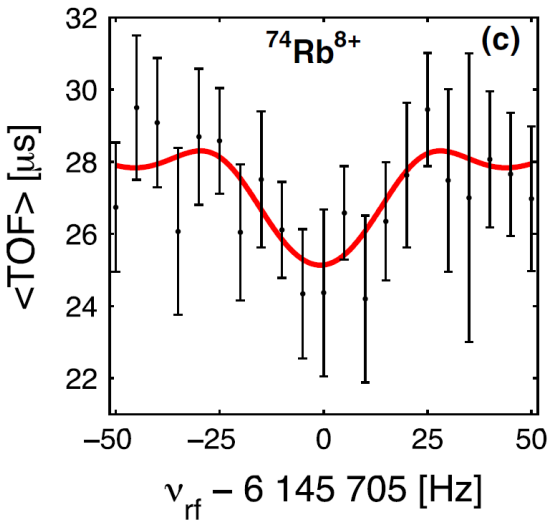

Figure 2.4: TOF resonance of $^{74}Rb^{8+}$ using the TOF-ICR technique and a quadrupole excitation time of 30 ms. The mass is determined from the center-frequency of the time-of-flight resonance where ν_{rf} is the applied radio frequency. Taken from [27]

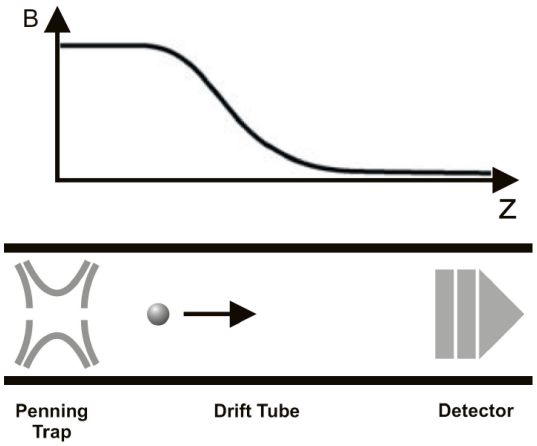

Figure 2.5: Time-of-Flight Ion Cyclotron Resonance (TOF-ICR) setup. While leaving the Penning trap, the extracted ion is accelerated by a magnetic field gradient and the TOF onto an ion detector is measured. Taken from [28]

2.2 Definitions of beam properties

An ideal beam consists of particles which travel in the same direction with the same velocity (see Figure 2.6a). However, in reality, such a beam is typically not achieved. Instead, the particles will have a distribution in energy which is called energy spread. This spread depends on the methods of production and acceleration. In order to describe the quality of a beam and its properties, the concept of emittance is introduced. The emittance of the beam will be used to describe the transversal energy spread of the ions (see Figure 2.6b). In longitudinal beam direction, the width of the ions distribution in the energy spread will provide a measure for the beam quality.

2.2.1 Emittance

The emittance ϵ, as used in this work, is defined as the product of the width of the particle distribution in position and momentum space and provides a figure of merit for the beam properties. For the ideal beam, a so defined emittance will be zero. With increasing emittance the beam properties worsen, since for most applications an ideal beam is desired. However, the emittance defined here should not be confused with the area or volume V covered by the particles in phase space

$$V = \int\int\int\int\int\int dx\,dy\,dz\,dp_x, dp_y, dp_z, \tag{2.6}$$

where $dx\,dy\,dz$ denotes integral over the position and dp_x, dp_y, dp_z the angle space.
Emittance is a quantity of a six dimensional phase space $((x, y, z), (p_x, p_y, p_z))$. For the purpose of measuring it, it is of great use that the six dimensional emittance can be divided into a longitudinal $\epsilon_{\parallel}$ and an transverse emittance $\epsilon_{\perp}$. This description assumes that the particle motion in the beam is uncorrelated. If this is not the case, the phase space grows into $6N$ dimensions, where N is the number of particles in the beam.
In addition to this, for a radially symmetric beam, it is enough to determine the emit-

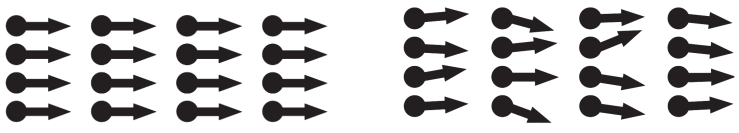

(a) Ideal beam **(b)** Non-ideal

Figure 2.6: In an ideal beam (a) all particles travel with same velocity-vector. In reality, the beam is non-ideal (b) and the absolute velocity of the particles as well as their directions can differ from each other. Taken from [10]

tance in one transverse direction. However, if the beam experiences forces which couple the transverse directions, like focusing via a quadrupole triplet, the radial symmetry is broken and the directions must be measured separately.

Further, when working with non-relativistic beam energies, as done at TITAN, the angle x' of the particles with respect to their common direction of motion is measured. This is preferable because it can be directly measured and is approximated for small angels via

$$x' = \frac{p_x}{p_z}, \tag{2.7}$$

with $p_\mathrm{z} \gg p_\mathrm{x}$ and $p_\mathrm{z} \gg p_\mathrm{y}$. The result is commonly given in units of (π mm mrad), where the π indicates that it is the product of widths, rather than an area in phase space. The use of an angle, however, is only well defined for the directions transverse to the beam.

Another important property of emittance is that it is conserved under conservative forces because of Liuville's Theorem. For measurement of beam properties, this is a crucial property since the beam often needs to be guided by electromagnetic optics that could influence the phase space and distort the measurement. The conservation can be explained using the close relation of emittance to the area of the particles in phase space as described in equation (2.6). If all applied forces can be expressed via scalar potentials $\Psi(x, y, z)$ as well as vector potential $\mathbf{A}(x, y.z)$, Liouville's Theorem, known from classical mechanics, can be applied. It states that the particle density n of a finite element in phase space is constant with respect to time. Hence, for a beam with N particles, the area or volume in phase space stays constant even though its shape can change.

In reality, however, non-conservative forces are acting on the beam, like particle collisions with rest gas or Coulomb interaction between particles caused, for example, by space charge. As a result, the beam does not obey Liouville's theorem any more and the emittance or phase space area can increase. On the other hand, this also provides the opportunity to actively reduce the emittance using non-conservative forces, like acceleration.

Emittance, as defined here, is inversely proportional to the particle momentum ($p \approx p_z$) in beam direction and therefore varies with the used beam energy. In order to compare emittances at different beam energies, it can be normalized by multiplication with the relativistic factor $\epsilon^* = \beta\gamma\epsilon$ where $\beta = v_z/c$ and $\gamma = 1/\sqrt{1-\beta^2}$.

Table 2.1: Percentage of enclosed particles in the RMS emittance for conversion to other definitions. Taken from [10]

$\epsilon/\epsilon_{\mathrm{rms}}$	$1/4$	1	4	6	9
Particles enclosed (%)	15	39	87	95	99

Root Mean Square emittance

A statistical approach to describe a beam is the Root Mean Square (RMS) emittance which makes use of the second order momenta of the particle distribution in phase space. To calculate the spread of the particles in phase space the variance of ions distribution in position $\langle x^2 \rangle$ and angle $\langle x'^2 \rangle$ is used

$$\langle x^2 \rangle = \frac{\sum (x - \bar{x})^2 \cdot c(x, x')}{\sum c(x, x')} \tag{2.8}$$

where $c(x, x')$ is the number of ions with the respective beam property and $\bar{x}$ the average of x given by:

$$\bar{x} = \frac{\sum x \cdot c(x, x')}{\sum c(x, x')}, \tag{2.9}$$

and analogous for $\langle x'^2 \rangle$.
Further, the covariance $\langle x x' \rangle$ of the data accounts for possible tilts of the area in phase space, caused by dispersion or focusing

$$\langle x x' \rangle = \frac{\sum (x - \bar{x}) \cdot (x' - \bar{x'}) \cdot c(x, x')}{\sum c(x, x').}. \tag{2.10}$$

With the above the Root Mean Square (RMS) emittance can be defined by ([29])

$$\epsilon_{\mathrm{rms}} = \sqrt{\langle x^2 \rangle \langle x'^2 \rangle - \langle x x' \rangle^2} = \sqrt{\det \begin{pmatrix} \langle x^2 \rangle & \langle x x' \rangle \\ \langle x x' \rangle^2 & \langle x'^2 \rangle \end{pmatrix}} \tag{2.11}$$

In order to compare the RMS emittance to other definitions, Table 2.1 provides the amount of enclosed particles for conversion.
The RMS is a good description for thermally distributed beams and a rather conservative measure of the beam properties. Even for distorted beams or beams with a high correlation between position and angle, the RMS emittance will not underestimate the quality of the beam properties.
On the downside, particles far away from the center of the beam (beam halos for example)

increase the RMS emittance drastically. Noise can therefore result in an overestimation of the emittance.

Longitudinal emittance

The longitudinal emittance is given by the product of width of the particles distribution in position Δz and momentum Δp_z

$$\epsilon_z = \langle \Delta z \rangle \frac{\langle \Delta p_z \rangle}{p_0} \tag{2.12}$$

where p_0 is the average longitudinal particle momentum and Δp_z and Δz are the longitudinal width of the ion bunch in momentum and space.

2.2.2 Longitudinal energy spread

Instead of the longitudinal emittance, the energy distribution of the particles in the beam is used as quantity in this work because it can be directly measured. This so-called energy spread is defined via the Full Width at Half Maximum (FWHM) of the ions' distribution in energy around the beam energy E_{beam}.
For the case of a thermally distributed beam, the energy distribution can be approximated by a Gaussian distribution. For further information see Section 5.2.2.

2.3 Improvement of the precision in Penning trap mass measurements

In order to overcome the limited precision in the measurement of unstable isotopes, HCIs are used at TITAN. The increase in mass measurement precision due to HCIs will be explained in the context of using the TOF-ICR technique. However, connected effects arising from the use of HCIs are investigated. Following up on the effects, the importance of low energy spread is discussed.

2.3.1 Effect of HCI in TOF-ICR measurements

One way to improve the measurement precision in Penning trap mass spectroscopy is the use of HCIs. The impact of HCI on the precision ($\delta m/m$) of Penning trap mass measurements can be determined using [30]

$$\frac{\delta m}{m} \propto \frac{m}{qBT_{\text{rf}}\sqrt{N_{\text{ion}}}} \tag{2.13}$$

with the charge state q of the ion, the strength of the magnetic field B in the trap center, the excitation time T_{rf} of the ion and the number of measured ions N_{ion}.

As is visible from equation (2.13), there are various factors that influence the measurement precision. For example, the quadrupole excitation time of the ion could be increased. Since the isotopes of interest typically have short half-lives, the excitation time is limited.

Further, a stronger magnetic field would increase the precision. Current technical limits on magnets allow field strengths of up to 9 T [31, 32]. In the case of TITAN's MPET, which uses a magnetic field strength of only 3.7 T, the precision could be more than doubled by increasing the magnetic field strength to 9 T.

Nevertheless, the largest gain in precision can be achieved through increasing the charge state of the ion. Depending on the ion's half life, charge breeding of unstable ions up to the bare nucleus is possible with EBITs. Thus, a gain in precision of more than one order of magnitude is possible.

This increase in precision can be explained by the dependence of the TOF-ICR technique on the width of the resonance $\delta\omega_{\mathrm{c}}$ compared to its center frequency ω_{c}

$$\frac{\delta m}{m} \propto \frac{\delta\omega_{\mathrm{c}}}{\omega_{\mathrm{c}}} \tag{2.14}$$

For an ideally injected single ion, starting with a pure magnetron motion, the width of the TOF resonance scales only with the quadrupole excitation time of the ion ($\delta\omega_{\mathrm{c}} \propto T_{\mathrm{RF}}$). Therefore, it is independent of the charge state. In contrast, the cyclotron frequency of an ion scales directly with its charge ($\omega_{\mathrm{c}} \propto q$). As a result, the resolution of the TOF resonance increases. In addition, the ratio of the shortest and the longest TOF also becomes smaller, which means that the signal to noise ratio of the measurement improves.

For the above reasons, a higher precision can be achieved using HCIs. Faster measurements at the same precision level as with SCI become possible because a lower number of measurement cycles is needed [27].

The drawback of this technique is that charge breeding in an EBIT increases the overall loss of ions, as well as the overall cycle time and therefore reduces the number of ions available for the measurement. However, as long as the number of ions allow for enough statistic for a TOF-spectrum, the measurement gains in precision due to a higher charge state.

Another important effect in the use of HCIs produced with an EBIT is the increase in the energy spread of the ions caused by electron collisions during charge breeding as well

as the extraction process. This has disadvantageous effects on the beam properties and directly influences the measurement precision, as explained in the following Section 2.3.2.

2.3.2 Advantage of low energy spread in TOF-ICR measurements

The beam properties of ions injected into MPET plays a major role for the mass measurement precision.

The given theoretical description for Time-of-Flight (TOF) mass measurements requires a pure magnetron motion of the trapped ion prior to its quadrupole excitation. This can only be achieved by injecting ions along the magnetic field lines. With zero angle towards the magnetic field, the ions have no reduced cyclotron motion. In the case where the ions are injected on center, they can then be prepared into a pure magnetron motion using a dipole excitation with magnetron frequency ω_-.

However, a transversal energy spread of the ion bunch can not completely be omitted. Thus, the injected ions will have a reduced cyclotron motion upon injection into the Penning trap which depends on their transverse energy. In turn, the ions will have different TOFs for the same quadrupole excitation frequency and the resolution of the TOF spectrum worsens. Further, when ions are injected onto different radii in the trap, they have a varying initial magnetron radius and gain more or less energy during the

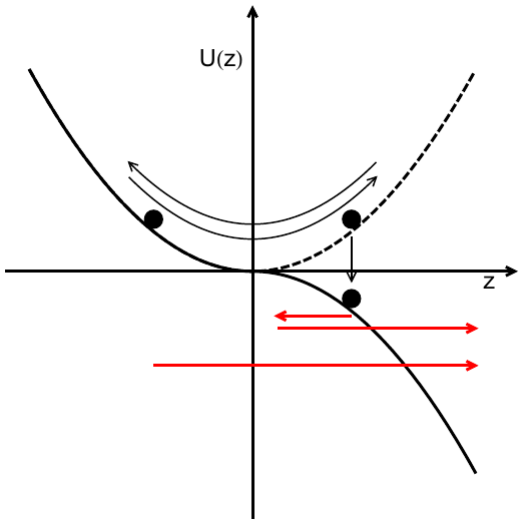

Figure 2.7: Extraction from the Penning trap. The ion on the left already travels to the right and in direction of the detector. In contrast, the right ion first travels to the left and first needs to be reflected at the potential, increasing its Time-of-Flight (TOF) onto the detector. Further, its energy is lowered, due to the extraction process. Taken from [26]

quadrupole excitation and the TOF spectrum broadens.
Further, problems are caused by an initial longitudinal energy spread of the ions. Being stored in the trap, the ions will maintain their energy spread and oscillate in the harmonic axial potential. When released, the ions travel with different initial axial velocities. Furthermore, due to the oscillation of the ions in the trap, ions might first move in the opposite direction of the detector (see Figure 2.7). These ions will only leave the trap after reflection at the trapping potential. Therefore, they have a different TOF. As as result of this, the signal to noise ratio of the TOF spectrum decreases.
If the energy spread is even bigger than the typical trap depth ($\approx 10\,\mathrm{V}$), ions will leave the trap. Therefore, the number of ions is reduced which can even prevent a complete measurement. Another related problem is the ion loss due to pulse width in time. If the fastest ions travel a distance of twice the trap length before the slowest enters the trap, ions are lost. In addition, the time spread can introduce further longitudinal energy spread due to the capturing method.
To capture ions in a Penning trap, the potential at the end caps is typically lowered upon arrival of an ion bunch. After the ions entered, the potential is raised again. If ions remain at the trap entrance while the electric fields are raised, these ions will gain energy. For extraction, the process is reversed and the end cap potential at the exit is lowered which can reduce the energy of ions in the region of the extraction end cap (see Figure 2.7).
For the given reasons, an energy spread less than $1\,\mathrm{eV}$ per charge is desired [33].

3 Electron Beam Ion Traps

Contents

EBITs are widely used for charge breeding of ions. In the following, the concept of an EBIT is explained, using the example of the TITAN EBIT. In order to understand the processes involved in the charge breeding process, the most important atomic processes in an EBIT will also be explained.
Additionally, HCIs from EBITs are used in Penning trap mass measurements. However, the achieved precision gain using HCIs at TITAN was not as high as possible because the precision is mainly limited due to the energy uncertainty of the HCIs. Therefore, the temperature of ions in an EBIT and the extraction mechanism of HCIs from an EBIT are investigated.

3.1 The TITAN EBIT

In general, an EBIT consists of an ion injection system, a magnet, drift tubes, an electron gun and an electron collector (Figure 3.1). Ions enter the EBIT through an injection

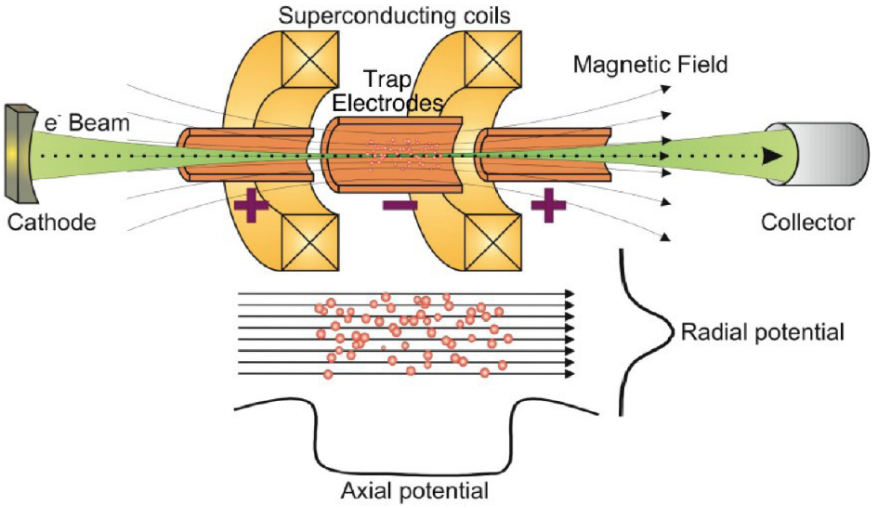

Figure 3.1: Scheme of an EBIT. The electron beam (green) is responsible for the ionization of ions. It travels from cathode to collector and is compressed to less than 100 µm diameter in the trapping region [19] using a magnetic field. The magnetic field is produced by two superconducting coils (yellow) in Helmholtz configuration. The ions are radially confined through the space charge of the electron beam as well as axially by the potential of the drift tubes (orange). Taken from [19]

system and when they interact with the electron beam (radius $\approx$ 100 µm), they are ionized by collisions with the electrons. During the charge breeding process, the ions are trapped due to the axial potential from the drift tubes and the radial potential from the electron beam. The breeding process is a dynamic process and is based on breeding parameters such as electron current, electron energy, etc. and an equilibrium in the charge stat distribution is reached .

3.1.1 Injection

To charge breed neutral atoms or ions, the particles need to be injected and stored in contact with the electron beam.
This can be done using two different methods. The first method uses a connection between the EBIT and a beam line on the collector side of the EBIT [22]. Through this connection, particles from an external ion source can enter via the EBIT collector.
After injection, the particles are stored via a trapping mechanism, described in section 3.1.3. The alignment and overlap with the electron beam is important to reach highest trapping efficiencies and shortest charge breeding times.
Apart from ion injection through the ring collector, atoms or molecules can enter the EBIT via an injection system on the side of the trapping region EBIT [19]. In the injec-

tion system, the particles enter the vacuum through a needle valve in the form of a gas stream. On its way into the trap, particles which are not directed at the electron beam are blocked by two slit apertures which also serve the purpose of differential pumping. Gas and liquids or solids with a high vapor pressure can be used for injection.

3.1.2 Electron gun

The source of the electron beam is a water cooled barium dispenser cathode consisting of tungsten and barium. To lower the work function of the gun surface and to enhance the electron emission, the cathode is coated with osmium and rubidium [21]. At an operation temperature of about 1300 K, electrons overcome the surface potential and are then accelerated towards the anode by a focus electrode. The voltage of the focus electrode allows one to control the emitted current.
For fast charge breeding, it is particularly important to achieve a small electron beam diameter in the trap. A small diameter increases the current-density and with it is the likelihood of collisions between electrons and ions. For this purpose, a compensation coil is installed around the gun. It shields the gun region from the residual magnetic field of the trap and therefore reduces the electron beam diameter.

3.1.3 Magnet, drift tubes and cold-head

The central part of an EBIT consists of a superconducting magnet and drift tubes.
The purpose of the superconducting magnet is the radial compression of the electron beam which is needed to reach high electron-current densities J_e for charge breeding in the trapping region. Due to the high current density, the electron beam's space charge also confines the ions in radial direction. Nevertheless, the main reason for high currents is a reduced charge breeding time.
For early breeding times the ionization process is dominating and a lower bound for the characteristic time, which is needed until the first appearance of charge state i, can be estimated using [34]

$$t_i^{app} = \frac{e}{J_e} \sum_{j=1}^{i} \frac{1}{\sigma_j^{EI}}. \tag{3.1}$$

Here, σ_j^{EI} denotes the electron impact ionization cross section.
For axial confinement, the TITAN EBIT trap consists of 9 Drift Tubes (DTs) (DT1-DT9). The number of DTs provides the opportunity to form specific axial potentials and allows for longitudinal trap sizes from 20 to 270 mm. Furthermore, the central drift

tube is radially cut into eight segments. In this way, new techniques like resistive cooling [35, 36] or Fourier Transform Ion Cyclotron Resonance (FT-ICR) of ions in an EBIT can be explored [37]. Seven ports allow in-trap spectroscopy of HCIs. Port number eight is blocked by the cold-head, generating cryogenic conditions in the EBIT for the magnet. This 4 K environment also has a cryogenic pumping effect and a vacuum of better than 10^{-12} mbar is reached in the trap.

To trap ions bunches injected through the collector, their kinetic energy is progressively reduced by the DTs on the collector side of the EBIT. The DT used for trapping is biased just below beam energy in order to trap the ions. To prevent the ions from escaping, the subsequent DT on the gun side is biased several hundred volts above beam potential and hence above the kinetic energy of the ions. After the ions arrive in the trapping DT, the bias is ramped down in few hundred nanoseconds. Next, the ions are charge bred for some milliseconds. The charge bred HCIs are released via the collector side, typically by ramping up the bias of trapping DT.

3.1.4 Collector

After passing the trapping region, the electron beam is absorbed by a so-called collector. The collector is biased at the cathode's ground. To fully absorb the beam, the residual magnetic field from the trap is canceled by a surrounding coil. Without magnetic field, the repelling Coulomb forces expand the electron beam and it is absorbed by the collector.

During the absorption process, secondary electrons can be emitted. These need to be prevented from reentering the trap as well as from leaving the EBIT to avoid recombination with HCIs. To shield the trap from secondary electrons, a suppressor electrode is installed between the trap and collector with a more positive bias than the collector. Facing the TITAN beam line, an extractor electrode prevents electrons from leaving the EBIT. With a more negative bias than the cathode, the extractor stops electrons from passing and it further works as an extraction Einzel lens for HCI at the same time[19].

3.2 Atomic processes in an EBIT

For a better understanding of the charge breeding process and the involved dynamic in process, an overview of the most important atomic processes in an EBIT is given in the following.

3.2.1 Electron impact excitation

Let's consider an electron e colliding with an ion X of charge q. If the energy of the electrons in the electron beam is smaller than the ionization potential I_{P} of one of the bound electrons ($E_{\mathrm{beam}} < I_{\mathrm{P}}$), electron impact excitation can take place [38]

$$\begin{aligned} X^{q+}(n,l) + e^- &\rightarrow [X^{q+}(n',l')]^* + e^- \\ &\rightarrow X^{q+}(n,l) + e^- + \gamma(\hbar\omega). \end{aligned} \tag{3.2}$$

The kinetic energy transferred due to the impact is converted to potential energy inside the ion. Thereby, an electron of the ion is excited to a higher energy level (n', l'). This additional energy is released subsequently by photon emission. Depending on the excited state and the atomic structure, the ion emits several photons until it reaches its ground state.

3.2.2 Electron impact ionization

If the energy of the electron beam is greater than the ionization potential $E_{\mathrm{beam}} > I_{\mathrm{P}}$, it is possible to remove an electron from the potential of the nucleus. This process is called electron impact ionization [38]

$$e_1^-(E_{\mathrm{Beam}}) + X^{q+} \rightarrow e_1^-(E_1) + X^{(q+1)+} + e_2(E_2). \tag{3.3}$$

The condition for the kinetic energy of the particles E_1, E_2 is

$$E_{\mathrm{Beam}} - I_P = E_1 + E_2 \geq 0. \tag{3.4}$$

3.2.3 Recombination processes

The production of high charge states competes with recombination processes. One of the most important effects is Radioactive Recombination (RR) (Figure3.2). RR corresponds to an inverse photo ionization process and lowers the charge state

$$X^{q+} + e^-(E_{\mathrm{Beam}}) \rightarrow X^{(q-1)+} + \gamma(\hbar\omega), \tag{3.5}$$

with the photon energy $\hbar\omega = E_{\mathrm{Beam}} + I_P$.

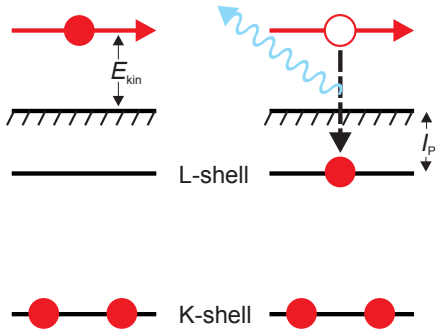

Figure 3.2: Schematic representation of radioactive recombination with the example of a He-like ion. Taken and modified from [39]

3.2.4 Charge exchange

During impact of an ion X^{q+} with a residual gas atom Y, charge exchange between those particles can occur. In addition, electrons of the residual gas atom can be freed

$$X^{q+} + Y \rightarrow X^{(q-p)+} + Y^{k+} + (k-p)e^{-}. \tag{3.6}$$

This process varies the charge balance of the ion cloud. Residual gas in the trapping region plays the main role in this process.

3.3 Evolution of emittance and energy spread during charge breeding and extraction of HCI

Charge breeding in an EBIT not only increases the charge state, it also generally increases the ions energy spread. As seen in the last section, an increase in the ions' energy spread directly translates into a reduced mass measurement precision and should be minimized. The evolution of energy spread can be divided into two generation mechanisms:

1. The charge breeding process

2. The extraction process

To improve the beam properties and achieve optimal beam behavior, these parameters need to be optimized and at the same time, they need to maintain short pulses in time to allow for capture in a Penning trap.

3.3.1 Ion temperature and charge breeding

The ion temperature, and with it the ions' energy spread in an EBIT, is typically determined by two processes. The first process is Landau-Spitzer heating during which the temperature is increased by the electron impact. The rate at with which the ions are heated generally scales with the square of the charge state q_i^2 and is linear to the used electron current J_e [34]. Therefore, higher charged ions are generally hotter. At the same time, they experience a deeper trapping potential due to their charge ($V_{\text{eff}} = qU_{\text{trap}}$). The second counteracting process is ion loss. With increasing ion temperature, ions start to escape the trapping potential axially or radially, depending on which is lower. However, only the hottest ions can leave the trap. Thereby it reduces the overall temperature of the ion cloud. This process is also often called evaporative cooling.

For most operating conditions a thermal equilibrium is achieved for each charge state, that follows a Maxwell Boltzmann distribution [40]. Further, the thermal energy of the ions can, in good approximation, be assumed to be equally distributed over all degrees of freedom, due to Coulomb interactions between the trapped ions and between ions and electrons.

The cooling of ions can be enhanced and the ion temperature lowered via injection of lighter ions with smaller proton number Z. Due to the Coulomb interactions in the trap, the heavier ions of interest will transfer parts of their kinetic energy to the coolant ions, which will escape the trap after sufficient collisions. To optimize the cooling process, typically inert gases are used, which generally reach lower charge states at the same electron beam energy due to their greater ionization energies. Therefore, they can escape more easily and provide an increased cooling rate.

An additional factor for the ion temperature, which is often neglected is ionization heating [41]. It stems from the ionization of the ions and can dominate the temperature at short charge breeding times of less than $T_{\text{breeding}} \leq 100\,\text{ms}$ [34]. It can be approximated with $k_B T \approx qV_0/5$, where k_B is the Boltzmann constant and V_0 is the potential reduction due to the electrons' space charge [34].

The calculation of the actual ion temperature, however, is very complex and requires numerical computer simulations for the respective operating conditions of the charge breeder. Nevertheless, a maximum temperature for single charge states in the ion cloud can be approximated via the minimal trapping potential V_T which the ions need to overcome [34]

$$k_B T \leq 0.1 - 0.4\, q\, V_T. \tag{3.7}$$

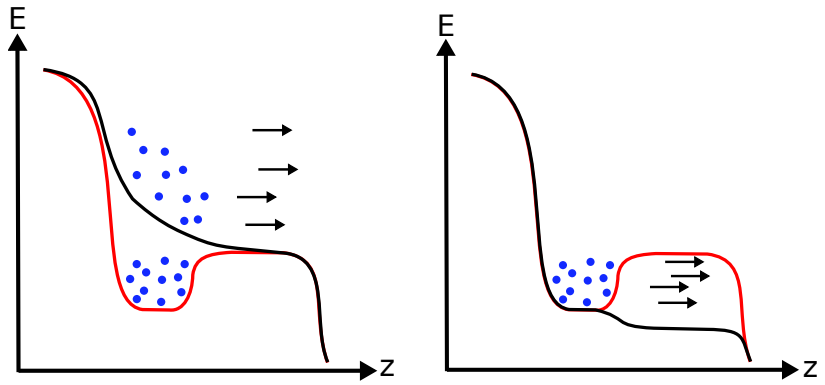

(a) Rasing **(b)** Lowering

Figure 3.3: Extracting ions from the EBIT by raising the trapping potential (a) and lowering the neighboring potential (b). The red line represents the potential while charge breeding and the black line represents the potential during extraction

3.3.2 Ion extraction and energy spread

After charge breeding, the ions are released as HCI on the collector side. For this to happen, the potential of the trapping DT is raised or the potential of the neighboring DT towards the collector is lowered (see Figure 3.3).
In the first method, the ions' energy is increased by a rapid rise in the DT potential until the ions can overcome the axial potential on the extraction side (see Figure 3.3a). The change in potential on the order of tens nanoseconds produces short pulses as needed for a Penning trap. This, however, can influence the Maxwellian velocity distribution of the ions since there is a super-position of the electric field of the trapping DT and the neighboring DT. Due to the rapid ramping of the trapping DT, the ions are almost at the same position during the process and in turn, the increase in energy of the ion is dependent on their position in the trap. Therefore, energy spread is mainly introduced in axial direction.
In the second method, the DT potential next to the trap on the collector side is lowered (see Figure 3.3b). Again, the super-position of the electric field lowers the ions' energy dependent on its position, but this time only on the collector side. Therefore, the introduced longitudinal energy spread will be less, but in turn, the time spread of the extracted ions will be larger due to a smaller initial axial energy.
To achieve the lowest energy spread of the ions during extraction and still maintaining short pulses in time, the extraction potential must be optimized.

4 The TITAN setup at TRIUMF

Contents

This chapter introduces the experimental setup of TITAN at Canada's National Laboratory for Particle and Nuclear Physics (TRIUMF) (Figure 4.1). At TITAN, mass measurements of rare unstable isotopes, delivered from Isotope Separator and Accelerator (ISAC), are performed. The current setup of TITAN can measure masses of SCIs or HCIs.

Isotopes from the ISAC beamline or stable ions from the Titan Ion Source (TIS) are cooled and bunched in a Radio-Frequency Quadrupole Trap (RFQ) (see figure 4.1). From there on, the ions are guided to MPET for the mass measurement.

Alternatively, the beam is sent into an EBIT after extraction from the Radio-Frequency Quadrupole Trap (RFQ). Here, the ions are charge bred. The HCIs are extracted and their mass is measured in MPET.

The individual parts of the experiment are described in the following.

4.1 Ion sources

The TITAN setup can either receive stable or unstable isotopes from the Isotope Separator and Accelerator (ISAC) or use stable ions from the Titan Ion Source (TIS). For this work, stable isotopes from the TIS were used.

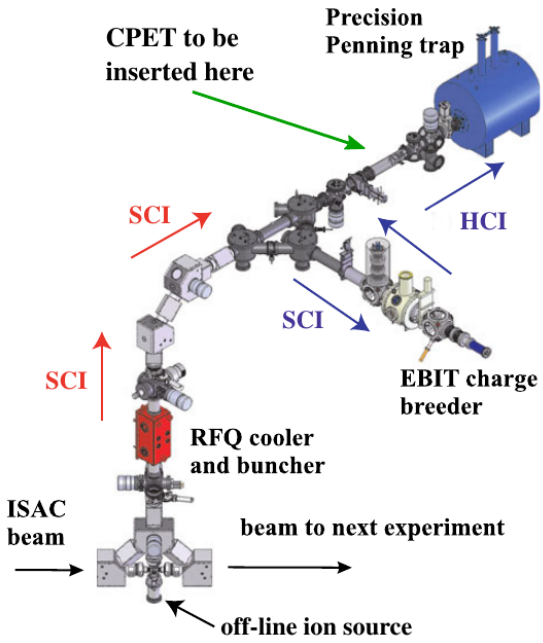

Figure 4.1: Overview of the TITAN-setup. Isotopes from the ISAC beamline or from the Titan Ion Source (TIS) (red arrows) are cooled and bunched before their mass measurement in MPET. To increase the charge state, the ions can be sent into an EBIT charge breeder prior to the mass measurement (blue arrows). Due to the increased energy uncertainty of the ions after charge breeding, the installation of a Cooler Penning Trap between EBIT and MPET is planned. Taken from [42]

4.1.1 ISAC facility

The Isotope Separator and Accelerator (ISAC) facility at Canada's National Laboratory for Particle and Nuclear Physics (TRIUMF) is capable of producing a wide range of rare, unstable isotopes for nuclear physics [43] which are available for mass measurements at TITAN. To produce rare unstable isotopes, a proton beam with an energy of $\approx 500\,\mathrm{MeV}$ and an intensity of up to $\approx 100\,\mu\mathrm{A}$ from TRIUMF's main cyclotron is directed onto a production target. The target consists of metal foils with a thickness of $\approx 10\,\mu\mathrm{m}$ [44]. The foils, made of various materials like UC, SiC, Ta, react with the proton beam and isotopes are produced from spallation, fragmentation or fission processes [45, 46]. Using the various target materials, a variety of unstable isotopes can be produced [47]. After production in the hot target ($\approx 2000\,\mathrm{K}$ [44]), the particles are ionized using methods like surface or laser ionization and are delivered to the different experiments [43].

As the beam typically contains multiple other isotopes, a magnetic mass separator is installed. With a resolution of up to $R \approx 3000$, it filters out isotopes using their mass

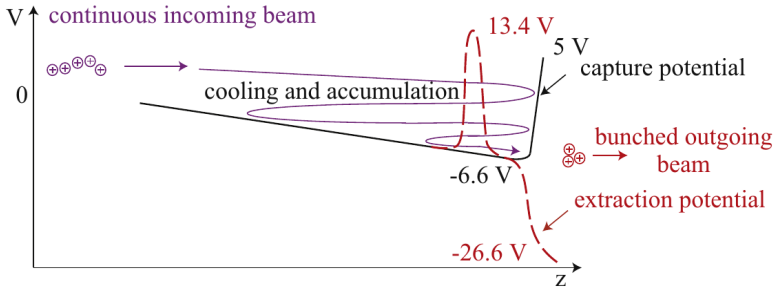

Figure 4.2: Schematics of the bunching and cooling process in the RFQ.

to charge ratio A/q. However, due to the limited resolution, the beam can still contain isobaric contamination when it reaches the TITAN experiment.

4.1.2 TITAN's ion source

The Titan Ion Source (TIS) is used for the optimization of TITAN's operation as well as for calibration purposes of MPET during measurements of unstable isotopes from ISAC. The source is electrically heated and releases singly or double charged ions using surface ionization. Due to the used ionization method, chemical elements, like alcalides, are available. The ions produced are focused with ion optical elements to form a continuous beam, which is directed to the experiment.

4.2 RFQ - cooler and buncher

The continuous beam from the ion sources typically has significant energy spread caused by the production methods. In order to match the acceptance parameters of the devices in the TITAN setup and to minimize ion losses during the measurement, the ions are cooled and bunched in a linear Paul trap also called Radio-Frequency Quadrupole Trap (RFQ) [48] (see Figure 4.2). The trap region of the RFQ consists of four segmented, hyperbolically shaped rods and the ions are trapped due to applied radial RF fields. Axially, the ions are accumulated in a potential well formed by DC voltages on the trap electrode segments. While the ions are stored, collisions with He buffer gas cool the ions. After cooling, the beam is extracted as a pulsed bunch. The bunched ions are delivered to the next component in the TITAN experiment at an adjusted transfer energy of $E_{\mathrm{beam}} = 1\,\mathrm{to}\,4\,\mathrm{keV}$.

4.3 Mass measurement in MPET

After beam preparation, the ions are sent into MPET [49] as described in Section 2.1. Using a 3.7 T magnet, the mass is measured via the TOF technique explained in section 2.1.1. To prepare the ion in an initial magnetron motion, a dipole excitation would be too time expensive since its duration typically needs to be longer than 10 ms [26]. Instead, at TITAN a Lorentz steerer deflects the ions slightly off trap center during injection. In order to capture the ions after Lorentz steering in MPET, their energy ($E_{\text{beam}} \approx 1$ to 4 keV) is reduced by a pulsed DT to $E_{\text{beam}} \approx 100$ eV. The residual energy is needed to enter the trap.
With this method, the mass of ^{11}Li with a half life of 8.8 ms was measured; the shortest-lived isotope ever measured with a Penning trap. At TITAN, mass measurement precisions on the order of 10^{-8} were achieved so far. To further improve the precision, the ions can be charge bred in an EBIT prior to injection into MPET.

4.4 EBIT: charge breeding of HCI for MPET

In order to increase the mass measurement precision of isotopes with a half-life of more than 50 ms, the ions can be sent into an EBIT charge breeder (see Chapter 3).
The EBIT was built at the Max Plank Institut für Kernphysik (MPIK) in Heidelberg [20] and provides sufficiently fast charge breeding; it is designed for currents of up to 5 A.

4.5 CPET: improving beam properties of HCI

Highly charged ions extracted from the EBIT will have affected beam properties, due to the electron collisions during charge breeding. However, as explained in Chapter 2, a low energy spread of the beam is crucial for high precision Penning trap mass measurements. To address this problem, a Cooler Penning Trap (CPET) [33] (see Figure 4.3) between EBIT and MPET to cool the ions after charge breeding has been developed to be used. To cool HCIs, a method buffer gas cooling cannot be applied. Since the electron recombination rate increases strongly with charge state, the charge state of the HCIs would decrease.
Therefore, it is planned to use either electrons or protons for the cooling process in the CPET [42]. Whereas using protons has the advantage of preserving the charge state of the HCIs, they need to be injected pre-cooled into CPET. Accordingly, this option

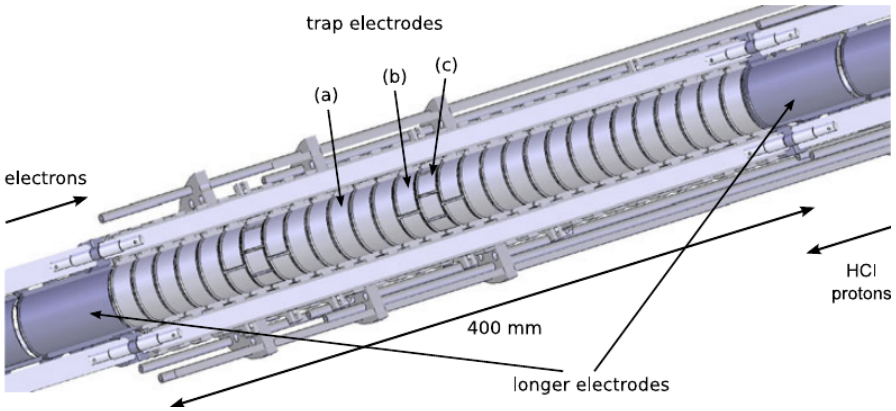

Figure 4.3: Trapping region of the Cooler Penning Trap (CPET). Electrons for cooling will come in from the left and HCIs from the right. Due to the number of trapping electrodes and a segmentation into 2 (a), 4 (b), and 8 (c) folded segments, a high flexibility for shaping the trapping potential will be possible. Taken from [42]

is technically more complex. Thus, tests with electron cooling will be performed first. Electrons cool themselves via emission of synchrotron radiation in the strong magnetic field of the CPET and can be easily produced. The cold electrons then cool the HCIs via Coulomb interactions. Even though electrons will recombine with HCI, extensive simulations have shown that the recombination rate is low enough to cool the HCIs down to 1 eV per charge state as required for MPET with moderate losses [42].

5 Experimental setup

Contents

This chapter describes the trapping section of the EBIT used for charge breeding as well as the ion optics in the EBIT beamline through which the ions pass on their way to the Allison-type and Retarding Field Analyzer detectors. Later on, the measurement concept and design of the Allison and RFA detectors, built during this thesis , are described. (Section 5.2). For the installation, significant changes to the TITAN switch yard section of the beamline were made (Section 5.3). The chapter closes with a description of the control system and the electronics for the Allison and RFA detectors.

5.1 The trapping region of the EBIT and used ion optics

From their production in the EBIT trap, described here in more detail, until they reach the emittance detectors, the HCIs pass several ion optical elements. For emittance and energy measurements, the ion optics play an important role, since emittance is only conserved when conservative forces are used to guide the ions.

5.1.1 Trapping region of the EBIT

The EBIT trap, as mentioned in Section of 3.1.3, consists of nine DTs. They are named in ascending order DT1 to DT9, starting at the collector (see Figure 5.1). The trap as a whole is built symmetrically around the center of DT5. DT5 is also the DT with the biggest radius and it has ports to allow for spectroscopy measurements on HCIs. For extraction of charge bred ions towards MPET, DT5 is too long and the spacial spread of the ion bunch would be too big. Therefore, either DT6 or DT4 is used for charge breeding of HCIs for MPET, as they are the shortest available DTs in the TITAN EBIT.

For calculation of the exact trap depth in the EBIT, the potentials applied to the DTs need to be corrected for the space charge of the electron beam which reduces the experienced potential of the ions in the trap [34].

Before the HCI leave the EBIT through the collector, they pass the DTs 3 to 1. Their horn shape provides an additional acceleration of the ions towards the collector and assures that the ions will leave the trap once they overcome the axial trapping potential on the collector side [34].

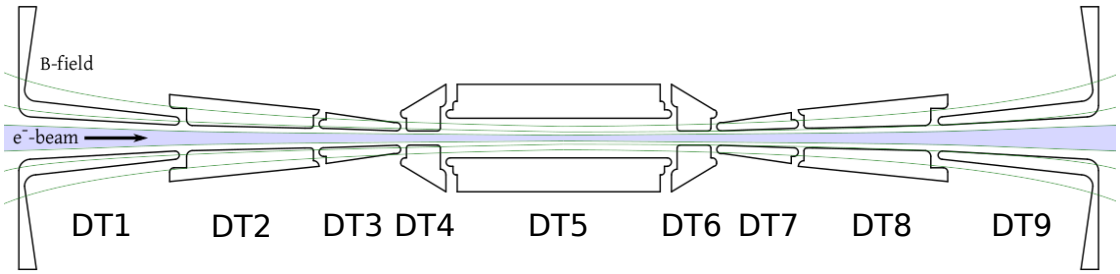

Figure 5.1: Schematic of the region in the EBIT. The electron beam (blue line), coming from the gun on the left, passes the Drift Tubes DT1-DT9 and is absorbed in the collector after exiting on the right side.

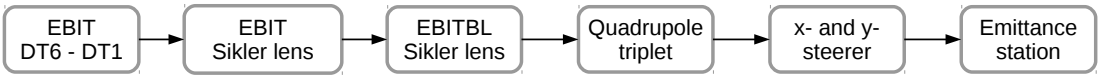

Figure 5.2: Optical elements the beam passes on its way from the EBIT towards the emittance station which is situated in the switch yard. Important to note is that the Quadrupole tripplet is currently operated as an Einzel lens triplet. For further information, see text.

5.1.2 Ion optics of EBIT extraction and in EBIT beamline

After charge breeding in the EBIT the ions are extracted through the collector into the EBIT beamline, which leads to the so-called switch yard (see Figure 5.2). The latter connects the EBIT beamline with the RFQ and MPET and provides space for the detectors. Since the EBIT beamline is used for injection into as well as extraction out of the EBIT, most optical elements can be switched between an injection and an extraction setting. Following the extracted beam path, the optical elements are presented.

Starting in the EBIT, the extracted ion bunch passes two Sikler lenses [50]. These are Einzel lens, which are divided into four pieces and can simultaneously focus and steer ions. The Sikler lens in the EBIT extraction is only used to focus the ion bunch because no switches are installed. Misalignments of the extracted ions with the beamline axis, are corrected by the second Sikler lens.

After extraction, the ions pass a quadrupole triplet which is used as an Einzel lens triplet. The operation an Einzel lens triplet is important for the measurement because a quadrupole triplet can introduce correlations between the two transversal emittances. In the following, the ion bunch can be corrected for misalignment with respect to the beamline axis via a set of x- and y-steering plates.

5.2 Determination of beam properties of extracted HCIs

In order to determine the beam properties, the appropriate detectors have to be selected. This section provides the reasoning for the choice of the Retarding Field Analyzer (RFA) and Allison detectors and an explanation of their measurement concepts. Further, their design and measurement uncertainties are discussed. At the end of the section, the built Bradbury Nielsen gate (BNG), used for charge state separation of HCIs from the EBIT, is described.

5.2.1 Requirements of the detectors

The main requirements for the detectors arise from the measurement range and precision. In terms of energy spread, a range of 1 to 50 eV from beam energies of 1.5 to 4 keV are needed. Here the upper limit arises from assuming the expected energy spread of the EBIT of less than $\Delta E_{\mathrm{beam}} \leq 50\,\mathrm{eVq}$. The lower limit is determined by the desired energy spread of less than 1 eV for injection into MPET. For the transversal emittance, a range of 1 to 30 π mm mrad is needed. The lower value is provided by the designed emittance of EBIT charge breeder of $\epsilon \approx 1\,\pi$ mm mrad [51] and the upper one is given by a preliminary measurement of the EBIT emittance of $15.7(5)\,\pi$ mm mrad [22] plus a safety margin.
Furthermore, there are very tight constraints due to the limited space in the beamline and the installation was limited to an 8 " port or less than 30 cm of beamline. Moreover, the small design is desired, as it allows the beam properties to be measured at different beamline locations in the future.
For the above reasons, an RFA was chosen to measure the lonitudinal energy distribution and an Allison-type detector for the transversal emittance of the beam. In addition, the data evaluation and the operation of the devices is comparatively simple.

5.2.2 Retarding Field Analyzer

The longitudinal energy distribution of an ion bunch will be measured with an RFA [52]. The central part of an RFA is a finely woven metal mesh, to which a voltage V can be applied. If the applied voltage is of same polarity as the ion's charge q, it forms a potential barrier of height $\Phi = qV$ and only ions with a greater kinetic Energy $E_{\mathrm{kin}} > \Phi$ can overcome it. Therefore, the mesh functions as an energy high-pass filter. After passing the mesh, the number of ions is counted by an ion detector, e.g. a Multi Channel Plate (MCP) [53]. The energy and energy spread of the bunch is determined by scanning the retarding potential.
To understand this, let's assume a bunched beam with energy distribution $n(E)$. In case of a symmetric distribution, the beam energy is given by the maximum of $n(E)$ and the energy spread is defined due to the distribution's FWHM [54] (see Figure 5.3).
The number of ions impinging on the detector at a certain retarding potential $N(\Phi)$ is then determined by the integral over the energy distribution $n(E)$

$$N(\Phi) = \int_{\Phi}^{\infty} n(E)dE \tag{5.1}$$

in the limits of the retarding potential and infinite particle energy. In order for this to

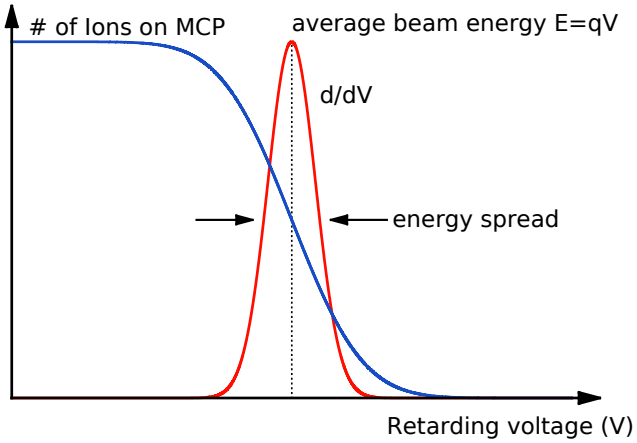

Figure 5.3: Number of ions which passed an ideal mesh on which a retarding Voltage is applied following (5.4) (blue). The first derivative (red) represents the corresponding energy distribution.

be valid, the number of particles in each bunch needs to be constant.
To reduce the uncertainty of the measurement, the accumulated curve $N(\Phi)$ is fitted to the data instead of building the numerical derivative of the spectrum. For this, the energy distribution must be known. In the case of extracted ions from the EBIT, the trapped ions are assumed to have a Maxwell-Boltzmann distribution after sufficient charge breeding time. To simplify the calculation, we approximate the Maxwell distribution by a Gaussian

$$n(E) = \frac{A}{\sqrt{2\pi\sigma}} \exp\left(-\frac{(E-E_0)^2}{2\sigma^2}\right), \tag{5.2}$$

with mean E_0, standard deviation σ and total particle number A. In the case of a Gaussian distribution, the Full Width at Half Maximum (FWHM) and with it the longitudinal energy spread, is defined as FWHM $= 2\sqrt{2\ln 2}\sigma$.
Integrating (5.2) using (5.1) yields the number of particles impinging on the detector

$$N(\Phi) = \int_{\Phi}^{\infty} n(E)dV = \int_{0}^{\infty} n(E)dV - \int_{0}^{\Phi} n(E)dV \tag{5.3}$$

$$N(\Phi) = \frac{1}{2}A\left(1 - \mathrm{erf}\left(\frac{\Phi - E_0}{\sigma\sqrt{2}}\right)\right) \tag{5.4}$$

where $\mathrm{erf} = \frac{2}{\sqrt{\pi}} \int_0^z e^{-t^2} dt$ is the error function. Equation (5.4) was used to fit the measured data.

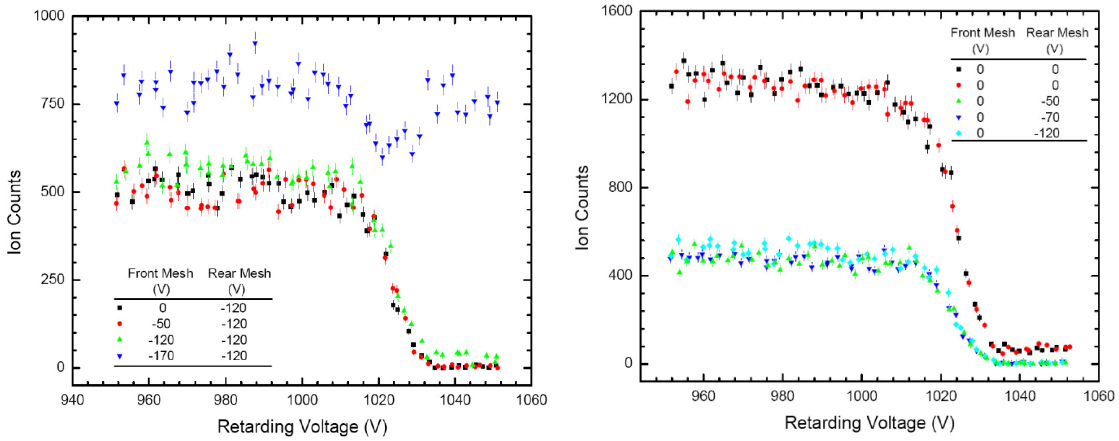

(a) Variation of the front-mesh potential **(b)** Variation of the rear-mesh potential

Figure 5.4: Influence of the suppression meshes of the old RFA onto the parasitic current. (a) The parasitic current drops significantly if the front mesh potential is less negative than the rear mesh potential. For greater potential difference between the front and the rear mesh, the parasitic current gets stronger suppressed. (b) A bias of 50 V or more results in a major reduction of the parasitic current. For the scans a $^6Li^+$ beam with 1 keV beam energy was used, coming from the RFQ. Taken from [28]

5.2.3 Design and construction of the Retarding field energy analyzer

Starting from a previously used design [28], a new, optimized RFA was developed. Therefore, the uncertainties and systematic errors of the device are investigated. Subsequently, the systematic errors were analyzed using a simulations. They could be reduced by the use of two retarding meshes. Further, a much higher transmission was achieved by means of a new method of secondary electron reduction.

Secondary electron reduction

In order to achieve a precise measurement, the detector needs to be shielded from secondary electrons, produced by collisions of ions with the detector. To achieve this, two meshes were installed in the previous RFA detector; one before and one after the retarding mesh. More meshes, however, significantly reduce the transmission in the detector. Investigating the need for the secondary electron suppression, measurements from [28] were re-evaluated. It was found that the mesh in front of the retarding mesh can be omitted without negatively impacting the result. The results from [28] prove that the first suppression mesh after the aperture makes no significant difference in parasitic current on the MCP and can therefore be omitted (see Figure 5.4a).
Instead, the mesh affects the direction of flight of the ions due to its reduced potential in

the transition point of the mesh which introduces systematic errors to the measurement. This will be discussed later.
In contrast, the rear mesh for second electron shielding is required, as can be seen in Figure 5.4b. Nonetheless, the mesh reduces the transmission, which would increase the measurement time. Therefore, it is left out and instead the MCP front plate is negatively biased, resulting in the comparative reduction of secondary electrons.
Due to these changes a major gain in transmission is achieved, while reducing systematic errors of the device.

Space charge limitations

Space charge is a crucial consideration in beam property measurements. Due to the non-conservative forces, the emittance and energy spread could increase. However, in terms of measurements at TITAN, space charge imposes no limitations. This can be estimated using the law of Child-Langmuir current density [55]

$$J = \frac{4\epsilon_0}{9}\sqrt{\frac{2q}{m_\mathrm{e}}}\frac{V_\mathrm{a}^{3/2}}{d^2}, \tag{5.5}$$

with vacuum permittivity ϵ_0, electron mass m_e, ion acceleration voltage V_a and distance d. The law describes current-density limitations due to space charge in sources. If the current density is on the order of the Child Langmuir current-density, space charge effects need to be considered.
For all operation conditions at TITAN, the current-density of the beam is on the order of $1\,\mathrm{mm\,cm^{-1}}$ and the Langmuir current density is not reached. Therefore, space charge does not need to be considered.

Potential depression and focusing effect

The used meshes which operate as a potential barrier, introduce two additional unwanted effects.
Firstly, in the open areas of the meshes, the potential is depressed and therefore lower than the bias on the mesh $V_\mathrm{open} < V_\mathrm{wire}$. In turn, ions passing the center of the opening see a lower potential than do ions close to the wires. This variation in the retarding potential introduces an error [54].
Secondly, as result of the potential depression, the ions are deflected (see Figure 5.5). In particular, ions with a potential energy close to the retarding potential are strongly deflected, because they spent more time in the inhomogeneous field region. Resulting

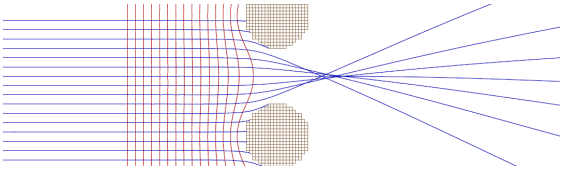

Figure 5.5: Visualization of the focusing effect. $^{133}Cs^{27+}$ ions (blue lines) of energy 1950 eV pass a non-ideal mesh (gray area) biased to 1900 V. The red lines represent equipotential lines of the electric field around the mesh.

from this, ions which would hit the mesh due to their ballistic path are now able to pass it. This causes an enhanced ion count for retarding potentials close to the beam potential (Figure 5.6a).
The thereby introduced error in longitudinal energy is small and can be approximated analytically by a circular aperture with focal length f and ion energy $E = qV_0$

$$\frac{1}{f} = \frac{E_1 - E_2}{4V_0}. \tag{5.6}$$

E_1 and E_2 are the electric field strengths before and behind the aperture, respectively. The introduced energy uncertainty can then be calculated using the deflection angle

$$\frac{\Delta E}{E} = \sin^2(\theta) = \sin^2\left(\frac{r}{f}\right) = \sin^2\left(\frac{r(E_1 - E_2)}{4V_0}\right) \tag{5.7}$$

where r is the radius of the opening.
For typical experimental values of $E_1 = 200\,\mathrm{kV\,m^{-1}}$, $E_2 = -250\,\mathrm{kV\,m^{-1}}$, $V_0 = 2.3\,\mathrm{kV}$ and $r \approx 8\,\mu\mathrm{m}$ this results in a relative energy uncertainty of $\Delta E/E \approx 4 \times 10^{-4}$.
Still, the analytical fit function does not take this enhanced ion count rate into account and results in a systematic error.

Simulation and improvement of the device

During the design process, a simulation study of the properties of the RFA was made using the commercial computer software SIMION 8.1 [56] to determine systematic uncertainties of the device.
In particular, the deviations in the measurement, caused by an initial energy distribution of the ions as well as by a deflection of ions due to a potential suppression in the open are of the mesh, were studied.
The software SIMION simulates ion optical geometries by numerically solving 2d and 3d Laplace equations. Solutions for individual elements, so called Potential Arrays (PAs), can then be merged together in a workbench. The ion trajectory through the workbench

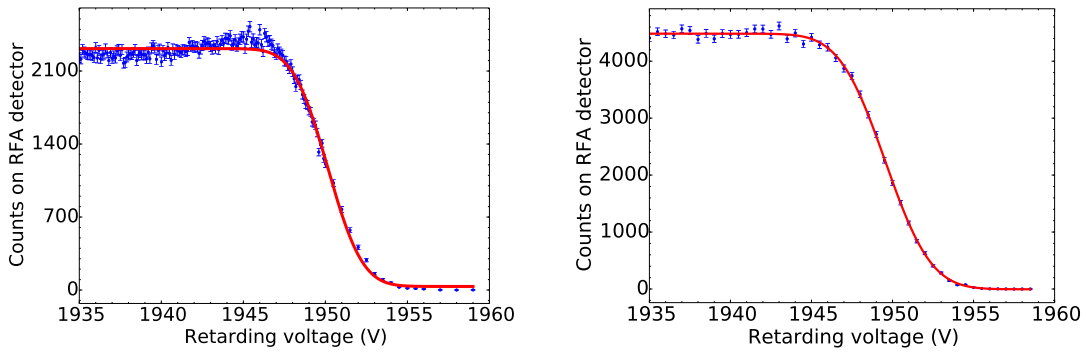

(a) One mesh **(b)** Two meshes

Figure 5.6: Example of the simulation results from Figure 5.7 for a RFA with one (a) and two (b) retarding meshes, respectively. Both simulations were done with a $^{133}Cs^{27+}$ beam of energy 1950 eV and an energy spread of 5 eV. Simulation (a) uses 1×10^4 ions and (b) 1×10^5 ions. In (a) a deviation of the simulation result and the fit (red) is clearly visible at 1945 V and can be reduced due to a second retarding mesh (b).

is calculated using the Runge-Kutta algorithm [57].

To reduce the potential suppression in the open areas of the mesh, a fine mesh is needed. Because of the fine meshes (wire diameter $d = 21.69\,\mu m$, 635 wires per inch), the simulation was split up into several PAs to save computational time. A rough structure of the RFA was designed as one PA and the fine mesh as a second superimposed PA. If an ion is in a region with several PAs it only experiences the PA with the highest priority. This also implies that the boundary conditions need to be carefully matched in the overlapping region. For computational reasons, only a small subsection of the non-ideal mesh was modeled. In order to still let every ion fly through the mesh, a Lua [58] script was written which detects the position of the ions and moves the mesh PA along the plane of the mesh into the ions' path of flight. The displacement was done in multiples of the length of the mesh PA.

$^{133}Cs^{27+}$ was chosen as an ion for the simulations since cesium is available from the TIS. With an $A/q = 4$ it has a low charge to mass ratio and can be produced in the EBIT with little contamination because 27+ represents a closed shell for cesium. Furthermore, the ions were simulated with a beam energy of E_{beam} =1950 eV and a three dimensional Gaussian energy distribution. For the beam-shape, a three dimensional Gaussian distribution was chosen as well, using a FWHM of 1 mm. To simulate the influence of transversal energy of the ions, they were programmed to follow a cone

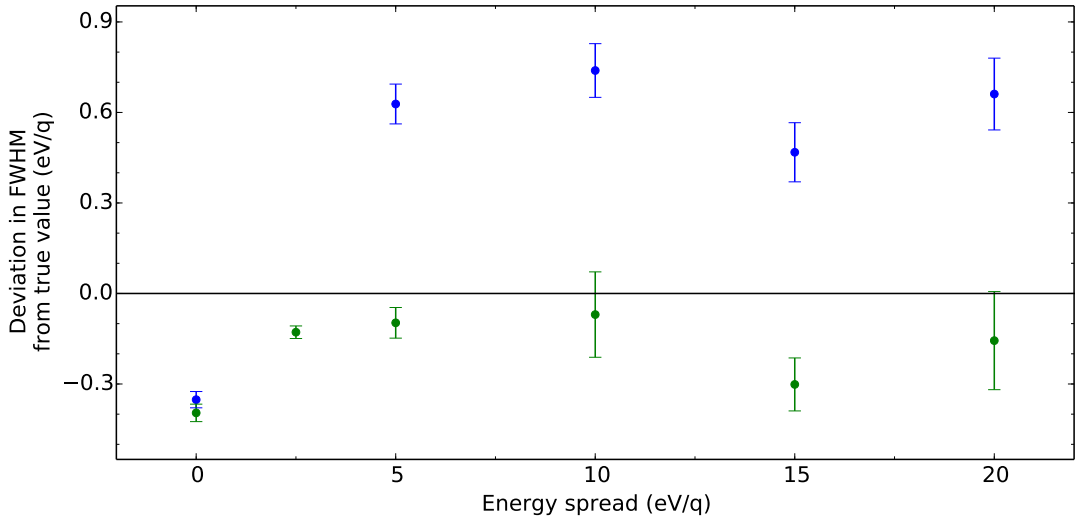

Figure 5.7: RFA simulations with one (black) and two (blue) meshes for different FWHM of the ion beam energy (energy spread) and 1×10^5 particles per simulation. The error is given by the 1σ uncertainty of the FWHM fit.

distribution with an opening angle of 1.3°. In the later device, the transversal energy was limited by a double hole aperture.

With this simulation, multiple values for the FWHM of the beam energy were tested. The simulation results were then fitted with a least square minimization routine written in Python [59] which uses Equation 5.4.

For a comparison of the results, the difference between the initial parameter and the values resulting from the fits were evaluated. Here, a systematic deviation of the FWHM of 0.6 eV towards higher values was found (see Figure 5.7), whereas the deviation of the beam energy was not significant.

The systematic deviation can be explained by the simulation results (see Figure 5.6a). At the end of the plateau region, before the count rate goes down, the fit clearly deviates from the data. This deviation is a result of an increased transmission through the mesh due to the focusing effect (see last section). However, in order to measure the longitudinal energy spread with high precision, the transmission through the detector should be independent of the retarding voltage and the ions' longitudinal energy.

In order to reduce this systematic effect, a second retarding mesh at an arbitrary distance of 1 cm was introduced. Due to the second mesh at the same potential, the deflection of the ions at the first retarding mesh drastically decreases. This can be understood using equation (5.6), where $E_1 - E_2$ goes to zero. In the following, another simulation study

Table 5.1: Most important dimensions of the RFA detector.

Measurement	Value
Spacing between mesh wire	12 µm
Mesh wire diameter	21 µm
Aperture diameter	52 thou
Distance between apertures	4 "

was done to find the systematic effect. As clearly visible in Figure 5.6b, the increased count rate from the focusing effect is strongly reduced. In the same way, the systematic shift is reduced to about $-0.2\,\mathrm{eV}$ (see Figure 5.7 for comparison).
To further reduce the ion deflection, the electric field gradient between the aperture and the first mesh needs to be reduced. Therefore, the respective spacing was increased to 1 cm.

Final design and precision of the detector

The final design was optimized for great flexibility while the results from the simulation were included. Also, lots of parts from the old detector, such as the meshes or the housing for example, could be reused. To keep the detector small and portable, it was designed to fit onto an 8 " vacuum flange that is horizontally installed in the beamline (see Figures 5.8, 5.9 as well as Appendix B for drawings of the detector). For this reason, the detector is also aligned with the beamline axis.
To filter out ions with a relative transversal energy of more than $\Delta E/E = 2 \times 10^{-4}$, two hole apertures are used (for dimensions of the devise see table 5.1). The size of the aperture can easily be varied by installing two new aperture plates.
Following the apertures, two retarding meshes are mounted on three studs and are separated by macor spacers of 1 cm length (see Figure 5.9). To hold everything in place, conical springs are used on the flange side. The meshes themselves are welded onto a support structure. Resulting from this, the mesh distance can be varied or meshes with other specifications can be installed. The number of electrical feed-troughs on the flange allows for up to three meshes. A housing around the detector prevents stray particles from entering the detector.
For the ion detection, two matched MCPs in Chevron configuration are used. To prevent secondary electrons from impinging on the MCP assembly, its front-plate can be biased. To be able to vary the front-plate bias, while maintaining the amplification factor of the MCP assembly, the bias of the back-plate can be varied as well. For a simple exchange

Figure 5.8: Foto of the full assembly of the used Retarding Field Analyzer (RFA). Ions, coming from the top of the picture, fly through a double hole aperture centered on the beamline axis. After passing two biased wire meshes, they impinge on an MCP detector.

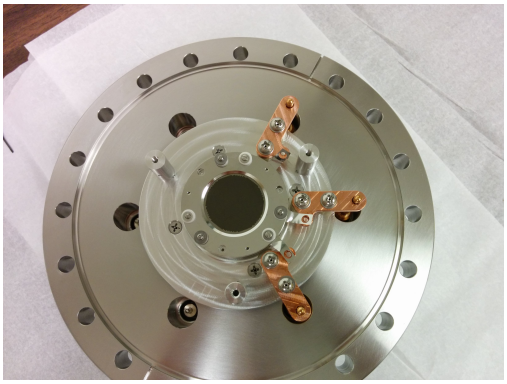

(a) RFA flange with installed MCP

(b) Meshes installed in the holder.

Figure 5.9: Pictures of partial assemblies of the RFA. (a) The mesh holder as well as apertures are detached from the vacuum flange and the MCP plates can be accessed. (b) Mesh holder with installed meshes, before cleaning. The surrounding housing as well as the apertures are detached. For test purposes a third mesh was assembled.

of the MCP assembly, all pieces of the RFA are detachable as a whole.

5.2.4 Allison emittance meter

To measure the transversal emittance, a so-called Allison emittance meter is used [60]. The advantages of an Allison detector are its compact design and its ability to measure angular resolution in the order of 1 mrad. Typically, Allison-type measurements can be distorted because of space charge in the beam [60]. However, at TITAN the effect of space charge is negligible (see Section 5.2.3).
In an Allison detector, particles pass two deflection plates situated between two slit apertures (Figure 5.10) [22]. The slit apertures are of width s and arbitrary length. To gain all information about the trace space $d^2\Phi/dxdx'$ of the particles, their angle x' with respect to the beamline-axis is measured dependent on the position x.
To vary the position of the apertures in the beam, the entire device is moved.
For each position in the beam, the angle x' of the particles is measured. Therefore, a voltage V_{plate} is applied across the deflection plates. The voltage results in an electric field $\boldsymbol{E} = V_{\text{plate}}/g$ and the ions experience a linear deflection force $\boldsymbol{F} = q\boldsymbol{E}$.
Depending on V_{plate}, only ions of an initial angle

$$x' = \frac{qV_{\text{plate}}}{E_{\text{ion}}} \frac{L_{eff}}{4g} \tag{5.8}$$

can pass the apertures. Here g is the gap between the deflection plates and $L_{eff} = L - 2\delta$ is their length.
Due to the space between the apertures and the deflection plated, fringe fields on the edges of the plates could potentially disturb the measurement. However, these can be neglected since their influence is small because of the detector geometry $L >> g$ [61].
The maximal detection angle x_{max} of the device is determined by ions which strike the

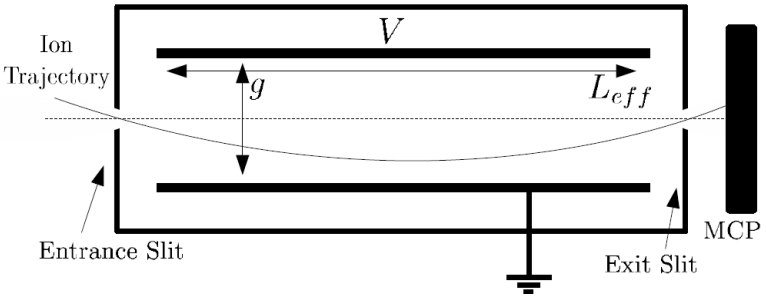

Figure 5.10: Scheme of an Allison detector. Taken from [22]

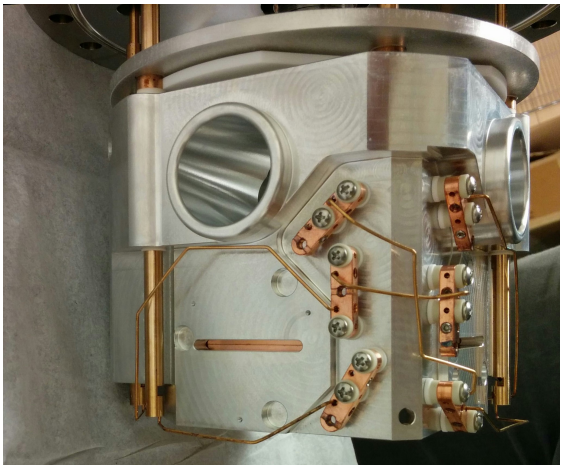

Figure 5.11: The new Allison emittance meter. Coming out to the left of the picture plane is the direction of ions from the RFQ toward EBIT. The MCPs are not yet installed on this picture.

deflection plates [60]

$$x'_{\max} = \frac{\pm 2g}{L + 2\delta}. \tag{5.9}$$

Therefore, a maximal voltage of

$$V_{\mathrm{m}} = \frac{\pm 8g^2 V_{\mathrm{ion}}}{L^2 - 4\delta^2} \tag{5.10}$$

is required to operate the detector.

5.2.5 Construction of Allison emittance meter

The new Allison emittance meter is based on the existing design from the ISAC group at TRIUMF [22]. Even though the geometrical parameters of the detector have not changed, major modifications to its design were made as explained in the design note. At the end of the section, the measurement uncertainties with this device are discussed.

Design

The original design was limited to an emittance measurement in one direction. However, at TITAN there are two orthogonally positioned devices – RFQ and EBIT – where an emittance measurement is crucial. Therefore, the design was altered to allow for measurements from two sides to avoid an opening of the beamline (see Figures 5.11, 5.12, as well Appendix A for the drawings).

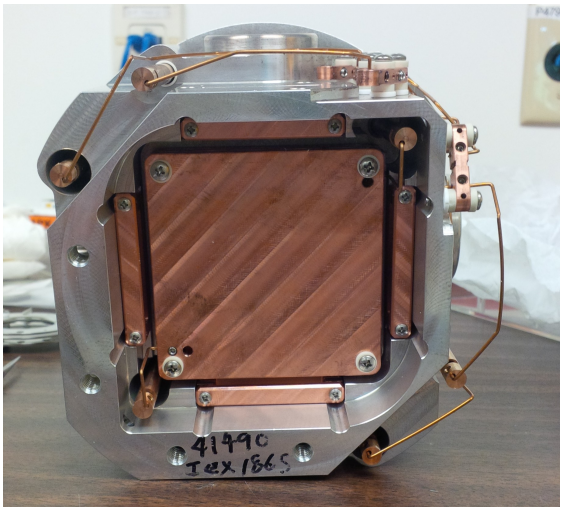

Figure 5.12: Picture of the bottom of the Allison detector during test assembly. In the center, the lower deflection plate is visible. Surrounding the deflection plate, the four apertures are can be seen.

Starting from the top, the detector is mounted on an 8" vacuum flange. To be able linearly move the detector through the beam, a rotary actuated feedthrough is used in combination with a stepper motor.

On the feedthrough, the device is attached to its housing. In the housing, two intersecting DTs of 3.175 cm diameter provide space for the beam to pass the detector unit undisturbed. This is important because the device will be installed in the beamline between RFQ and MPET.

In the lower part of the housing, the actual Allison detector is installed. Again, beam from two sides can pass the detector. For this reason, the deflection plates are square-shaped (all relevant measurements of the device can be found in table 5.2). They are attached to the bottom of the detector (see Figure 5.12). Further, they are separated with Macor spacers and can be biased individually.

To be able to adjust for the amount of beam which can pass the detector, each aperture is made out of two single pieces. Metal spacers between the two pieces of the slit apertures provide a modifiable spacing of the aperture slit. Their installation via the open configuration of the detector system allows for an easy exchange.

Since the device is movable, the electrical connections from the device to the feedthroughs are made out of two pieces; a beryllium-copper rod attached to the feedthrough slides in a tube of slightly bigger radius and the final connection is made, by means of a beryllium-copper spring attached to the rods tip (see also Appendix A).

Table 5.2: Most important dimensions of the Allison detector.

Measurement	Value
Slit aperture spacing d	0.1 mm
Distance between apertures	82.3 mm
Length of deflection plate L_{eff}	69.9 mm
Gap g between deflection plates	4.0 mm
Translation of rotary actuated feedthrough per turn	1.27 mm
Stepper motor steps/turn	200
Drift tube diameter	31.8 mm

For the Allison detector, MCPs stacks in Chevron configuration were used. Since the number of electrical feedthroughs were limited due to space constrains, the front- and back-plates of both MCP stacks share the same connection.

Measurement uncertainties of the Allison emittance meter

The measurement uncertainties of the Allison detector can be divided into components of the position and angle measurement.
The position is determined by the stepper motor position and its uncertainty is given by the used stepper motor and rotary feedthrough. The motor itself has a resolution of 200 steps per turn. In combination with the translation of the feedthough, the uncertainty in position follows to 6.35 µm.
Uncertainties in the angle measurement are derived from equation (5.8) using Gaussian error propagation

$$\frac{\Delta x'}{x'} = \sqrt{\left(\frac{\Delta V}{V}\right)^2 + \left(\frac{\Delta U}{U}\right)^2 + \left(\frac{\Delta L_{eff}}{L_{eff}}\right)^2 + \left(\frac{\Delta g}{g}\right)^2}. \tag{5.11}$$

The uncertainty caused by the deflection voltage V is controlled by the stability and accuracy of the power supply. Therefore, it can be adapted to be on the order of magnitude as the other uncertainties.
The next uncertainty is derived from the uncertainty in transversal energy of the ions, which can be expressed by the extraction voltage U. In the case of measurements of extracted ions from the EBIT, this term is assumed to be the dominating factor since the energy spread is predicted to be on the order of $\Delta U/U \leq 1 \times 10^{-2}$ to 1×10^{-1} per charge state for a beam energy of $E_{\text{beam}} = 2\,\text{keV}$.
Further, a variation in the effective deflection length L_{eff} can give rise to an uncertainty.

Due to the used slit apertures, ions can pass the Allison detector diagonal, which alters the interaction time with the electric field. The difference in length $\Delta L_{eff} = L'_{eff} - L_{eff}$ can be expressed by

$$\frac{\Delta L_{eff}}{L_{eff}} = \frac{1}{\cos\alpha} - 1 \tag{5.12}$$

with $\tan\alpha = D/2L$. Here, D is the length of the slits. For an aperture separation of $L = 82.55\,\text{mm}$ and a slit length of $D = 25\,\text{mm}$, one finds a maximal uncertainty of 1.2×10^{-2}. The relative uncertainty of the alignment of the deflection plates is on the order of $\Delta g/g \approx 1 \times 10^{-2}\,\text{mm}$ due to machining.
The uncertainty in $\Delta s/s$, caused by the aperture width, can be neglected since it is on the order of 1×10^{-3}.

5.2.6 Bradbury Nielson gate

In order to separate in various ion charge states as well as to remove contaminants from the residual gas in the EBIT, a Bradbury Nielson Gate (BNG) [62] was built and installed (Figure 5.13). A BNG acts as gate that separates ions by their TOF and consists of two sets of parallel wires.
When the wires are grounded, the BNG is invisible to the ions and they can pass. This state is called 'open' (see Figure 5.14 left side).
In the 'closed' state, an electrical potential is applied to the wires, producing a linear

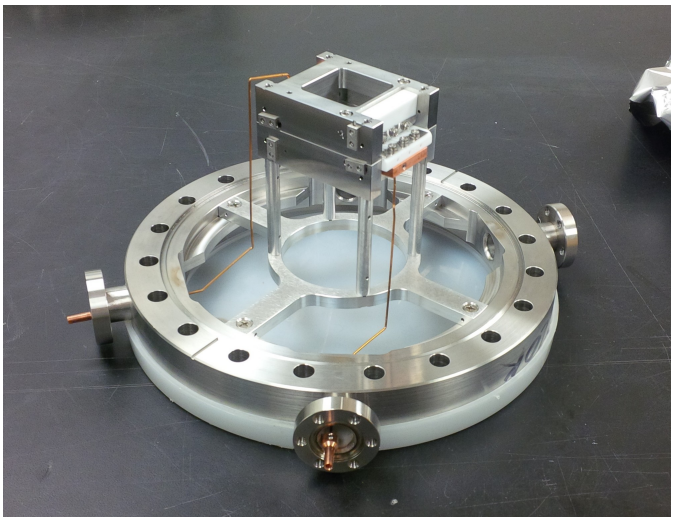

Figure 5.13: Picture of the fully assembled BNG. Beam, coming from the top of the picture, is going into the square shaped opening, where the meshes are installed.

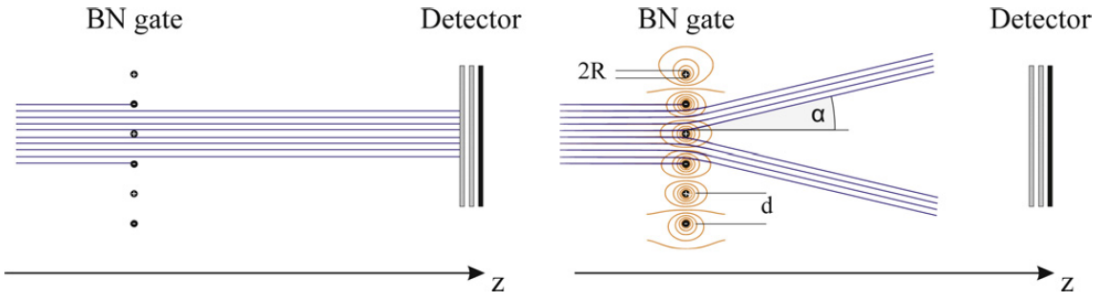

Figure 5.14: Schematic working principle of a BNG. When the BNG is 'open', ions (shown as purple lines) don't 'see' the BNG and hit the detector (left). When the BNG is 'closed', all ions of the same charge state are deflected under the deflection angle α and don't hit the detector (right). The orange lines represent the equipotential lines. Taken from [63]

potential gradient between the wires (see Figure 5.14 right side).

Since the direction of the gradient changes signs from one opening to the next, the ions are deflected in different directions. The average deflection angle for an ideal BNG with round wires can be described as [64]:

$$\tan(\alpha) = \frac{\pi}{2\ln(\cot(\pi R/2d))} \frac{V_{\text{wire}}}{E_{\text{kin}}/q} \tag{5.13}$$

The deflection angle depends on the space between the single wires as well as on the diameter $2R$ of the wires. Further α is determined by the ratio of the wire potential $V_{\text{wire}}(V_{\text{pos}} = |V_{\text{neg}}|)$ and the ion potential, meaning the kinetic energy divided by the charge state E_{kin}/q. During the rise time of the potential the deflection angle varies. Therefore, the capacitance of the wires are chosen as small as possible to allow for fast switching.

For application in the emittance measurement, a new BNG design of T. Brunner [63] is used. Instead of single wires, chemically etched grids are used, which allow for an easier and faster assembly. Due to their production method, the grid wires are diamond-shaped which slightly alters the electric field, in contrast to an ideal BNG with round wires. However, due to the small wire diameter - compared to their spacing d - the effect is negligible and only occurs close to the wires [63].

5.3 The emittance station

Instead of bending the extracted ions towards MPET (see Figure 5.15), the ions can be guided straight into the Emittance Station. The Emittance Station, built during this

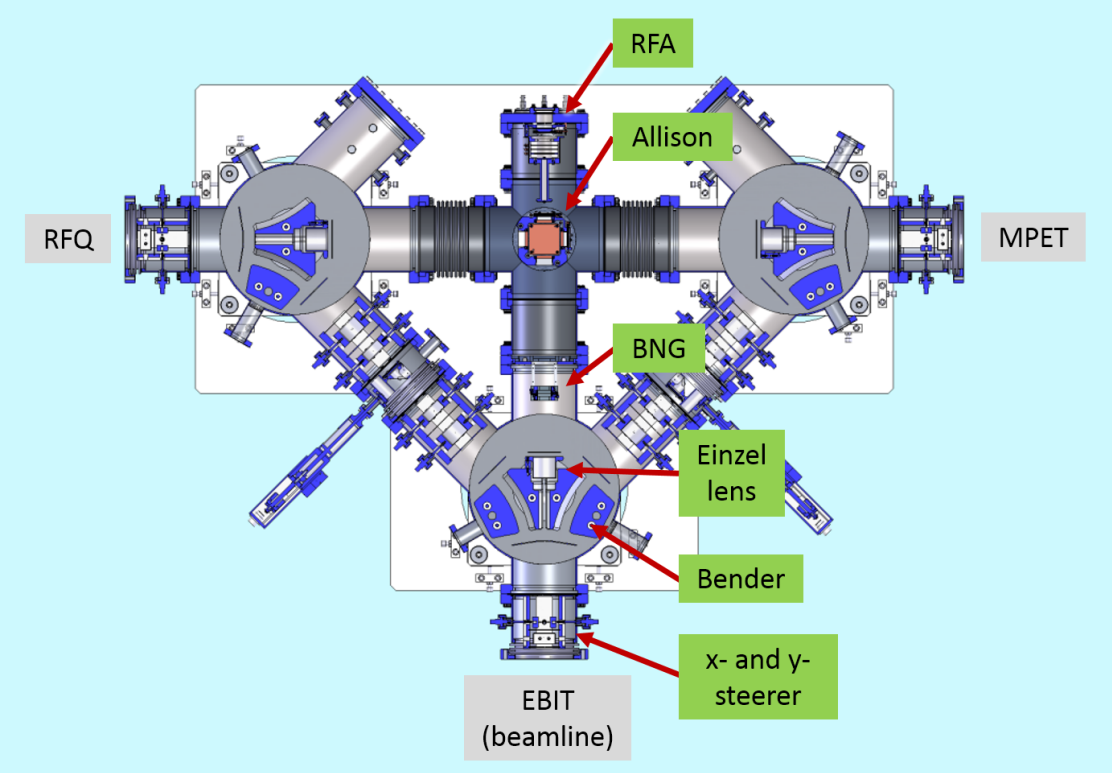

Figure 5.15: Rendered drawing of the TITAN switch yard. Cooled and bunched beam coming from the Radio-Frequency Quadrupole Trap (RFQ) on the left can be guided directly to Measurement Penning Trap (MPET) or bend toward the EBIT where it is charge bred. After charge breeding, the HCIs are sent to MPET. Alternatively, the beam can now also be sent straight through the bender. In the bender, the beam is refocused by an Einzel lens and sent towards the retractable Allison detector or the Retarding Field Analyzer (RFA). On the way, unwanted charge states as well as charge bred residual gas from the EBIT is separated by a Bradbury Nielsen gate (BNG).

work, is situated in the TITAN switch yard and consists of an Einzel lens, a BNG and the Allison, as well as the RFA detector. Further, the path of the ions and the changes on the vacuum system of the switch yard are described.

5.3.1 Detector installation

For an accurate measurement of the beam properties of ejected ions from the EBIT, it is of great importance that the beam solely experience conservative forces (see Section 5.1). Otherwise, the measurement can be distorted.
For this reason, the beam properties are measured in a straight line with the EBIT. Ion optical bender units have distorting affects on the beam properties [65]. Also the

detectors were placed as close as possible to the EBIT, to limit the amount of steering elements that effects the phase space of the extracted ions. Since the space in the EBIT beamline is limited, modifications to the switch yard were made to accommodate the Emittance Station. Another reason for the switch yard is the opportunity to have a permanently-installed Allison detector to measure the transversal emittance of beam from the EBIT, as well as beam towards the MPET from the RFQ.

5.3.2 Ion optical path towards the emittance station

Beam going into the Emittance Station first passes between two deflection plates of an electrostatic bender (TSYBL-B4) of the switch yard. Both deflection plates need to be equally biased to allow the ions to pass through the bender. To guarantee a high transmission through the RFA and Allison detector apertures, the same bender was modified to allow housing of an Einzel lens (TSYBL-EL4). Prior to its installation, the focusing voltage was simulated to be 1200 V for a 2 kV beam. For the simulation, beam properties were chosen based on a preliminary, unpublished measurement of the transversal emittance from 2010 [22]. He measured a transverse beam emittance of $\epsilon_{\mathrm{rms}} = 16\,\pi$ mm mrad with an extraction potential of 1950 V at position of a vacuum port between the EBIT and the bender.

Before the beam reaches the detectors, it is important to separate all contaminants like different charge states or charge bred residual gas from the EBIT. This is done with a new BNG (see Section 5.2.6) downstream of TSYBL-EL4 which separates the ions by their TOF. Its position was chosen at a maximum distance from the EBIT to give the HCIs enough TOF to spatially separate. At the same time, the BNG must deflect the ions by more than 1 cm for an estimated beam radius of ≤ 5 mm. Since deflection power is limited by the maximal voltage of 300 V for the BNG voltage switch, the deflection capabilities were verified by using the above mentioned simulation. At the position of the first detector, all ions are deflected more than 1.5 cm, which is sufficient.
After charge state separation, the beam arrives at the Allison detector (see Figure 5.15 and Section 5.2.5 in Chapter 5.2 installed in the intersection of the EBIT beamline and the beamline from RFQ to MPET. Furthermore, the stepper motor allows the DT of the Allison detector to align with the beamline axis. At a position of 72.4 mm of the linear actuated feedthrough, beam can pass from the EBIT onto the RFA detector or from the RFQ into MPET.

The beamline is terminated by the flange on which the RFA detector is installed. Since the apertures of the RFA are aligned with the beamline axis, the detector provides best opportunities to verify that extracted beam from the EBIT is extracted on beamline axis. Therefore it can also be used to find optimal extraction parameters for the Sikler lenses of the EBIT extraction optics (see Section 5.1.2).

5.3.3 Changes to the Vacuum system

To install the emittance meters, significant changes to the TITAN switch yard had to be made (see Figure 5.15). The beamline part between two benders in the switch yard was disassembled and replaced by two 6 " long bellows on both sides (see Figure 5.15). Between the bellows, a 6-way short cross with a length of 5.5 " from center to flange edge was installed. On its upper port, the Allison emittance meter is mounted.
The connection to TSYBL-B4 is provided by a double knife edge flange on which the BNG is attached to a mounting system. The mounting system ensures enough distance between the gate and the detectors. The final connection to the 6-way cross is then provided by a custom-built short nipple of length 51/8 ". A second nipple with same measures is used as housing for the RFA emittance meter on the opposite site of the short cross. All mentioned vacuum components have the standard diameter of the TITAN beamline of 8 ".

5.4 Measurement electronics and their uncertainties

Here, the electronics used for the RFA and the Allison detectors are described and their uncertainties discussed.

5.4.1 RFA

To measure the ions' energy spread and beam energy with a RFA, a precise bias for the retarding meshes is required. Here, a power supply with a high temporal stability was chosen in combination with a calibrated high voltage divider and a high precision multimeter (Agilent 34401A). For all voltage measurements, the input impedance of the multimeter was set to the standard value of 10 MΩ.
In order to ensure the precision of the high voltage divider, it was calibrated using a high precision power supply (ISEG EHS 8230p-F). The power supply's precision to set and read out voltages is 10 mV, when controlled by its computer interface. Unfortunately, this supply was not available for the measurements.

The voltage was then measured with the multimeter using the high voltage divider. The uncertainty of the multimeter, used for the calibration, is given by its readout uncertainty of one digit (10 µV in the range up to 10 V) and the linearity of the voltage measurement ($0.0002\,\% \cdot V_{\text{readout}} + 0.0001\,\% \cdot V_{\text{range}}$).
For the final calibration of the high voltage divider, a linear curve was fitted to the data with the least square method

$$V_{\text{RFA}}(x) = 996.42(2) \cdot (x - 2.3) + 2292.81 \pm 0.01 \tag{5.14}$$

For measurements of the absolute beam energy, the accuracy of the ISEG power supply also needs to be accounted for, which is dependent on the voltage output as well as the nominal voltage ($0.01\,\% \cdot V_{\text{out}} + 0.02\,\% \cdot V_{\text{nom}}$).

5.4.2 Allison detector

In order to optimize the achievable precision of the device, the deflection plates of the Allison detector need a bias with a relative uncertainty of better than 1×10^{-2}.
To fulfill this requirement, the stable voltage output from a Digital to Analog Converter (DAC) is used. The 16-bit DAC provides up to ±10 V. In case this voltage is not sufficient, it can be amplified up to ±200 V using an Apex Pa98 operational amplifier.
The amplified voltage is then measurement by the multimeter used for the RFA measurements. The accuracy of the voltage measurement is $\pm(0.0020\,\% \cdot V_{\text{readout}} + 0.0006\,\% \cdot V_{\text{range}})$ in a range of up to 100 V. Resulting from this, the total relative error is far below 1×10^{-2}.

5.5 Data acquisition and evaluation

This section describes the data accumulation and control system of the detectors and an overview of the ion detection setup of the RFA and Allsion detectors is given.

5.5.1 Controlsystem and Software

The control of the detectors is implemented in a software for the MCP readout, written by R. Klawitter [private communication] (see Figure 5.16). Due to its access to all important control systems of the TITAN experiment, it is an ideal tool to optimize the transport efficiency of ions at TITAN.
In particular, the software can send commands to the control system EPICS (Experimental Physics and Industrial Control System) of the beamline elements. EPICS is used

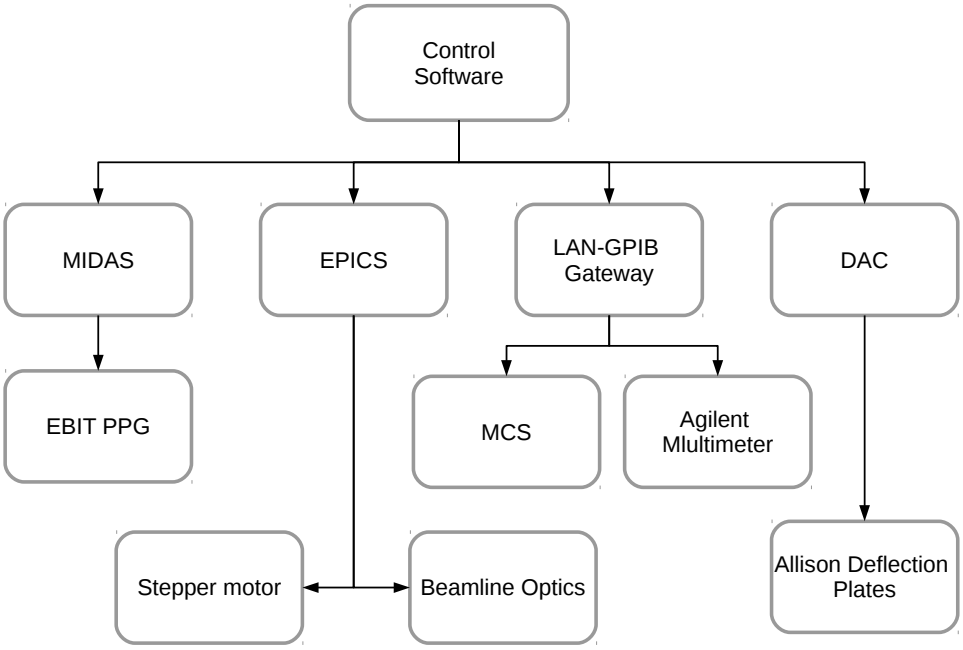

Figure 5.16: Overview of the control system of the experiment. For further information, see text.

to control the EBIT optics, Allsion stepper motor, TIS source, and the RFQ.

The software can send commands to the software MIDAS, used to control the timings for switching the EBIT, as well as the optical elements in the EBIT beamline, between injection and extraction. To do so, timings are set in the MIDAS web interface and sent to a Pule-Pattern-Generator (PPG). The PPG translates the MIDAS signal into NIM pulses with a temporal resolution of up to 10 ns to make them suitable for the solid state voltage switches.

For the control of the detectors, the software is able to read out an multimeter via a LAN-GPIB gateway (see Section 5.4). The voltages for the retarding meshes of the RFA as well as the position of the Allison stepper motor are set via commands sent to EPICS. To bias the Allison deflection plate, a DAC is controlled by the software via MIDAS.

All elements can be scanned via command line inputs in the software and the settings and data saved in a data base. Entries in the data base can be viewed and extracted for evaluation.

5.5.2 Ion detection

To detect the ions, both detectors use two MCPs in Chevron configuration. In the following, the surface of the plate facing the incoming ion is called front-plate (f-plate) and the surface of the second MCP facing away from the incoming ion, back-plate (b-plate). MCPs detect ions by amplifying the charge of the ion. This is done via production of an electron cascade in the MCPs. In order to maintain a steady charge amplification, the bias between the front- and back-plate was kept at $\Delta V = 1900\,\mathrm{V}$. To detect the electron cascade, an anode is biased 200 V more positive the back-plate.
The electrical signal from the anode is first capacitively decoupled from the anode bias. Afterward it is amplified by an operational amplifier and sent to a Multi Channel Scaler (MCS). Here, the incoming analog signals are counted and binned in time, up to a minimal bin-width of 40 ns. To avoid dead times in the MCP, the ion rate on the detector must be on the order of one ion per extraction from the EBIT. Further, two ions at the same time are seen as one count because the MCS triggers on the rising or falling slope of the incoming signal. In order to reduce noise, a discriminator level for the detection was chosen slightly below the ion pulse height.
The signal from the MCS is read out by the measurement software via a LAN-GBIB gateway. Using the software, the number of extractions over which the MCS accumulates can be chosen, as well as the discriminator level.
From the so measured Time-of-Flight (TOF) spectrum (Figure 5.17), the number of ions can be extracted by summing over all bins with ions of interest. This sum provides one data point in an Allison or RFA scan.

5.5.3 Data evaluation and correction

For data evaluation, the TOF spectra stored in the database were analyzed. For both types of measurements, all counts in the region in TOF with ions of interest were summed. The data of both detectors was then corrected for noise background from the electronics. Therefore, the sum over all counts in an equivalent time range of the TOF spectra was subtracted, where ions have been deflected by the BNG.

RFA

To obtain the beam energy and the energy spread, the data was fitted using Equation 5.4. The stated errors were calculated by multiplying the uncertainties of the fitted values with the chi-squared over degree of freedoms of the fit.

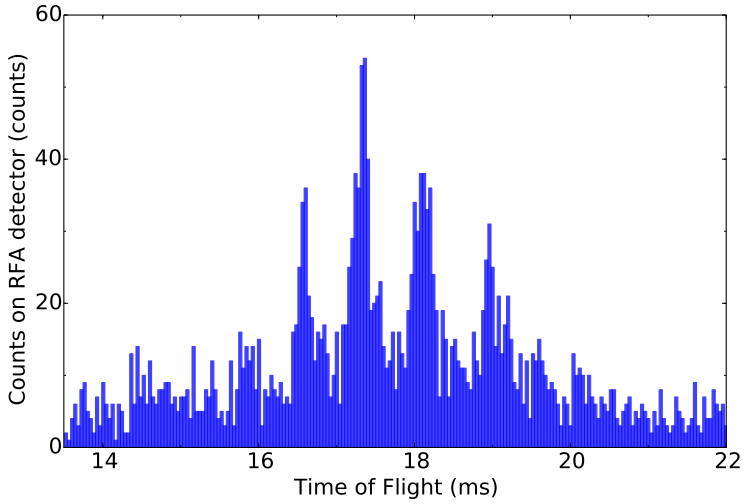

Figure 5.17: TOF spectrum of ^{85}Rb measured on the RFA detector. The single charge states are clearly separated by their TOF at the position of the detector. No BNG was set.

Allison detector

Prior to the calculation of the emittance values of the Allison detector measurements, the dataset was manually corrected for effects of contamination by other ions.
Afterwards, the RMS emittance was calculated (see Section 2.2.1) for a cutoff of zero percent. Because of the cutoff, all values smaller than the product of maximum value in the spectrum and cutoff are set to zero. The uncertainty of the RMS emittance was estimated by the absolute of the dereference in RMS emittance for zero and five percent. The cutoff of five percent was chosen because it represented the level of noise in the measurements.

6 Measurement of beam properties of extracted beam from the EBIT

Contents

This chapter describes the commissioning of the detectors with HCIs from the EBIT. After commissioning, the impact of secondary electrons onto the count rate of the detectors was measured because the Retarding Field Analyzer (RFA) and Allison detector make use of counting detectors (MCPs). Also a first investigation of the dependency of the beam properties onto the EBIT trap depth and the release voltage was made.

6.1 Commissioning

For the measurements, ^{85}Rb ions from the TIS were used. They were selected instead of ^{133}Cs because more rubidium was available from the source, reducing measurement times. For operation of the EBIT, the method of capture and release of ions by changing the bias of DT6 was used throughout all measurements. This method was chosen since it is typically used at TITAN for charge breeding of ions for Penning trap mass measurements.

Performing measurements, ^{85}Rb from the source was cooled and bunched in the RFQ for 12 ms. After extraction, its beam energy was reduced from 20 kV to about 2130 eV. While the ^{85}Rb ions entered the EBIT, DT6 was biased ($V_{\mathrm{DT6,high}} = V_{\mathrm{DT6,low}} + V_{\mathrm{DT6},\Delta}$) just below beam potential to reduce their kinetic energy and the ions were captured by

Table 6.1: Used EBIT settings and ^{85}Rb charge state for all made measurements. The settings for $V_{\mathrm{DT6,low}}$ and $V_{\mathrm{DT6},\Delta}$ are not listed since they were varied in the scope of the experiments.

Setting	Value
Charge breeeding time	10 ms
Electron beam current	100 mA
V_{DT5}	2070 V
Magnetic field in EBIT	4.5 T
Charge state of ^{85}Rb	13+

lowering the potential on DT6 ($V_{\mathrm{DT6,low}}$). During capturing, ^{85}Rb was separated from its isotope ^{87}Rb. In the EBIT the ions were charge bred for 10 ms with an electron current of 100 mA (see Table 6.1). After charge breeding, the ions were extracted towards the emittance station by raising the potential of DT6 to is initial value. Using the BNG, $^{85}Rb^{13+}$ was selected because it was easily separated from contamination as well as other charge states.
In order find the apertures of the RFA detector and steer extracted beam from the EBIT into the RFA, a simultaneous scan of the deflection voltages of x- (horizontal direction) and y-steerer (vertical direction) was made. With the injected beam, the extraction values of all optical elements in the EBIT beamline were optimized for a maximal count rate on the RFA detector. In doing so, maximal alignment of extracted beam from the EBIT with the beamline axis was assured since the two apertures of the RFA are well aligned. After detecting beam on the MPC of the RFA, the extraction settings were used to optimize beam on the Allison detector. This was done by stepping its position through the beamline. With unbiased deflection plates the maximum beam intensity was found for an EPICS set value for the stepper motor of 14 mm.

6.1.1 Impact of secondary electrons

Since the measurement methods are based on counting events on a MCP, the amount of secondary electrons was investigated, to avoid a possible impact on the results.
To this end, HCIs were extracted under stable experimental parameters while the number of detected ions was measured for varying negative front-plate potentials $V_{\mathrm{f-plate}}$ of the MCP (see Figure 6.2). Assuming a stable rate of incoming beam, a reduction in count rate is expected for more negative front plate bias due to repulsion of secondary electrons. While varying $V_{\mathrm{f-plate}}$, the MCP backplate bias was adjusted accordingly to maintain a

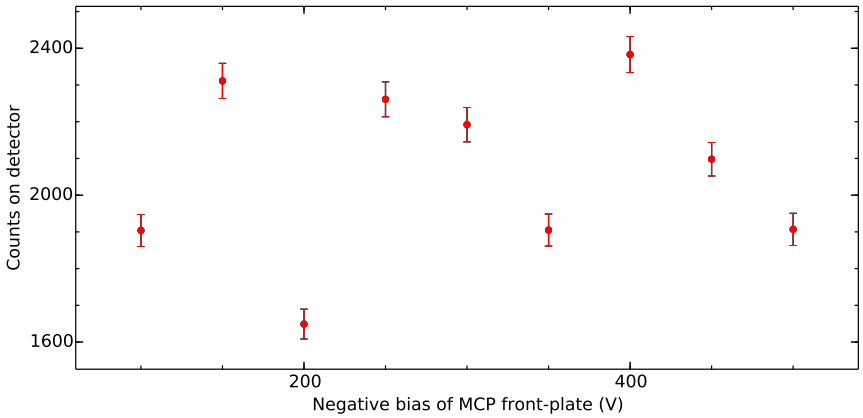

Figure 6.1: Reduction of secondary electrons on the Allison detector. Plotted are counts on the Allison MCP for six times 1000 extraction cycles from the EBIT. No general trend in counts is visible for more negative bias of the MCP front-plate. Note that the absolute value of the front plate bias is plotted for better visualization.

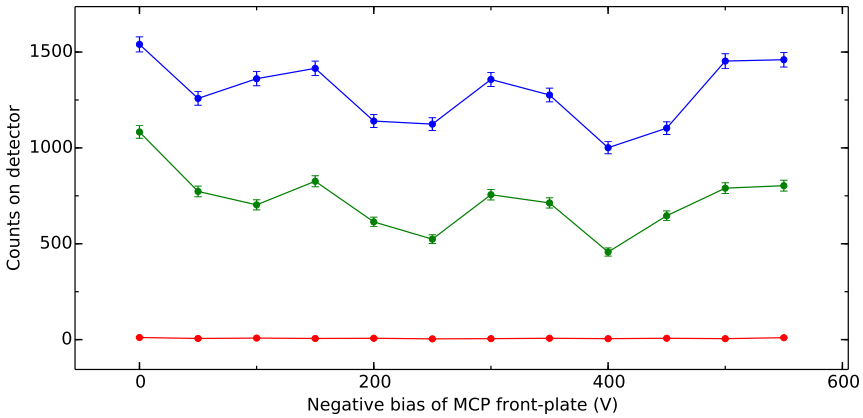

Figure 6.2: Reduction of secondary electrons on the RFA detector. Plotted are counts on the RFA MCP for six times 1000 extraction cycles from the EBIT, for different biases of the retarding meshes (red: V_{mesh} =1950 V, green: V_{mesh} =2150 V, blue: V_{mesh} =2250 V). A general decrease in counts is visible for more negative bias of the MCP front-plate due to reflection of secondary electrons. But the count rate is fluctuating and even increases for $V_{\mathrm{f-plate}} \leq -400$ V. Note that the absolute value of the front plate bias is plotted for better visualization.

constant amplification factor of the MCPs. For the MCP readout, the MCP anode was biased 200 V above the backplate potential, during all measurements.
To measure the effect of secondary electrons onto the count rate of the Allison detector, the front plate bias of its MCP was varied from 50 to 500 V in steps of 50 V. However, no general trend in the number of counts is visible (see Figure 6.1). Further, fluctuations of the count rate are recognizable, which can't be explained by the counting error.
For the RFA detectors, the count rates were measured in a range of 0 to 550 V in steps of 50 V. Additionally, the count rate was measured for different retarding voltages V_{mesh} to investigate a correlation between the incoming beam and the number of secondary electrons. As visible in Figure 6.2, detected events on the RFA follow a general trend of a reduced signal with more negative front plate bias. However, an increase in the number of detected events can be seen for highest front plate biases $V_{\mathrm{f-plate}} \leq -400$, which was not expected. Further, fluctuations in the number of events are visible, not following the general decrease in events.

6.1.2 Fluctuations of count rate from TIS or RFQ

Significant fluctuations and an un-expected increase of the count rate occurred in the measurements for secondary electrons.
To investigate the RFQ and the ion source as possible reasons for the fluctuations, ^{85}Rb ions were extracted from the RFQ and counted on a MCP. The sum of the detected events of 1000 extractions from the RFQ was measured every two minutes over a time period of five and a half hours. During this measurement, the TIS was operated at a lower extraction rate compared to measurements with the RFA and Allison detectors. This was necessary to limit the current on the MCP and with it the dead times of the counting setup (MCP, MCS) as well as possible space charge effects.
In the results of this measurement (Figure 6.3), clear fluctuation in the rate of detected events is visible. Furthermore, a sudden jump in the rate of extracted ions is visible, before the extraction rate stabilizes. To exclude that the jump in count rate is caused by the used electronics, the same measurement was done without ions. However, no indications were found that either the fluctuations or the jump in the count rate are correlated with the used electronics.

6.1.3 Problems of the control system electronics

During commissioning as well as after several hours of measurement, problems occurred in the use of the DAC, MCS, LAN-GPIB converter and power supplies for biasing the

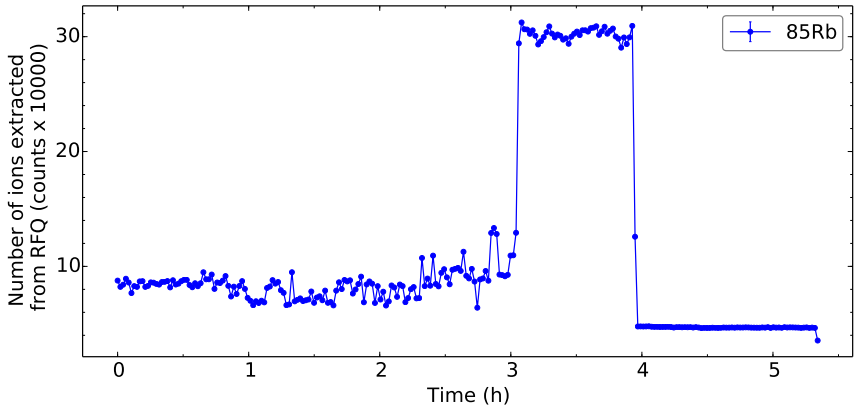

Figure 6.3: Number of ^{85}Rb ions extracted from the RFQ over time. With unchanged experimental settings, clear fluctuations of the extracted number of ions are visible in the first four hours. The error bars are too small to be seen.

EBIT DTs. These problems were a limiting factor for measurement series with the RFA and Allison detectors as well as for single Allison scans. This was because the duration of an RFA or Allison measurements was on the order of half an hour or five hours per scan, respectively.
The LAN-GPIB converter stopped responding to the measurement software after different periods of time, ranging from two days down to half an hour. Using a local- instead of a global-network connection to the measurement computer, the problems could be resolved. For the MCS, similar problems occurred and are suspected to have resulted from overheating of the device. The problem can be solved via an external cooling system. Even though the DAC kept responding to the measurement software, it stopped changing its output voltage after about 3000 cycles and potentially needs to be replaced, in order to do longer measurements. A further problem arose from the power supply of DT7, which reduced its voltage output during the measurements from 2950 V to 30 V. Controlling the current read back of the power supply, there was no indication that the supply reached its current limit, which would be an indication of the electron beam coming too close to the respective DT.

6.2 Beam property measurements

In addition to the detector commissioning, first systematic, measurements of the beam properties of ions extracted from the EBIT were carried out. Due to stability problems in the experimental setup and time constraints, it was not possible to obtain data from

the Allison detector for each individual RFA measurement. Therefore, the investigation of the energy spread and transversal emittance are separated into different sections. In the first section, results of measurements with the RFA detector are described. Using the detector, the reproducibility of the measured longitudinal energy spread was investigated, as well as its dependency on the trap depth and release voltage. In the second section, the transversal emittance was measured for different combinations of EBIT trap depths and release voltages, using the Allison detector.

6.2.1 Longitudinal energy spread measurements with the RFA

In order to investigate a possible influence of the count rate fluctuations on the RFA measurements, the reproducibility of the RFA measurements was tested. Further, the impact of the EBIT trap depth V_{Trap} and release voltage $V_{\mathrm{DT6},\Delta}$ onto the longitudinal energy spread of the ions was investigated.

Reproducibility of the measurements

To test the reproducibility of the measurements, several RFA spectra, with identical charge breeding and extraction settings, were taken (see Table 6.2 and Figure 6.4). For the measurements, the EBIT extraction was operated with $V_{\mathrm{DT6,low}} = 1905\,\mathrm{V}$ and $V_{\mathrm{DT6},\Delta} = 435\,\mathrm{V}$ and a charge breeding time of 10 ms. The voltage on the two retarding meshes was varied between 2050 to 2260 V in steps of 3 V. In order to reach sufficient statistic to reduce uncertainties, and still maintain short measurement times of less than one hour, 1500 extraction cycles from the EBIT were summed for each data point. Obtaining a spectrum as is seen here, took approximately one hour (see Figure 6.4). Narrowing the measurement range, the same results could be obtained in approximately half an hour of measurement time.
All measured values for the beam energy (see Table 6.2) are all in agreement with each other and an average of 2180.4(17) eV/q was calculated where the uncertainty is given by the standard deviation of the values.
With regards to the energy spread, a variation in the measured values is visible but not significant. Comparing the single spectra (Figure 6.4), scan 1 stands out because here the number of events was higher by approximately 300 compared to all other scans. Further, fluctuations outside the statical uncertainty are visible in the range of V_{mesh} =2050 to 2100 V. In this range, a stable number of detected ions was expected for a stable extraction rate because it is far below the measured beam energy. The fluctuations are particularly visible in the second scan (in green), causing an increased

Table 6.2: Result of five energy spread measurements under constant extraction parameters. The corresponding scans can be seen in Figure 6.4.

Scan	E_{beam} (eV/q)	ΔE_{beam} (eV/q)
1	2182(3)	19(8)
2	2179(4)	21(12)
3	2181(2)	17(5)
4	2178(1)	22(4)
5	2182(3)	20(9)

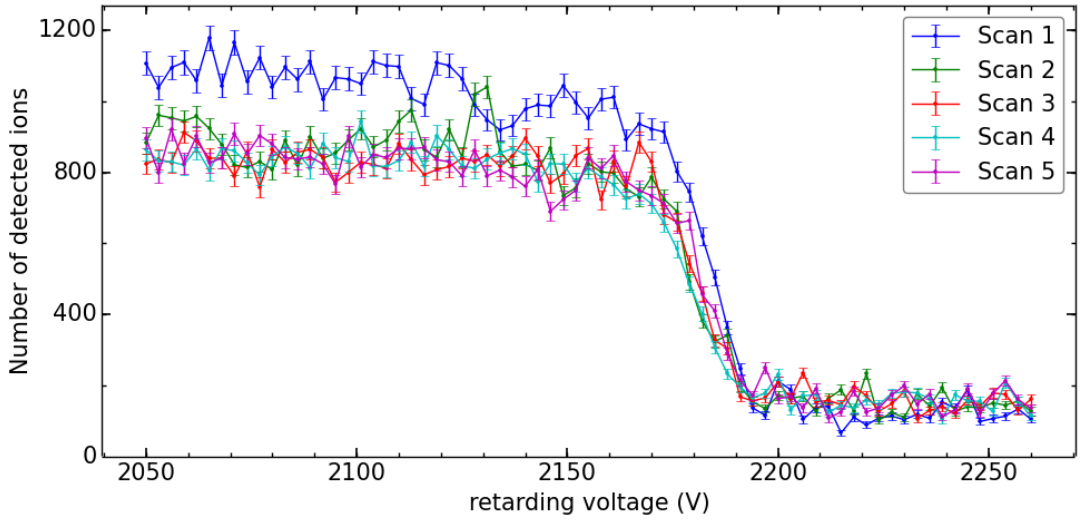

Figure 6.4: RFA scan for the same extraction settings, which was repeated five times over a time period of six hours. Each measured data point is the average of 1000 extractions from the EBIT. The measured energy spreads as can be seen in Table 6.2

uncertainty of 12 V unlike the other measurements.

Calculating the average and standard deviation of all values, an energy spread of 19.7(21) eV/q was measured.

Influence of the ions' potential gain during extraction and EBIT trap depth onto the energy spread

In this section, a possible correlation of the ions' energy spread and their potential gain during the extraction process was investigated. In the following, this potential gain will be called 'release voltage' to avoid confusion with the extraction voltage $V_{\text{DT,ext}} = V_{\text{DT6,low}} + V_{\text{DT6,}\Delta}$, which determines the overall beam energy.

Table 6.3: Dependency of the energy spread on the EBIT release voltage $V_{\mathrm{DT6},\Delta}$ and trap depth, represented by the lower potential of the trapping DT $V_{\mathrm{DT6,low}}$. Note that the DT voltages need to be corrected for the space charge of the electron beam.

$V_{\mathrm{DT6,low}}$	$V_{\mathrm{DT6},\Delta}$	E_{beam} (eV/q)	ΔE_{beam} (eV/q)
1915	450	2186(6)	63(18)
1920	445	2181(4)	37(11)
1925	440	2182(5)	48(13)
1930	435	2180(5)	34(15)
1935	430	2182(2)	36(7)
1940	425	2181(2)	38(5)
1945	420	2181(2)	39(7)
1950	415	2177(3)	57(8)
1955	410	2186(2)	44(5)

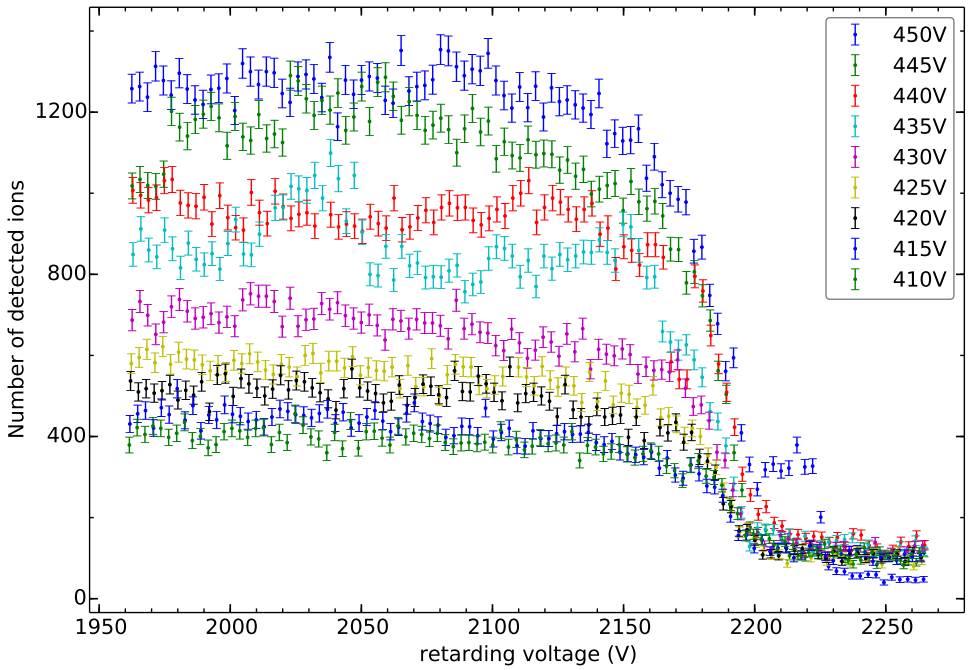

Figure 6.5: RFA scans for various release voltages $V_{\mathrm{DT6},\Delta}$. In order to avoid influences from the extraction optics, the beam energy ($V_{\mathrm{extr}} = V_{\mathrm{DT6}} + V_{\mathrm{DT6},\Delta}$) was kept constant. In turn, the trap depth changed $V_{\mathrm{Trap}} = V_{\mathrm{DT5}} - V_{\mathrm{DT6,low}}$. Each measured data point represents the average of 1000 extractions from the EBIT. The measured energy spreads can be seen in Table 6.3

During the measurements the release voltage was varied between $V_{\mathrm{DT6,\Delta}} = 410\,\mathrm{to}\,450\,\mathrm{V}$ (see Figure 6.5). At the same time, the EBIT trap depth $V_{\mathrm{Trap}} = V_{\mathrm{DT5}} - V_{\mathrm{DT6,low}}$ was decreased by lowering $V_{\mathrm{DT6,low}}$ (1955 to 1915 V) to maintain the used extraction voltage. This was done for two reasons. First, the extraction voltage equals the injection voltage on which ions from the RFQ are received and its change would require the re-optimization of the injection process into the EBIT. Second, the timings for the BNG would need to be adjusted.

Reducing the trap depth, the energy spread of the ions is expected to reduce as well because the trap depth limits the maximal temperature of trapped ions. Additionally, smaller energy spreads are expected for a decrease in release voltage. The measured beam energy should not change because the extraction voltage V_{extr} was stable throughout the measurement.

While scanning a range of $V_{\mathrm{DT6,\Delta}} = 410\,\mathrm{to}\,450\,\mathrm{V}$, the count rate on the detector clearly reduces, which is explained by the shallower EBIT trap. In the spectra, variations of the number of ions in the plateau-like regions ($V_{\mathrm{RFA}} = 1950\,\mathrm{to}\,2130\,\mathrm{V}$) can be seen. Especially for $V_{\mathrm{DT6,\Delta}} = 435\,\mathrm{V}$ and $V_{\mathrm{DT6,\Delta}} = 445\,\mathrm{V}$ they are visible. In the spectra of $V_{\mathrm{DT6,\Delta}} = 445\,\mathrm{V}$ and $V_{\mathrm{DT6,\Delta}} = 450\,\mathrm{V}$, an early decrease in count rate, starting in at about $V_{\mathrm{RFA}} = 2075\,\mathrm{V}$, can also be observed, which clearly deviates from the other spectra. Further, for $V_{\mathrm{DT6,Delta}} = 450\,\mathrm{V}$,the number of ions suddenly increases again at $V_{\mathrm{RFA}} = 2200\,\mathrm{V}$, before it reduces again until reaching the background.

From the obtained values in Table 6.3, no correlation of the energy spread with the release voltage and trap depth is visible and all measured values agree in their uncertainty margin. Expected, however, was a decrease in energy spread due to a shallower trap and reduced release voltage.

Summary

In the measurements some of the results, local deviations from the anticipated shape of the spectrum occurred. These deviations are not assumed to be of physical origin, but rather, to stem from fluctuations in the extraction count rate of the EBIT. Even though the RFA measurement precision was limited due to the problems, a value of $\Delta E_{\mathrm{beam}} = 19.7(21)\,\mathrm{eV/q}$ could be measured for a beam energy of $E_{\mathrm{beam}} = 2180.4(17)\,\mathrm{eV/q}$. This is in agreement with prior expectations that the energy spread will be below $50\,\mathrm{eV/q}$ [33]. An investigation of a varying trap depth and release voltage showed no correlation to the energy spread. However, the trap depth was reduced by more than a factor of two while the release voltage was only reduced by less than 9 % (note that the given DT

potentials need to be corrected for the electron beams' space charge). This shows that the release energy is the dominating factor for the energy spread.
Since the measurements were limited by fluctuations, the number of ions could be normalized by simultaneous measurement of the EBIT extraction rate on another MCP. This could be done by monitoring the number of ions on MCP0, situated in front of MPET. By deflecting every several hundred extraction from the EBIT into direction of MPET using the x-steerer, temporal fluctuations on the scale of minutes could be detected and accounted for. Another option would be the use of deflected ions from the BNG. If settings of the deflection plates in the Allison detectors can be found which allow the beam to pass onto its MCP, the ion extraction rate could be monitored for every single extraction from the EBIT.

6.2.2 Measurements of transversal emittance with the Allison detector

The measurements with the Allison detector were performed with sole bias of the upper deflection plate, whereas the lower plate was grounded. In all measurements, the deflection voltage was varied for each step of the stepper motor. In this manner, an accumulation of positioning uncertainties was prevented. This is important since the position of the Allison detector is not measured but calculated via the amount of turns of the stepper motor. For minimal uncertainties of the detectors position, the stepper motor position was calibrated before each measurement. The voltage was monitored during the entire measurement.
The measurements were typically performed in a range of -10 to 10 V in deflection voltage and 5 to 20 mm in position of the stepper motor (EPICS set value). Using a resolution of 20 to 25 steps in position and voltage, as well as 1000 EBIT extractions per position, the duration of one Allison measurements was approximately five hours. The minimal required resolution was found to be 20 steps in position and deflection voltage. Due to the needed measurement duration for one scan as well as time constrains, the number of measurements with the Allison detector was limited compared to that of the RFA. Further, because of the technical problems described in Section 6.1.3, transversal emittance measurements commonly failed and needed to be repeated.
Like the energy spread, the transversal emittance was investigated for correlations with the release voltage and the trap depth (see Table 6.4). Again, throughout the measurements, the extraction energy was kept constant (see Section 6.2.1). In the measurement results a decrease in emittance was expected for shallower trap and decreased release voltage because lower values are assumed to decrease the energy spread of the extracted

Table 6.4: Emittance values for extracted beam from the EBIT for varied extraction voltages and trap depths as well as beam energies.

E_{beam} (eV/q)	$V_{\mathrm{DT6,low}}$ (V)	$V_{\mathrm{DT6},\Delta}$ (V)	ϵ_{rms} (π mm mrad)
2080	1960	315	6.97(271)
2080	1950	325	5.79(178)
2080	1950	325	4.76(44)
2080	1940	335	6.14(59)
2180	1955	410	8.47(148)
2180	1930	435	8.65(113)

particles.

All measurement results (see Figures 6.6, 6.7 are provided as examples) showed, in first approximation, an elliptical shaped phase space area, as it would be expected for a thermal distributed beam. In some measurements, the count rate was locally increased in the vicinity of the elliptical shape. These ions, assumed to be from neighboring charge states, are not completely deflected due to the finite rise time of the deflection voltage on the BNG.

Two different sets of measurements were performed at $E_{\mathrm{beam}} = 2080\,\mathrm{eV/q}$ and $E_{\mathrm{beam}} = 2180\,\mathrm{eV/q}$. At a beam energy of $E_{\mathrm{beam}} = 2080\,\mathrm{eV/q}$, three different values for the release voltage and trap depth were measured, as can be seen in Table 6.4. The setting of $V_{\mathrm{DT6},\Delta} = 325$ was measured a second time in a repetition of the measurement. All values agree within their measurement uncertainty, but a decrease in emittance for a release voltage of V_{325} can be seen. Calculating the average value the two measurements at $E_{\mathrm{DT6},\Delta} = 325\,\mathrm{V}$, the emittance follows to ϵ_{rms} =5.27(73) $\pi\,\mathrm{mm\,mrad}$, where the uncertainty is given by the standard deviation.

In addition, the emittance was measured at a beam energy of $E_{\mathrm{beam}} = 2180\,\mathrm{eV/q}$, which is expected to have a reducing effect onto the emittance. However, at the same time the release voltage was about 100 V higher than for the previous set of measurements. Again, the trap depth was reduced while decreasing the release voltage, but only two measurements were possible due to time constraints and problems with the used electronics. The results (see Table 6.4 as well as Figure 6.7) show a tendency towards an increased transversal emittance but agree within their uncertainties.

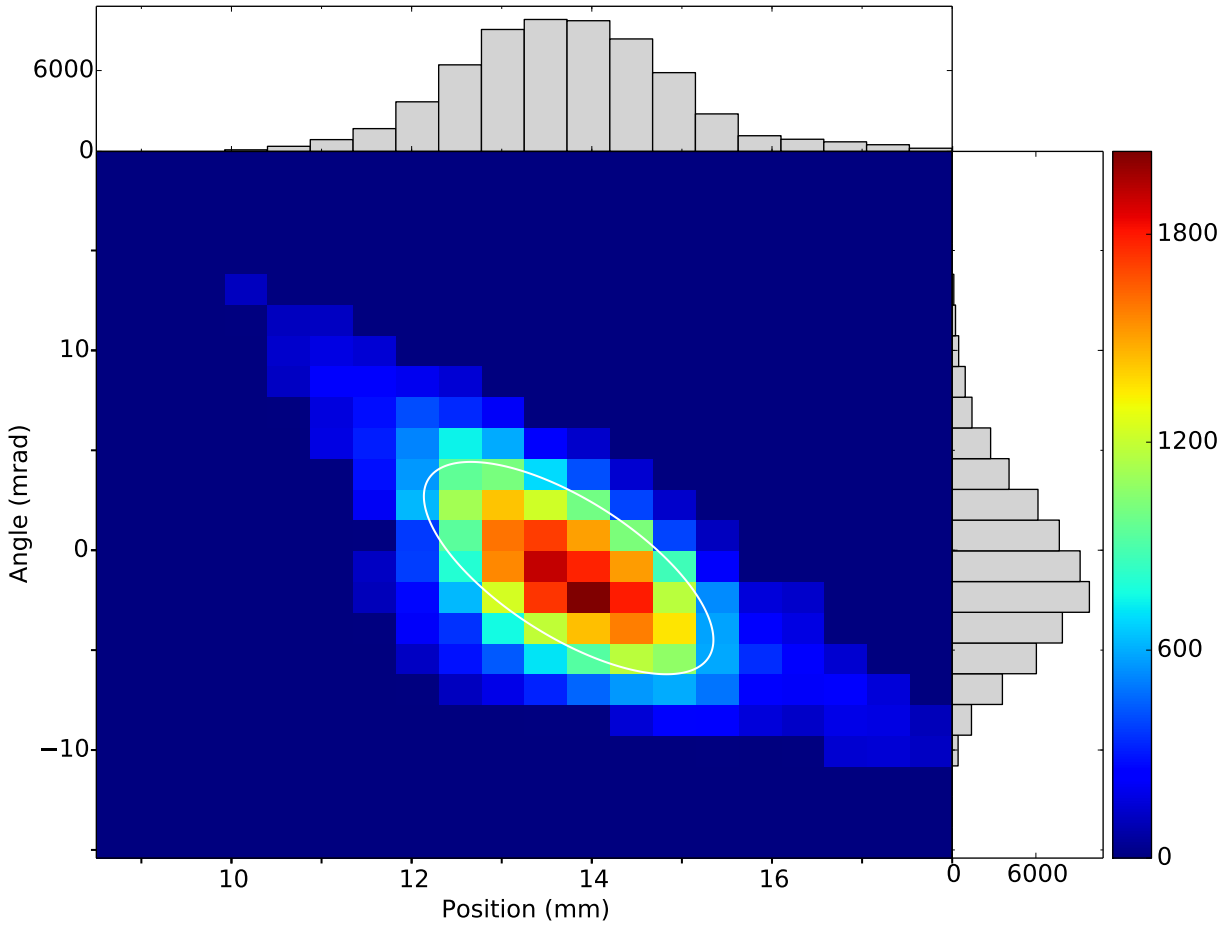

Figure 6.6: Result of an Allison emittance measurement of extracted beam from the EBIT by switching DT6. In white, the one RMS ellipse of $\epsilon_{\mathrm{rms}} = 5.79(178)\,\pi\,\mathrm{mm\,mrad}$. $E_{\mathrm{beam}} = 2080\,\mathrm{eV/q}$, $V_{\mathrm{DT6,low}} = 1955\,\mathrm{V}$, $V_{\mathrm{DT6},\Delta} = 325\,\mathrm{V}$

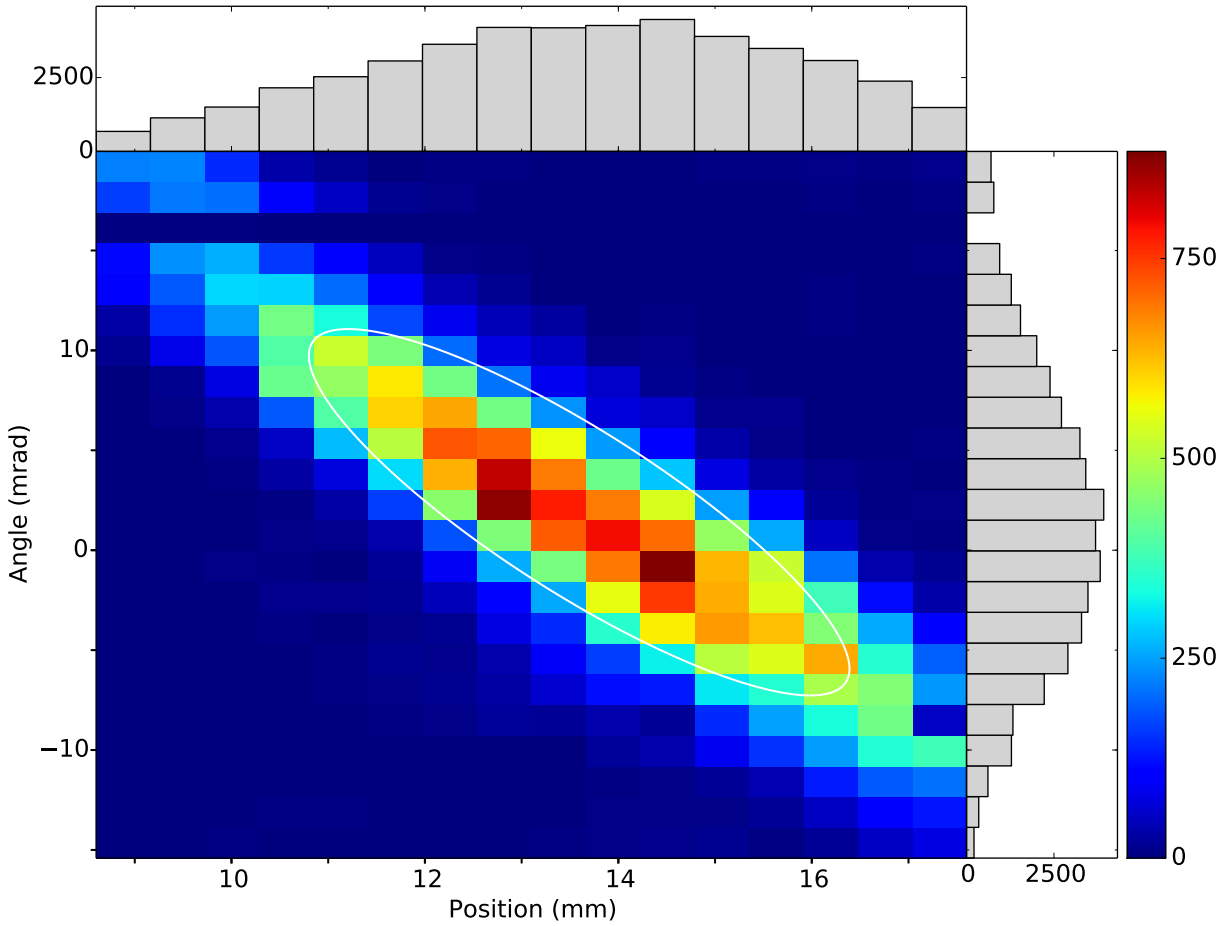

Figure 6.7: Result of an Allison emittance measurement of extracted beam from the EBIT by switching DT6. In white, the one RMS ellipse of $\epsilon_{\mathrm{rms}} = 8.47(148)\,\pi\,\mathrm{mm\,mrad}$. $E_{\mathrm{beam}} = 2180\,\mathrm{eV/q}$, $V_{\mathrm{DT6,low}} = 1955\,\mathrm{V}$, $V_{\mathrm{DT6},\Delta} = 410\,\mathrm{V}$

Summary

The measurements with the Allison detector delivered a first bench mark result for the transversal emittance of extracted ions from the EBIT of $\epsilon_{\mathrm{rms}} = 5.27(73)\,\pi\,\mathrm{mm\,mrad}$ at a beam energy of $E_{\mathrm{beam}} = 2080\,\mathrm{eV/q}$. All measurement results showed an in first approximation elliptical shape of the beam, indicating a thermal distribution as well as no deformations due to non-linear forces of the ions optics. Even though the measurement method relies on a stable extraction rate from the EBIT, no significant influences on the results could be found, compared to the RFA. Further, limitations in the ion deflection capabilities of the BNG were visible, caused by the finite rise time of its deflection voltage. This did not prevent measurements even though the installation of a Wien-Filter would be beneficial which separates particles depending on their velocity. A Wien-Filter would also separate contamination which can not be separated by TOF as, for example, protons which are extracted from the EBIT in small numbers at all times. For in installation in the EBIT beamline, this Wien-Filter would need to be switchable.
Two sets of measurements were done at different beam energies and the release voltage, as well as the trap depth were varied. The emittance was expected to reduce for higher beam energy as well as for lower release voltage and trap depth. Against the expectations, no correlation of the emittance with the varied parameter was found within the single measurements sets. Nevertheless, at a beam energy of 2080 V, a minimum in transversal emittance was found.
Comparing between the two measurement sets, a correlation of the transversal emittance with the release voltage can be seen.

6.3 Summary and Conclusion

During the experimental part of the theses, two detectors were successfully commissioned. The secondary electron impact onto the count rate was investigated but no significant influence was found. This indicates that secondary electrons are negligible for the measurements. Another reason for the non-significance could be count rate fluctuations from the EBIT which were found. These could be traced back to either RFQ or the TIS, but no apparent reasons for fluctuations were found. The fluctuations could potentially result from problems of the RFQ electronics for generation of the radio-frequency. A different explanation is a loss of ions due to temporal fluctuations of the beam energy. This could be caused during the reduction of the beam energy after the RFQ. It is important for TITAN to further investigate this potential ion loss in the

system.
The extraction rate fluctuations further affected the precision of the RFA measurements. Since the measurement method of the RFA relies on a stable ion rate, the precision of the energy spread measurements was reduced. However, where no count rate fluctuations were obvious, the fits indicated a good approximation of the energy spread with the Gaussian fit-function. Further, no correlation of the energy spread of the extracted ions with the extraction voltage and the trap depth could be found. But because the trap depth was more than halved, whereas the release voltage was only lowered by less than 9 %, the results indicate the release voltage as the main cause for the energy spread. To prove this assumption, the energy spread should be measured for a more drastic change in release voltage. In order to do measurements with a reduced amount of ions from the source, the size of the aperture holes could be doubled. This would provide the opportunity to reduce the number of ions needed from the EBIT and approach conditions closer to the conditions for ion extraction into MPET without affecting the precision.
Using the Allison detector, an RMS emittance of $\epsilon_{\mathrm{rms}} = 5.27(73)\,\pi\,\mathrm{mm\,mrad}$ at a beam energy of $E_{\mathrm{beam}} = 2080\,\mathrm{eV/q}$ was measured. This is well above the planned value [51]. Nevertheless, it is a significant reduction compared to a preliminary value of $\epsilon_{\mathrm{rms}} = 15.7\,\pi\,\mathrm{mm\,mrad}$ [22]. Further, a correlation of the emittance with the release voltage was found. To investigate this, more measurements need to be done at same beam energy and with a more drastic variation of the release voltage. In this work, the number of measurements was limited by the long duration of approximately five hours per measurement as well as problems with the used MCS and DAC which resulted in regular restarts and failures of measurements. To overcome the technical problems with the MCS, the device could be cooled since it is assumed to overheat. To avoid problems with the DAC, it could be replaced with a newer type of DAC, that can be controlled directly without the use of MIDAS.
The measured values of the energy spread as well as the transverse emittance are much higher than the requirements of MPET ($\Delta E_{\mathrm{beam}} \leq 1\,\mathrm{eV/q}$ and smallest possible emittance). In order to improver the beam properties, HCIs are extracted from the EBIT by lowering DT5 in the future (see Section 3.3.2 in Chapter 3). It needs to be investigated, if the beam properties can be improved using this extraction method. For future measurements like this, it will be important to also investigate the time spread of the ion bunch as well as the efficiency during the charge breeding and extraction process. Overall efficiencies of more than ten percent are important at the TITAN setup.
Despite the insufficiency of the here measured beam properties for MPET, they could be sufficient for the use in the future CANadian Rare-isotope facility with Electron-Beam

ion source (CANREB) facility for acceleration and purification of rare isotope beams from TRIUMF's Advanced Rare IsotopE Laboratory (ARIEL) [66] accelerator. The CANREB project will make use of an EBIT of similar construction.

7 Conclusion and outlook

In this work, the beam properties of HCIs extracted from an Electron Beam Ion Trap (EBIT) charge breeder were investigated. Measuring beam properties is an important step for TITAN towards higher precision (ppb) in Penning trap mass spectrometry using HCIs.

In order to measure the beam properties, an Allison type emittance meter as well as a Retarding Field Analyzer (RFA), were designed and built. Whereas the first device was used to investigate the transversal beam emittance, the latter was used to measure the longitudinal energy spread of the beam. During the detector design, systematic errors of the RFA could be evaluated and minimized by means of simulations.

Throughout the measurements, using HCI extracted from the TITAN EBIT, a fluctuation in count rate was detected. The count rate fluctuations could be traced back to either the used ion source or Radio-Frequency Quadrupole Trap. However, a stable count rate is a requirement for precise measurements with the Allison and RFA detectors and the fluctuations limited the precision achievable.

In a first step, the transversal emittance was measured to be ϵ_{rms} =5.27(73) π mm mrad at a beam energy of E_{beam} = 2080 eV/q, using the Allison detector. This number represents the lower bound of all measurements done and is well above the predicted value of $\epsilon_{\mathrm{rms}} = 1\,\pi$ mm mrad [51]. The longitudinal energy spread was measured to be 19.7(21) eV/q, which is below the theoretical predicted maximum of 50 eV/q [33].

Furthermore, the influence of the depth of the trapping potential and the potential increase, used for extraction of the HCI, onto the beam properties were investigated. During the measurements, no significant correlation of the trap depth of the EBIT with the beam properties of the extracted beam was found. However, the measurements indicate that the ions' longitudinal energy spread as well as the transversal emittance is dominated by the used extraction method of raising the potential of the trapping drift tube.

Throughout the measurements, the double apertures of the RFA provided a beneficial tool to align the extracted beam with the beamline axis after extraction from the EBIT. This alignment vital for optimal transportation of the beam to the Penning trap and its injection into the Penning trap.

For future beam property measurements at TITAN, an investigation of the count rate fluctuations is essential, since they suggest potential ion losses in the RFQ. In order to achieve higher precision in the measurement of beam properties, despite count rate fluctuations, the RFA and Allison measurements could be normalized by simultaneous measurement of the extraction rate of beam from the EBIT. To do so, the extracted pulses could be guided onto another MCP in the TITAN beamline at a regular interval during the measurements.

Additionally, more measurements of extracted beam from the EBIT are necessary to confirm the results. To minimize the energy spread and transverse emittance as far as possible, beam properties of extracted ions using different charge breeding and extraction methods should be measured (see Seection 6.3 in Chapter 6). Of particular interest are different extraction mechanisms, since the beam appears to gain most of its energy spread during the extraction process. The ions could, for example, be extracted by lowering the barrier of the trapping potential on the extraction side (Section 3.3.2). Performing these measurements, it will be important to simultaneously investigate the efficiency of the charge breeding and extraction form the EBIT, since an overall efficiency of more than ten percent is desirable for mass measurements at TITAN.

In the future, measurements of beam properties at different positions in the TITAN beamline using the RFA and Allison detectors will be carried out. In doing so, the beam properties of HCI after cooling in the Cooler Penning Trap will be investigated and with them CPET's ability to cool HCI.

Further improvements of the detector system in the future could include the improvement of the used electronic setup and an increase of the RFA aperture diameter. Because of problems in the electronic setup a lot of measurements failed and needed to be repeated. Here, for example, a new Digital to Analog Converter (DAC) could be installed. Further, the measurement precision using the RFA was not limited by the aperture size and it could therefor be increased. This would allow to work with less beam from the EBIT.

Acknowledgments

This work would not have been possible without the help of many people. Especially I want to thank my supervisor Renee Klawitter who provided me with a lot of support and advice during my time as a master student at TRIUMF. Also I am grateful for the great technical design of the detectors done by of Mel Good. His work made a trouble free assembly and installation of the detectors possible. I want to thank all people in the TITAN group for being so welcoming and the great time I had working with them. Furthermore, I want to thank Prof. Jens Dilling and Priv.-Doz. Dr. José Crespo for all their support as well as giving me the opportunity to carry out this work at TRIUMF. Also a special thanks to all the people who proof read my thesis. And of course, I want to thank my family who made all this possible and provided lots of support throughout my whole studies.

Acronyms

ARIEL Advanced Rare IsotopE Laboratory.

BNG Bradbury Nielsen gate.

CANREB CANadian Rare-isotope facility with Electron-Beam ion source.

CKM Cabibbo–Kobayashi–Maskawa.

CPET Cooler Penning Trap.

CVC Conserved Vector–Current.

DAC Digital to Analog Converter.

DT Drift Tube.

EBIT Electron Beam Ion Trap.

FT-ICR Fourier Transform Ion Cyclotron Resonance.

FWHM Full Width at Half Maximum.

HCI Highly Charged Ion.

ISAC Isotope Separator and Accelerator.

MCP Multi Channel Plate.

MCS Multi Channel Scaler.

MPET Measurement Penning Trap.

MPIK Max Plank Institut für Kernphysik.

PA Potential Array.

PPG Pule-Pattern-Generator.

RFA Retarding Field Analyzer.

RFQ Radio-Frequency Quadrupole Trap.

RMS Root Mean Square.

RR Radioactive Recombination.

SCI Singly Charged Ion.

TIS Titan Ion Source.

TITAN TRIUMF's Ion Trap for Atomic and Nuclear Science.

TOF Time-of-Flight.

TOF-ICR Time-of-Flight Ion Cyclotron Resonance.

TRIUMF Canada's National Laboratory for Particle and Nuclear Physics.

Bibliography

[1] K. Blaum, Yu. N. Novikov, and G. Werth. Penning traps as a versatile tool for precise experiments in fundamental physics. *Contemporary Physics*, 51(2):149–175, 2010. ISSN 0010-7514. doi:10.1080/00107510903387652.

[2] Klaus Blaum. High-accuracy mass spectrometry with stored ions. *Physics Reports*, 425(1):1–78, 2006. ISSN 03701573. doi:10.1016/j.physrep.2005.10.011.

[3] Hans Dehmelt. Experiments with an isolated subatomic particle at rest. *Reviews of Modern Physics*, 62(3):525–530, 1990. ISSN 0034-6861. doi:10.1103/RevModPhys.62.525.

[4] S Sturm, F Köhler, J Zatorski, A Wagner, Z Harman, G Werth, W Quint, C H Keitel, and K Blaum. High-precision measurement of the atomic mass of the electron. *Nature*, 506(7489):467–70, 2014. ISSN 1476-4687. doi:10.1038/nature13026.

[5] D. Lunney, J. M. Pearson, and C. Thibault. Recent trends in the determination of nuclear masses. *Reviews of Modern Physics*, 75(3):1021–1082, 2003. ISSN 0034-6861. doi:10.1103/RevModPhys.75.1021.

[6] Marianne Dufour and Andrés P. Zuker. Realistic collective nuclear Hamiltonian. *Physical Review C*, 54(4):1641–1660, 1996. ISSN 0556-2813. doi:10.1103/PhysRevC.54.1641.

[7] J. Jänecke and P.J. Masson. Mass predictions from the Garvey-Kelson mass relations. *Atomic Data and Nuclear Data Tables*, 39(2):265–271, 1988. ISSN 0092640X. doi:10.1016/0092-640X(88)90028-9.

[8] Takahiro Tachibana, Masahiro Uno, Masami Yamada, and So Yamada. Empirical mass formula with proton-neutron interaction. *Atomic Data and Nuclear Data Tables*, 39(2):251–258, 1988. ISSN 0092640X. doi:10.1016/0092-640X(88)90026-5.

[9] M Smith, M Brodeur, T Brunner, S Ettenauer, A Lapierre, R Ringle, V L Ryjkov, F Ames, P Bricault, G W F Drake, P Delheij, D Lunney, F Sarazin,

and J Dilling. First Penning-trap mass measurement of the exotic halo nucleus 11Li. *Physical review letters*, 101(20):202501, 2008. ISSN 0031-9007. doi:10.1103/PhysRevLett.101.202501.

[10] M.J. Smith. A Square-Wave-Driven Radiofrequency Quadrupole Cooler and Buncher for TITAN, 2005.

[11] G. Audi, A.H. Wapstra, and C. Thibault. The Ame2003 atomic mass evaluation. *Nuclear Physics A*, 729(1):337–676, 2003. ISSN 03759474. doi:10.1016/j.nuclphysa.2003.11.003.

[12] George Wallerstein, Icko Iben, Peter Parker, Ann Merchant Boesgaard, Gerald M. Hale, Arthur E. Champagne, Charles A. Barnes, Franz Käppeler, Verne V. Smith, Robert D. Hoffman, Frank X. Timmes, Chris Sneden, Richard N. Boyd, Bradley S. Meyer, and David L. Lambert. Synthesis of the elements in stars: forty years of progress. *Reviews of Modern Physics*, 69(4):995–1084, 1997. ISSN 0034-6861. doi:10.1103/RevModPhys.69.995.

[13] H. Schatz, A. Aprahamian, J. Görres, M. Wiescher, T. Rauscher, J.F. Rembges, F.-K. Thielemann, B. Pfeiffer, P. Möller, K.-L. Kratz, H. Herndl, B.A. Brown, and H. Rebel. rp-process nucleosynthesis at extreme temperature and density conditions. *Physics Reports*, 294(4):167–263, 1998. ISSN 03701573. doi:10.1016/S0370-1573(97)00048-3.

[14] Nicola Cabibbo. Unitary Symmetry and Leptonic Decays. *Physical Review Letters*, 10(12):531–533, 1963. ISSN 0031-9007. doi:10.1103/PhysRevLett.10.531.

[15] Makoto Kobayashi and Toshihide Maskawa. C P -Violation in the Renormalizable Theory of Weak Interaction. *Progress of Theoretical Physics*, 49(2):652–657, 1973. ISSN 0033-068X. doi:10.1143/PTP.49.652.

[16] E. (Univ. of Chicago) Blucher and W.J. (BNL) Marciano. Vud, Vus, THE CABIBBO ANGLE, AND CKM UNITARITY. *Particle Data Group*, 090001 (September 2013):1–10, 2014.

[17] K.S. Krane. Introductory nuclear physics. 1987.

[18] Klaus Blaum, Jens Dilling, and Wilfried Nörtershäuser. Precision Atomic Physics Techniques for Nuclear Physics with Radioactive Beams. page 63, 2012. ISSN 0031-8949. doi:10.1088/0031-8949/2013/T152/014017.

[19] Michael Wayne Froese. *The TITAN Electron Beam Ion Trap: Assembly, Characterization, and First Tests.* PhD thesis, University of Manitoba, 2006.

[20] G. Sikler, J. R. Crespo López-Urrutia, J. Dilling, S. Epp, C. J. Osborne, and J. Ullrich. A high-current EBIT for charge-breeding of radionuclides for the TITAN spectrometer. *European Physical Journal A*, 25:63–64, 2005. ISSN 14346001. doi:10.1140/epjad/i2005-06-072-6.

[21] A. Lapierre, M. Brodeur, T. Brunner, S. Ettenauer, A.T. Gallant, V. Simon, M. Good, M.W. Froese, J.R. Crespo López-Urrutia, P. Delheij, S. Epp, R. Ringle, S. Schwarz, J. Ullrich, and J. Dilling. The TITAN EBIT charge breeder for mass measurements on highly charged short-lived isotopes—First online operation. *Nuclear Instruments and Methods in Physics Research Section A: Accelerators, Spectrometers, Detectors and Associated Equipment*, 624(1):54–64, 2010. ISSN 01689002. doi:10.1016/j.nima.2010.09.030.

[22] a T Gallant, M Brodeur, T Brunner, S Ettenauer, M Good, A Lapierre, R Ringle, V V Simon, P Delheij, and J Dilling. TITAN-EBIT — charge breeding of radioactive isotopes for high precision mass measurements. *Journal of Instrumentation*, 5(08): C08009–C08009, 2010. ISSN 1748-0221. doi:10.1088/1748-0221/5/08/C08009.

[23] A. T. Gallant, M. Brodeur, T. Brunner, U. Chowdhury, S. Ettenauer, V. V. Simon, E. Mané, M. C. Simon, C. Andreoiu, P. Delheij, G. Gwinner, M. R. Pearson, R. Ringle, and J. Dilling. Highly charged ions in Penning traps: A new tool for resolving low-lying isomeric states. *Physical Review C*, 85(4):044311, 2012. ISSN 0556-2813. doi:10.1103/PhysRevC.85.044311.

[24] S. Ettenauer, M. C. Simon, T. D. Macdonald, and J. Dilling. Advances in precision, resolution, and separation techniques with radioactive, highly charged ions for Penning trap mass measurements. *International Journal of Mass Spectrometry*, 349-350:74–80, 2013. ISSN 13873806. doi:10.1016/j.ijms.2013.04.021.

[25] G. Gräff, H. Kalinowsky, and J. Traut. A direct determination of the proton electron mass ratio. *Zeitschrift für Physik A: Atoms and Nuclei*, 297(1):35–39, 1980. ISSN 0340-2193. doi:10.1007/BF01414243.

[26] Aaron T Gallant. *Penning trap mass measurements to test three-body forces in atomic nuclei by.* PhD thesis, The University of British Columbia, 2015.

[27] S. Ettenauer, M. C. Simon, A. T. Gallant, T. Brunner, U. Chowdhury, V. V. Simon, M. Brodeur, A. Chaudhuri, E. Mané, C. Andreoiu, G. Audi, J. R. Crespo López-Urrutia, P. Delheij, G. Gwinner, A. Lapierre, D. Lunney, M. R. Pearson, R. Ringle, J. Ullrich, and J. Dilling. First Use of High Charge States for Mass Measurements of Short-Lived Nuclides in a Penning Trap. *Physical Review Letters*, 107(27):272501, 2011. ISSN 0031-9007. doi:10.1103/PhysRevLett.107.272501.

[28] Christian Champagne. Characterizing and Optimizing the TITAN Facility from Energy Spread Determinations with a Retarding Energy Field Analyzer, 2009.

[29] Jean Buon. Beam phase space and emittance. Technical report, Laboratoire de l'Accélérateur Linéaire, Orsay, France, 1990.

[30] G. Bollen. Mass measurements of short-lived nuclides with ion traps. *Nuclear Physics A*, 693(1-2):3–18, 2001. ISSN 03759474. doi:10.1016/S0375-9474(01)00353-0.

[31] M Block, D Ackermann, and D Beck. The ion-trap facility SHIPTRAP. *Epj a*, 50: 49–50, 2005. doi:10.1140/epjad/i2005-06-013-5.

[32] R. Ringle, G. Bollen, A. Prinke, J. Savory, P. Schury, S. Schwarz, and T. Sun. The LEBIT 9.4 T Penning trap mass spectrometer. *Nuclear Instruments and Methods in Physics Research, Section A: Accelerators, Spectrometers, Detectors and Associated Equipment*, 604(3):536–547, 2009. ISSN 01689002. doi:10.1016/j.nima.2009.03.207.

[33] V L Ryjkov, L Blomeley, M B, P Grot, M Sm, P B, F Bu, and J Crawford. TITAN project status report and a proposal for a new cooling method of highly charged ions. *EPJ A direct*, 56, 2005. doi:10.1140/epjad/i2005-06-122-1.

[34] F. Currell and G. Fussmann. Physics of electron beam ion traps and sources. *IEEE Transactions on Plasma Science*, 33(6):1763– 1777, 2005. ISSN 0093-3813. doi:10.1109/TPS.2005.860072.

[35] F.G. Major, V.N. Gherorghe, and G. Werth. *Charged Particle Traps*. Springer-Verlag Berlin Heidelberg, 2005. ISBN 978-3-540-22043-5.

[36] D. F. a. Winters, M. Vogel, D. M. Segal, and R. C. Thompson. Electronic detection of charged particle effects in a Penning trap. 3131:16, 2006. ISSN 0953-4075. doi:10.1088/0953-4075/39/14/019.

[37] M B Comisarow and a G Marshall. The early development of Fourier transform ion cyclotron resonance (FT-ICR) spectroscopy. *Journal of mass spectrometry : JMS*, 31(April):581–585, 1996. ISSN 1076-5174. doi:10.1002/(SICI)1096-9888(199606)31:6<581::AID-JMS369>3.0.CO;2-1.

[38] U. Fano and Joseph Macek. Impact Excitation and Polarization of the Emitted Light. *Reviews of Modern Physics*, 45(4):553–573, 1973. ISSN 0034-6861. doi:10.1103/RevModPhys.45.553.

[39] Sascha W. Epp. *No Title*. PhD thesis, Ruprecht-Karls-University Heidelberg, 2007.

[40] D. W. Savin, P. Beiersdorfer, S. M. Kahn, B. R. Beck, G. V. Brown, M. F. Gu, D. a. Liedahl, and J. H. Scofield. Simulating a Maxwellian plasma using an electron beam ion trap. *Review of Scientific Instruments*, 71(9):3362, 2000. ISSN 00346748. doi:10.1063/1.1287045.

[41] F J Currell, H Kuramoto, S Ohtani, C Scullion, E J Sokell, and H Watanabe. Measurements of Temperature Dynamics of Ions T rapped Inside an Electron Beam Ion T rap and Evidence for Ionisation Heating. 147:147–149, 2001.

[42] V. V. Simon, P. Delheij, J. Dilling, Z. Ke, W. Shi, and G. Gwinner. Cooling of short-lived, radioactive, highly charged ions with the TITAN cooler Penning trap. *Hyperfine Interactions*, 199(1-3):151–159, 2011. ISSN 0304-3843. doi:10.1007/s10751-011-0309-5.

[43] G C Ball, L Buchmann, B Davids, R Kanungo, C Ruiz, and C E Svensson. Physics with reaccelerated radioactive beams at TRIUMF-ISAC. *Journal of Physics G: Nuclear and Particle Physics*, 38:024003, 2011. ISSN 0954-3899. doi:10.1088/0954-3899/38/2/024003.

[44] M. Dombsky, D. Bishop, P. Bricault, D. Dale, A. Hurst, K. Jayamanna, R. Keitel, M. Olivo, P. Schmor, and G. Stanford. Commissioning and initial operation of a radioactive beam ion source at ISAC. *Review of Scientific Instruments*, 71(2000): 978, 2000. ISSN 00346748. doi:10.1063/1.1150364.

[45] P.G. Bricault, M. Dombsky, P.W. Schmor, and G. Stanford. Radioactive ion beams facility at TRIUMF. *Nuclear Instruments and Methods in Physics Research Section B: Beam Interactions with Materials and Atoms*, 126(1-4):231–235, 1997. ISSN 0168583X. doi:10.1016/S0168-583X(96)01037-3.

[46] P. Bricault, M. Dombsky, A. Dowling, and M. Lane. High power target developments at ISAC. *Nuclear Instruments and Methods in Physics Research, Section B: Beam Interactions with Materials and Atoms*, 204:319–324, 2003. ISSN 0168583X. doi:10.1016/S0168-583X(03)00504-4.

[47] TRIUMF. TRIUMF Yield database, 2015.

[48] T. Brunner, M.J. Smith, M. Brodeur, S. Ettenauer, A.T. Gallant, V.V. Simon, A. Chaudhuri, A. Lapierre, E. Mané, R. Ringle, M.C. Simon, J.A. Vaz, P. Delheij, M. Good, M.R. Pearson, and J. Dilling. TITAN's digital RFQ ion beam cooler and buncher, operation and performance. *Nuclear Instruments and Methods in Physics Research Section A: Accelerators, Spectrometers, Detectors and Associated Equipment*, 676:32–43, 2012. ISSN 01689002. doi:10.1016/j.nima.2012.02.004.

[49] J. Dilling, R. Baartman, P. Bricault, M. Brodeur, L. Blomeley, F. Buchinger, J. Crawford, J.R. Crespo López-Urrutia, P. Delheij, M. Froese, G.P. Gwinner, Z. Ke, J.K.P. Lee, R.B. Moore, V. Ryjkov, G. Sikler, M. Smith, J. Ullrich, and J. Vaz. Mass measurements on highly charged radioactive ions, a new approach to high precision with TITAN. *International Journal of Mass Spectrometry*, 251(2-3): 198–203, 2006. ISSN 13873806. doi:10.1016/j.ijms.2006.01.044.

[50] P Mandal, G Sikler, and M Mukherjee. Simulation study and analysis of a compact einzel lens-deflector for low energy ion beam. *Journal of Instrumentation*, 6(02): P02004–P02004, 2011. ISSN 1748-0221. doi:10.1088/1748-0221/6/02/P02004.

[51] J. Dilling, P. Bricault, M. Smith, and H.-J. Kluge. The proposed TITAN facility at ISAC for very precise mass measurements on highly charged short-lived isotopes. *Nuclear Instruments and Methods in Physics Research Section B: Beam Interactions with Materials and Atoms*, 204:492–496, 2003. ISSN 0168583X. doi:10.1016/S0168-583X(02)02118-3.

[52] J. Arol Simpson. Design of retarding field energy analyzers. *Review of Scientific Instruments*, 32(1961):1283–1293, 1961. ISSN 00346748. doi:10.1063/1.1717235.

[53] Joseph Ladislas Wiza. Microchannel plate detectors. *Nuclear Instruments and Methods*, 162(1-3):587–601, 1979. ISSN 0029554X. doi:10.1016/0029-554X(79)90734-1.

[54] Yoshiyuki Sakai and Ituso Katsumata. An Energy Resolution Formula of a Three

Plane Grids Retarding Field Energy Analyzer. *Japanese Journal of Applied Physics*, 24:337–341, 1985. ISSN 0021-4922. doi:10.1143/JJAP.24.337.

[55] Irving Langmuir. The Effect of Space Charge and Residual Gases on Thermionic Currents in High Vacuum. *Physical Review*, 2(6):450–486, 1913. ISSN 0031-899X. doi:10.1103/PhysRev.2.450.

[56] J David Manura and David A Dahl. SIMION 8.1, 2011.

[57] J. C. Butcher. The numerical analysis of ordinary differential equations: Runge-Kutta and general linear methods. 1987.

[58] Frederic P. Miller, Agnes F. Vandome, and John McBrewster. *Lua (programming language)*. Alpha Press, 2009. ISBN 6130256981, 9786130256982.

[59] Charles Severance. Python for Informatics Exploring Information. *Computer*, pages 1–236, 2010.

[60] Paul W. Allison, Joseph D. Sherman, and David B. Holtkamp. An Emittance Scanner for Intense Low-Energy Ion Beams. *IEEE Transactions on Nuclear Science*, 30(4):2204–2206, 1983. ISSN 0018-9499. doi:10.1109/TNS.1983.4332762.

[61] H. Wollnik and H. Ewald. The influence of magnetic and electric fringing fields on the trajectories of charged particles. *Nuclear Instruments and Methods*, 36:93–104, 1965. ISSN 0029554X. doi:10.1016/0029-554X(65)90410-6.

[62] Norris E. Bradbury and Russell a. Nielsen. Absolute values of the electron mobility in hydrogen. *Physical Review*, 49(1929):388–393, 1936. ISSN 0031899X. doi:10.1103/PhysRev.49.388.

[63] T. Brunner, a. R. Mueller, K. O'Sullivan, M. C. Simon, M. Kossick, S. Ettenauer, a. T. Gallant, E. Mané, D. Bishop, M. Good, G. Gratta, and J. Dilling. A large Bradbury Nielsen ion gate with flexible wire spacing based on photo-etched stainless steel grids and its characterization applying symmetric and asymmetric potentials. *International Journal of Mass Spectrometry*, 309:97–103, 2012. ISSN 13873806. doi:10.1016/j.ijms.2011.09.004.

[64] Oh Kyu Yoon, Ignacio A Zuleta, Joel R Kimmel, Matthew D Robbins, and Richard N Zare. Duty cycle and modulation efficiency of two-channel

Hadamard transform time-of-flight mass spectrometry. *Journal of the American Society for Mass Spectrometry*, 16(11):1888–901, 2005. ISSN 1044-0305. doi:10.1016/j.jasms.2005.07.025.

[65] P. Emma and R. Brinkmann. Emittance dilution through coherent energy spread generation in bending systems. In *Proceedings of the 1997 Particle Accelerator Conference (Cat. No.97CH36167)*, volume 2, pages 1679–1681. IEEE, 1997. ISBN 0-7803-4376-X. doi:10.1109/PAC.1997.750799.

[66] Jens Dilling, Reiner Krücken, and Lia Merminga, editors. *ISAC and ARIEL: The TRIUMF Radioactive Beam Facilities and the Scientific Program*. Springer Netherlands, Dordrecht, 2014. ISBN 978-94-007-7962-4. doi:10.1007/978-94-007-7963-1.

Appendices

A Drawings of the Allison detector

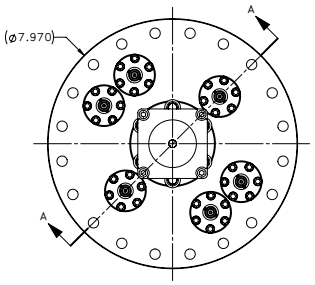

Top View

Refer to Note #2 Concerning the BOM Quantities Column.

ITEM	REF No.	DESCRIPTION	MATERIAL	QTY.
1	IEX1863	AD2-W Flange Details	AISI 304L	1
2	IEX1864	AD2-W Drift Tube Section Ass'y	Varies	1
3	IEX1878	AD2-W Cond. Bar Assembly	Varies	6
100	G-133	1 1/3 CF Non-Plated, Copper Gasket (Duniway Stock Room Corp. Part # Quoted or Equiv. (Pkg of 10))	Oxygen Free Cu	6
101	G-275	2 3/4 CF Non-Plated, Standard I.D. Copper Gasket (Duniway Stock Room Corp. Part # Quoted or Equiv. (Pkg of 10))	Oxygen Free Cu	1
102		#0-80 X 1/2 Lg Phillips Drive Pan Hd Machine Screw	SS	6
103		#0 Flat Washer Regular Series	SS	6
104		#0 Helical Lock Washer	SS	6
105	31602	#0 Advanced Performance Detector (APD) Mounting Washer (PHOTONIS USA Inc. Part # Quoted or Equiv.)	Ceramic	12
106	Stores # 1-2/2015	#4-40 X 3/16 Lg Phillips Drive Pan Hd Machine Screw	SS	6
107		#4 Flat Washer Narrow Series	SS	6
108	Stores # 1-2/3007	#4 Helical Lock Washer	SS	6
109	SAX-32-050	#8-32 X 1/2 Lg Soc Hd Cap Screw c/w Washer (Pkg. of 25 Cap Screws & 25 Washers) (Duniway Stockroom Corp. Part # Quoted or Equiv.)	Ag Plated SS	36
110		#10-32 X 9/16 Lg Phillips Drive Pan Hd Machine Screw	SS	4
111	SBX-28-087	1/4-28 X 7/8 Lg 12 Point Cap Screw c/w Washer (Pkg. of 25 Cap Screws & 25 Washers) (Duniway Stockroom Corp. Part # Quoted or Equiv.)	Ag Plated SS	6
200	FLMR-275-50-4/MS	4" Linear Stepper Motor Driven Manipulator (TLI Thermionics Vacuum Products Part # Quoted or Equiv.)	SS	1
201	APD 2 MA 25/12/10/12 D 60:1	Microchannel Plate Detector w/o Phosphor Screen (PHOTONIS USA Inc. Part # Quoted or Equiv.)	SS & Ceramic	2

Note: UHV Cleanliness Standards MUST Be Followed and Maintained During the Complete Assembly.
Also Refer to Document 44430; "TRIUMF UHV Cleaning and Assembly Procedures"

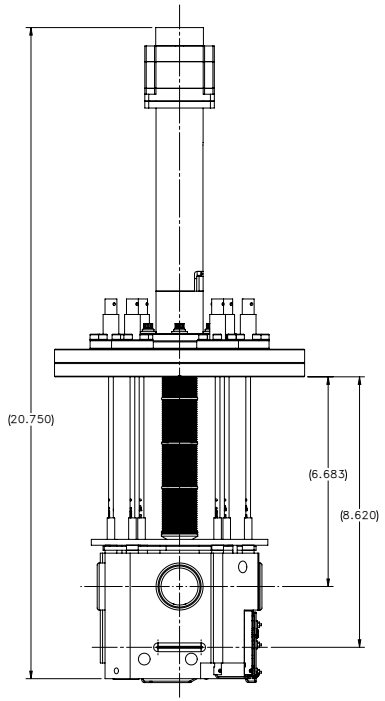

Front View
(Shown Fully Extended)

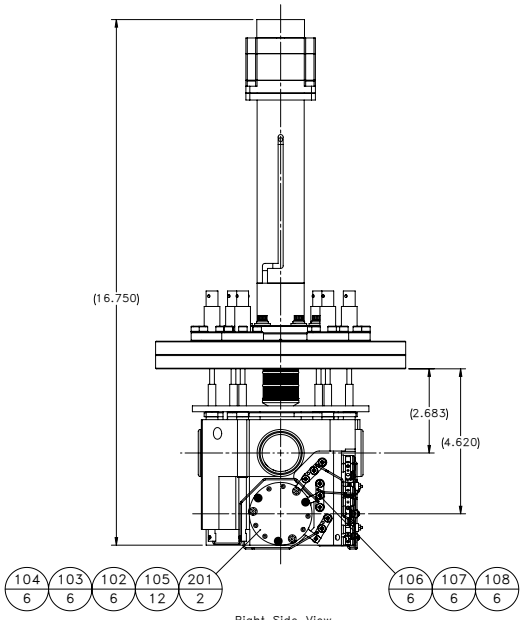

Right Side View
(Shown Fully Retracted)

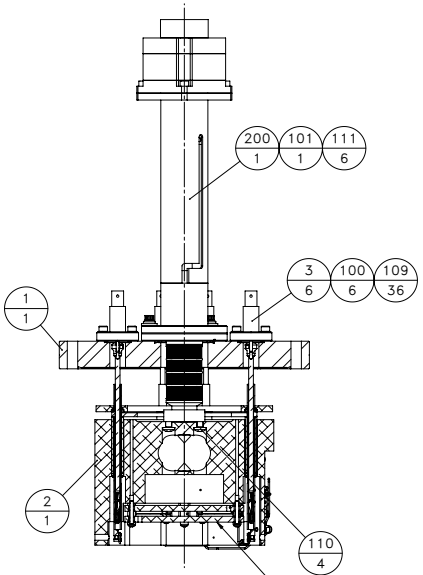

SECTION A-A

(Temporary Removal of the Deflection Plates is Required to Enable Installation of Item 2 to Item 200 (Using Item 110)).

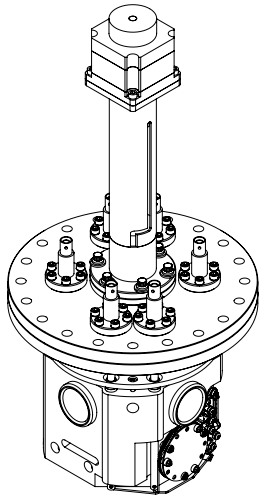

Isometric View

Notes:
1.) Quantities Listed in BOM are Required to Assemble and/or Install One (1) Assembly as Drawn.
2.) When Sets and/or Packages are Described in the BOM, the Number of Individual or Least Used Part is Listed in the Quantities Column. (Ex. Bolt, Washer & Platenut Sets; the Quantity of Platenuts is Listed as it is Understood that Two (2) Bolts & Two (2) Washers are Required for Each Platenut.)
3.) All Vacuum Surfaces in this Assembly and/or Installation MUST be Cleaned to Ultra High Vacuum (UHV) Standards. Refer to Document 44430; "TRIUMF UHV Cleaning and Assembling Procedures" Located on DocuShare.
4.) UHV Cleanliness Standards MUST be Followed and Maintained During the Complete Installation or Assembly.

REV	DATE	REVISION DESCRIPTION	BY	APPD
A	6/15/2015	ECO-3707 – Change Control Applies.	Mel Good	Jens Dilling

TOLERANCES UNLESS OTHERWISE SPECIFIED
DECIMALS .X ± 0.1, .XX ± 0.01, .XXX ± 0.005
ANGULAR ± 1.0°
SURFACE FINISH 63 μ Inch
ALL DIMS IN INCHES

DESIGNED TRIUMF/MSG
DRAWN Mel Good
CHECKED Renee Klawitter
REA/WPN # 3060
TRACKING # 0-068
SUB-ASSY:
ASSEMBLY: IEX1860

TRIUMF
4004 WESBROOK MALL
VANCOUVER, BRITISH COLUMBIA
CANADA V6T-2A3
CANADA'S NATIONAL LABORATORY FOR PARTICLE AND NUCLEAR PHYSICS

Ass'y (Allison Detector, 2-Way (AD2-W)) TITAN Switch Yard Emittance Station ISAC 1 – TITAN

SCALE 1:2
THIRD-ANGLE PROJECTION
DWG NO. IEX1862
SIZE D
SHEET 1 OF 1
REV A
DATE Feb. 2015

ITEM	DESCRIPTION	MATERIAL	QTY.
1	8 CF to 2 3/4 CF Reducing Flange (Kurt J. Lesker Co. Part # RF800X275 or Equiv.)	AISI 304L	1

DIMENSIONS QUOTED ARE FINISHED DIMENSIONS, NO ALLOWANCE HAS BEEN MADE FOR MANUFACTURE.

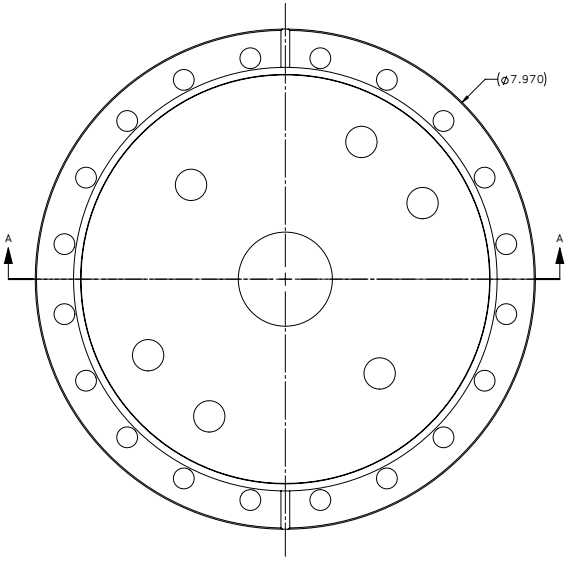

Top View

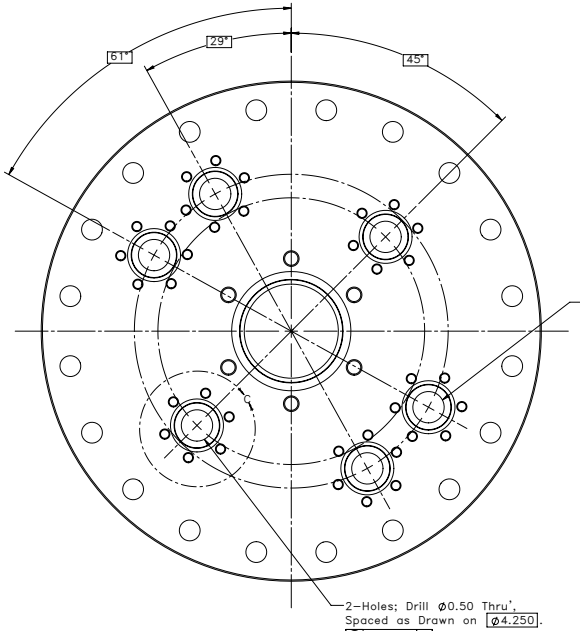

Bottom View
(Removed)

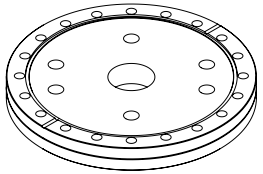

Isometric View
Scale: 1/2 X Full Size.

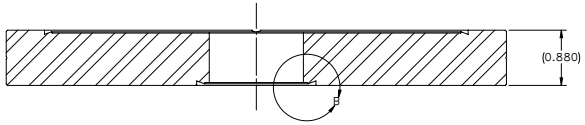

SECTION A–A
(Replaces Front View)

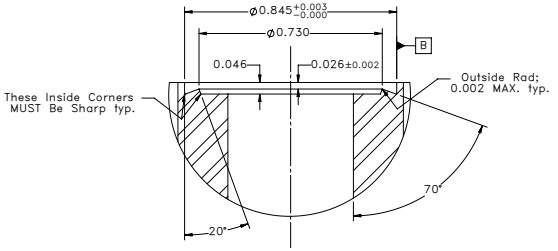

DETAIL E
SCALE 4 : 1
(Details Represented Here typ. for All Six (6) Instances)

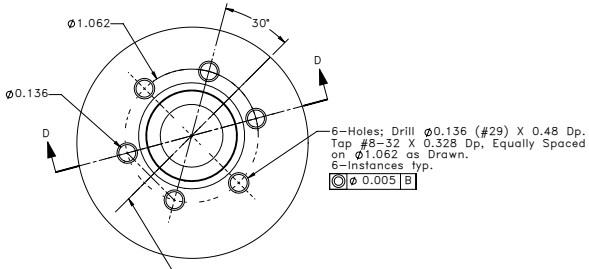

DETAIL C
SCALE 2 : 1

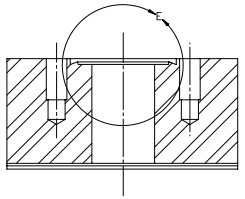

SECTION D–D
SCALE 2 : 1

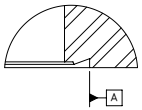

DETAIL B
SCALE 2 : 1

Notes: 1.) Break All Corners.
2.) Dimensions Listed in BOM Do NOT Include Machining Allowances.
3.) Maximum Inside Radius 0.020" Unless Noted.

REMOVE ALL BURRS AND SHARP EDGES

REV	DATE	REVISION DESCRIPTION	BY	APPD
A	6/15/2015	ECO–3707 – Change Control Applies.	Mel Good	Jens Dilling

TOLERANCES UNLESS OTHERWISE SPECIFIED
DECIMALS .X ± 0.1, .XX ± 0.01, .XXX ± 0.005
ANGULAR ± 1.0°
SURFACE FINISH 63 μ Inch
ALL DIMS IN INCHES

DESIGNED TRIUMF/MSG
DRAWN Mel Good
CHECKED Renee Klawitter
REA/WPN # 3060
TRACKING # 0–068
SUB–ASSY: IEX1862
ASSEMBLY: IEX1860

TRIUMF
4004 WESBROOK MALL
VANCOUVER, BRITISH COLUMBIA
CANADA V6T–2A3
CANADA'S NATIONAL LABORATORY FOR PARTICLE AND NUCLEAR PHYSICS

AD2–W Flange Details
TITAN Switch Yard Emittance Station
ISAC 1 – TITAN

SCALE 1:1
THIRD–ANGLE PROJECTION
DWG NO. IEX1863
SIZE D
SHEET 1 OF 1
REV A
DATE Feb. 2015

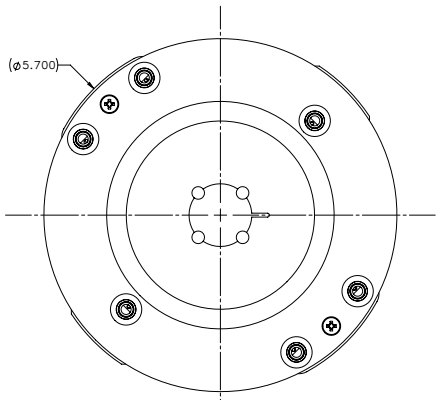

Top View

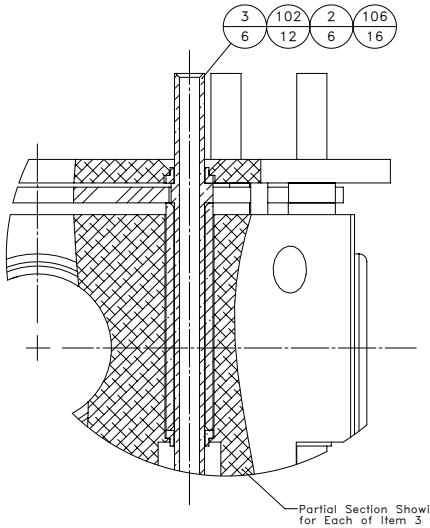

DETAIL B
SCALE 2 : 1

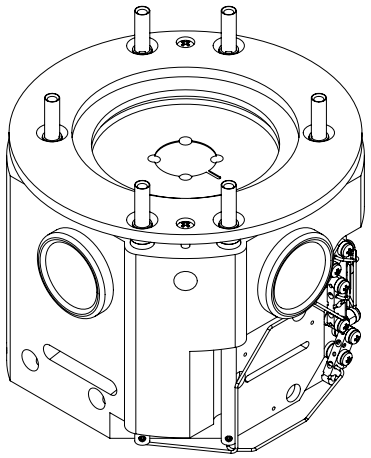

Isometric View
Scale: 1/4 X Full Size.

ITEM	REF No.	DESCRIPTION	MATERIAL	QTY.
1	IEX1865	AD2-W Main Body	6061-T6	1
2	IEX1866	AD2-W Insulative Sleeve	Unglazed Alumina	6
3	IEX1867	AD2-W Contact Recepticle	BeCu	6
4	IEX1868	AD2-W Anti-Rotation Plate	Macor	1
5	IEX1869	AD2-W Deflection Plate	Oxygen Free Copper	2
6	IEX1870	AD2-W 4mm Plate Spacer	Macor	4
7	IEX1871	AD2-W Entrance/Exit Skimmer Half	Oxygen Free Copper	8
8	IEX1872	AD2-W Entrance/Exit Skimmer Shim	AISI 304	8
9	IEX1873	AD2-W Conductor Block Type 1	Oxygen Free Copper	4
10	IEX1873	AD2-W Conductor Block Type 2	Oxygen Free Copper	2
11	IEX1874	AD2-W Top Fixture Plate	6061-T6	1
12	IEX1875	AD2-W Defl. Plate Cond. Wire Type 1	AISI 304	1
13	IEX1875	AD2-W Defl. Plate Cond. Wire Type 2	AISI 304	1
14	IEX1876	AD2-W Inter-Con. Cond. Wire Type 1	AISI 304	1
15	IEX1876	AD2-W Inter-Con. Cond. Wire Type 2	AISI 304	1
16	IEX1877	AD2-W MCP Cond. Wire Type 1	AISI 304	1
17	IEX1877	AD2-W MCP Cond. Wire Type 2	AISI 304	1
18	IEX1877	AD2-W MCP Cond. Wire Type 3	AISI 304	1
19	IEX1877	AD2-W MCP Cond. Wire Type 4	AISI 304	1
100	Stores # 1-1/1311	#4 Ceramic Bushing LP-76803	Ceramic	32
101	Stores # 1-1/1312	#4 Ceramic Washer LP-76803	Ceramic	12
102	10003630	1/4 Shoulder Washer (McAllister Technical Services Part # Quoted or Equiv.)	Ceramic	12
103		#2-56 X 5/8 Lg Phillips Drive Pan Hd Machine Screw	SS	8
104		#4-40 X 9/16 Lg Phillips Drive Pan Hd Machine Screw	SS	12
105	Stores # 1-2/2033	#4-40 X 3/4 Lg Phillips Drive Pan Hd Machine Screw	SS	4
106	Stores # 1-2/5051	#4-40 X 1/8 Lg Cup Piont Hex Drive Set Screw	SS	16
107	Stores # 1-2/2052	#6-32 X 1/2 Lg Phillips Drive Pan Hd Machine Screw	SS	2

Note: UHV Cleanliness Standards MUST Be Followed and Maintained During the Complete Assembly.
Also Refer to Document 44430; "TRIUMF UHV Cleaning and Assembly Procedures"

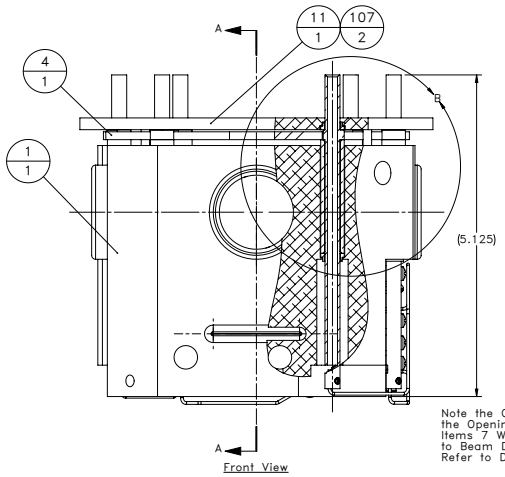

Front View

Beam Direction

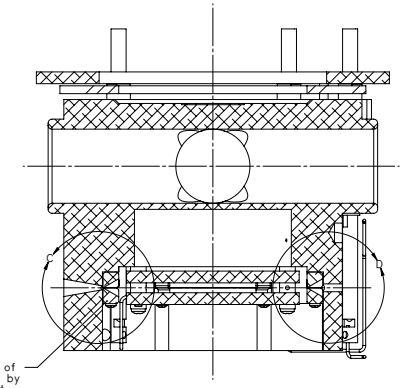

SECTION A-A
(Replaces Right Side View)

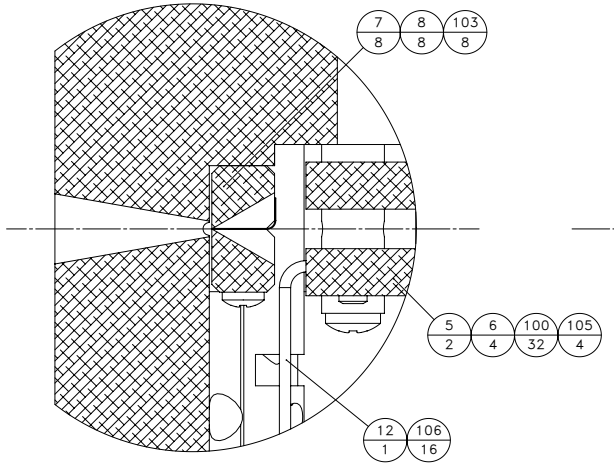

DETAIL C
SCALE 4 : 1

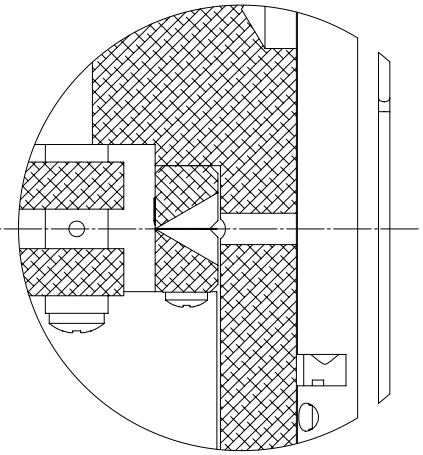

DETAIL D
SCALE 4 : 1

Notes: 1.) Quantities Listed in BOM are Required to Assemble and/or Install One (1) Assembly as Drawn.
2.) All Vacuum Surfaces in this Assembly and/or Installation MUST be Cleaned to Ultra High Vacuum (UHV) Standards. Refer to Document 44430; "TRIUMF UHV Cleaning and Assembling Procedures" Located on DocuShare.
3.) UHV Cleanliness Standards MUST be Followed and Maintained During the Complete Installation or Assembly.

REV	DATE	REVISION DESCRIPTION	BY	APPD
A	6/15/2015	ECO-3707 – Change Control Applies.	Mel Good	Jens Dilling

TOLERANCES UNLESS OTHERWISE SPECIFIED
DECIMALS .X ± 0.1, .XX ± 0.01, .XXX ± 0.005
ANGULAR ± 1.0°
SURFACE FINISH 63 μ Inch
ALL DIMS IN INCHES

DESIGNED TRIUMF/MSG
DRAWN Mel Good
CHECKED Renee Klawitter
REA/WPN # 3060
TRACKING # 0-068
SUB-ASSY: IEX1862
ASSEMBLY: IEX1860

TRIUMF
4004 WESBROOK MALL
VANCOUVER, BRITISH COLUMBIA
CANADA V6T-2A3
CANADA'S NATIONAL LABORATORY FOR PARTICLE AND NUCLEAR PHYSICS

AD2-W Drift Tube Section Ass'y
TITAN Switch Yard Emittance Station
ISAC 1 – TITAN

SCALE 1:1
DATE Feb. 2015
THIRD-ANGLE PROJECTION
DWG NO. IEX1864
SIZE D
SHEET 1 OF 2
REV A

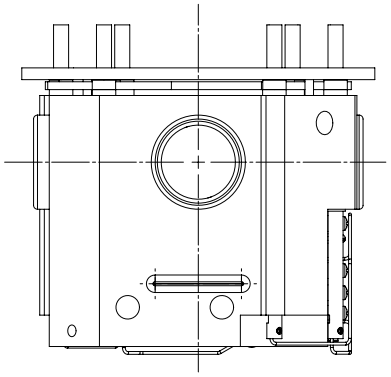

Front View
(Repeated)

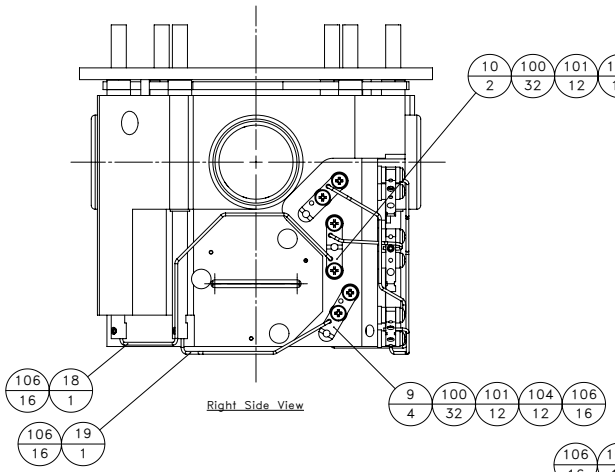

Right Side View

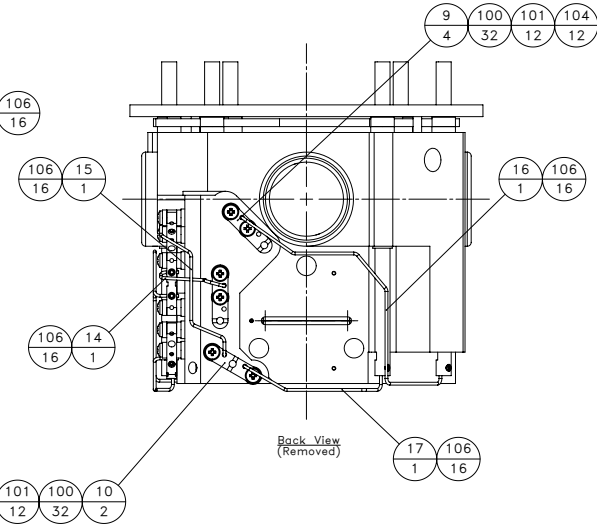

Back View
(Removed)

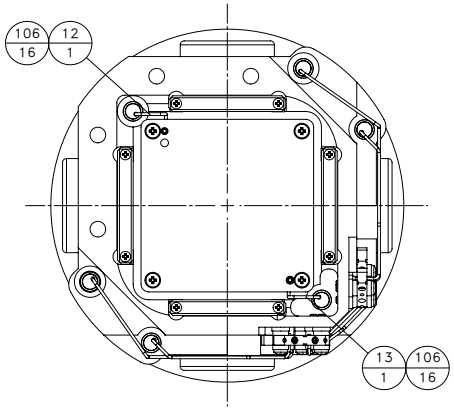

Bottom View

a	b	c	d	e	f	g	h

TRIUMF
4004 WESBROOK MALL
VANCOUVER, BRITISH COLUMBIA
CANADA V6T-2A3

CANADA'S NATIONAL LABORATORY FOR PARTICLE AND NUCLEAR PHYSICS

SCALE	DWG NO.	SIZE	SHEET	REV
1:1	IEX1864	D	2 OF 2	A

USE IN CONJUNCTION WITH SHEET No. 1

THIRD-ANGLE PROJECTION

ITEM	DESCRIPTION	MATERIAL	QTY.
1	5.250 Square X 4.000 Lg Block	6061-T6	1

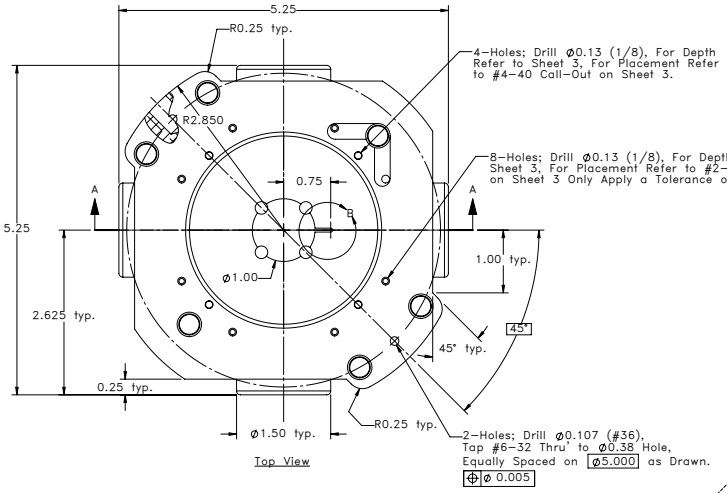

Top View

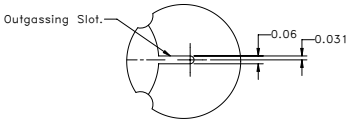

DETAIL B
SCALE 2 : 1

DIMENSIONS QUOTED ARE FINISHED DIMENSIONS, NO ALLOWANCE HAS BEEN MADE FOR MANUFACTURE.

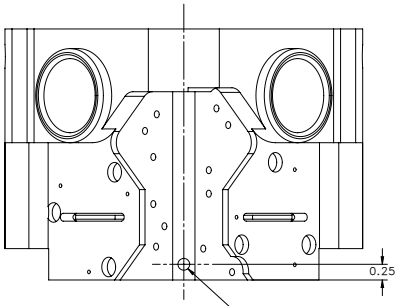

VIEW E-E
(Removed)

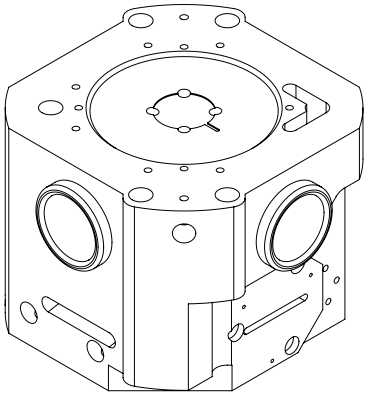

Isometric View

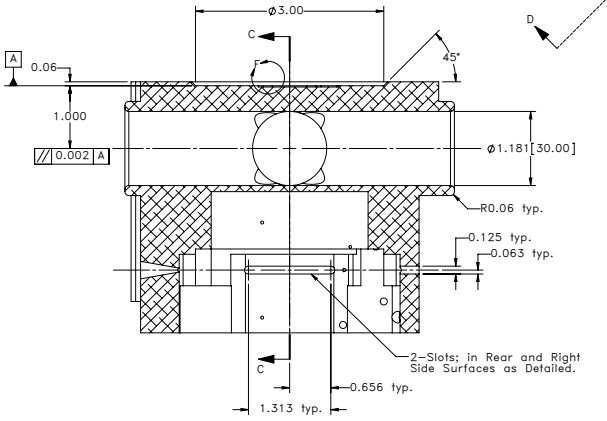

SECTION A-A

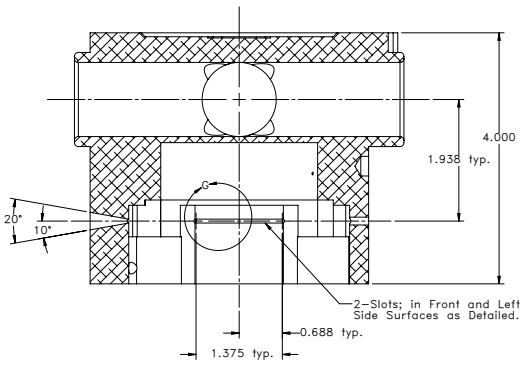

SECTION C-C

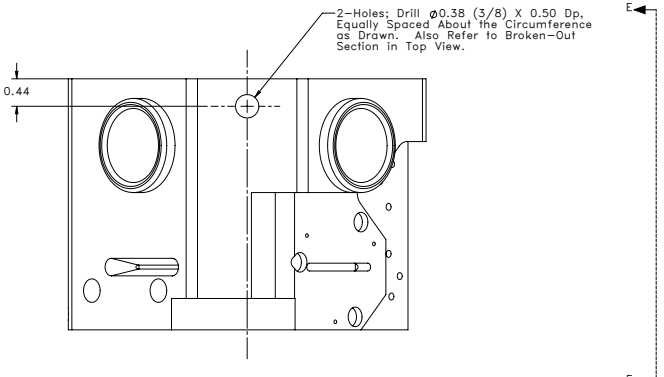

VIEW D-D
↷45.0°

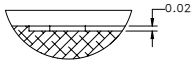

DETAIL F
SCALE 4 : 1

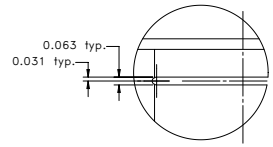

DETAIL G
SCALE 2 : 1

REMOVE ALL BURRS AND SHARP EDGES

Notes: 1.) Break All Corners.
2.) Dimensions Listed in BOM Do NOT Include Machining Allowances.
3.) Maximum Inside Radius 0.020" Unless Noted.

REV	DATE	REVISION DESCRIPTION	BY	APPD
A	6/15/2015	ECO-3707 – Change Control Applies.	Mel Good	Jens Dilling

TOLERANCES UNLESS OTHERWISE SPECIFIED
DECIMALS .X ± 0.1, .XX ± 0.01, .XXX ± 0.005
ANGULAR ± 1.0°
SURFACE FINISH 63 μ Inch
ALL DIMS IN INCHES

DESIGNED TRIUMF/MSG
DRAWN Mel Good
CHECKED Renee Klawitter
REA/WPN # 3060
TRACKING # 0-068
SUB-ASSY: IEX1864
ASSEMBLY: IEX1860

TRIUMF
4004 WESBROOK MALL
VANCOUVER, BRITISH COLUMBIA
CANADA V6T-2A3
CANADA'S NATIONAL LABORATORY FOR PARTICLE AND NUCLEAR PHYSICS

AD2-W Main Body
TITAN Switch Yard Emittance Station
ISAC 1 – TITAN

SCALE 1:1
THIRD-ANGLE PROJECTION
DWG NO. IEX1865
SIZE D
SHEET 1 OF 3
REV A
DATE Feb. 2015

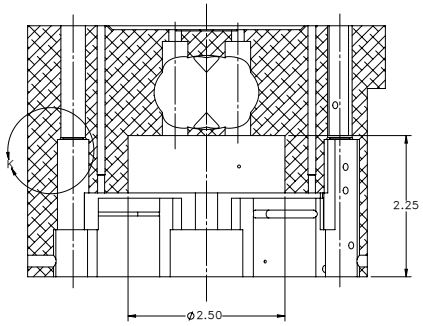

SECTION H–H
(Removed & Rotated)

1–Hole; Drill ⌀0.316 (Ltr. "O") Thru', C'Bore ⌀0.391 (25/64) X 1.781 Dp, From Top Surface, Equally Spaced on ⌀4.250, C'Bore X 2.188 Dp, From Bottom Surface as Shown by Detail N on Sheet 3.
⌖ ⌀ 0.005

1–Hole; Drill ⌀0.316 (Ltr. "O") Thru', C'Bore ⌀0.391 (25/64) X 1.781 Dp, From Top Surface, Equally Spaced on ⌀4.250, C'Bore ⌀0.50 X 2.188 Dp, From Bottom Surface as Drawn.
⌖ ⌀ 0.005

4–Holes; Drill ⌀0.316 (Ltr. "O") Thru', C'Bore ⌀0.391 (25/64) X 1.781 Dp, From Top Surface, Spaced as Drawn on ⌀5.000, C'Bore ⌀0.50 X 2.188 Dp, From Bottom Surface as Drawn.
⌖ ⌀ 0.005

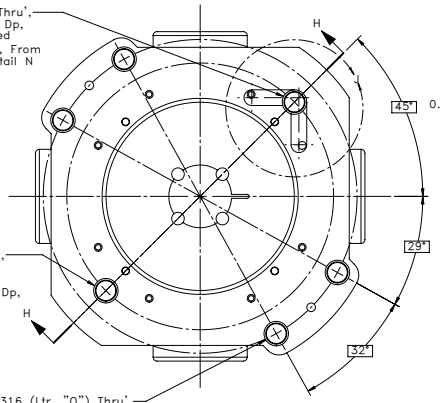

Top View
(Repeated)

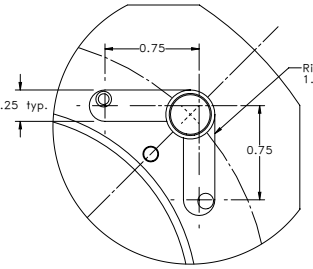

DETAIL J
SCALE 2 : 1

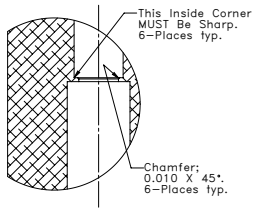

DETAIL K
SCALE 2 : 1

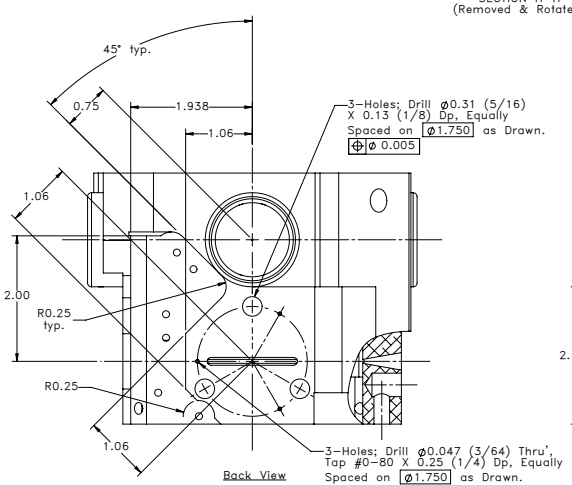

Back View

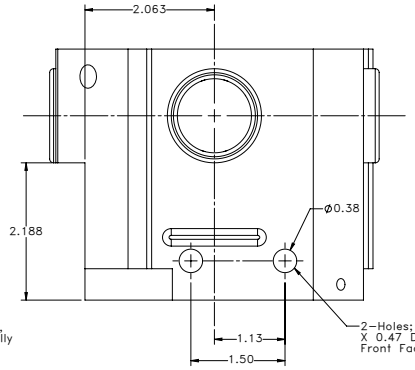

Left Side View

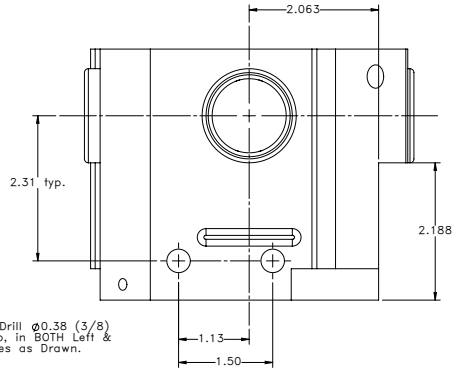

Front View

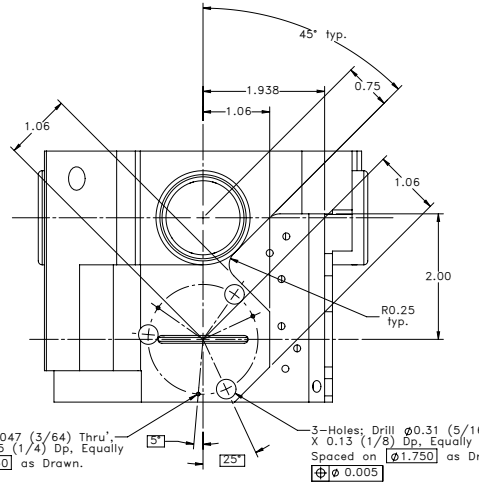

Right Side View

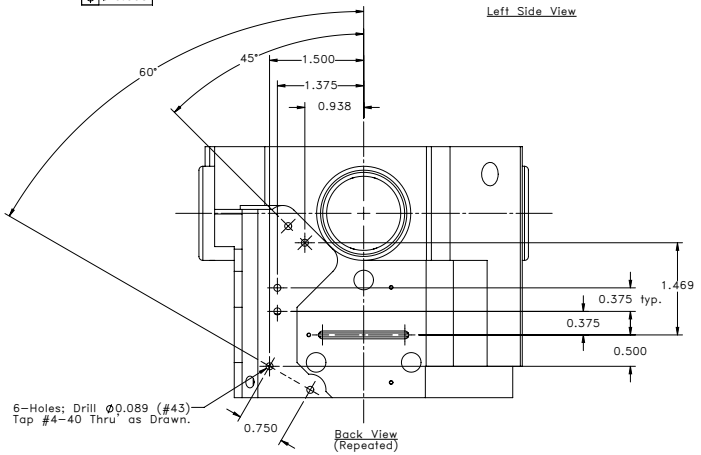

Back View
(Repeated)

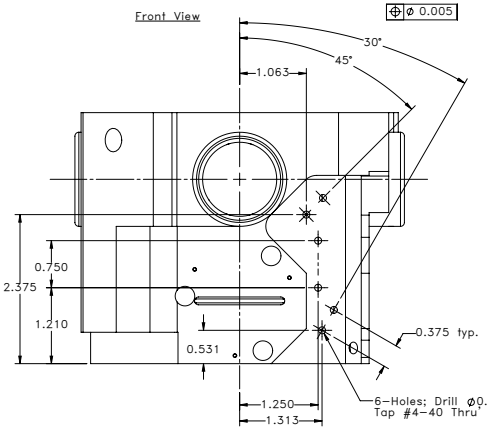

Right Side View
(Repeated)

TRIUMF 4004 WESBROOK MALL VANCOUVER, BRITISH COLUMBIA CANADA V6T-2A3					CANADA'S NATIONAL LABORATORY FOR PARTICLE AND NUCLEAR PHYSICS
SCALE 1:1		DWG NO. IEX1865	SIZE D	SHEET 2 OF 3	REV A
USE IN CONJUNCTION WITH SHEET No. 1	THIRD-ANGLE PROJECTION				

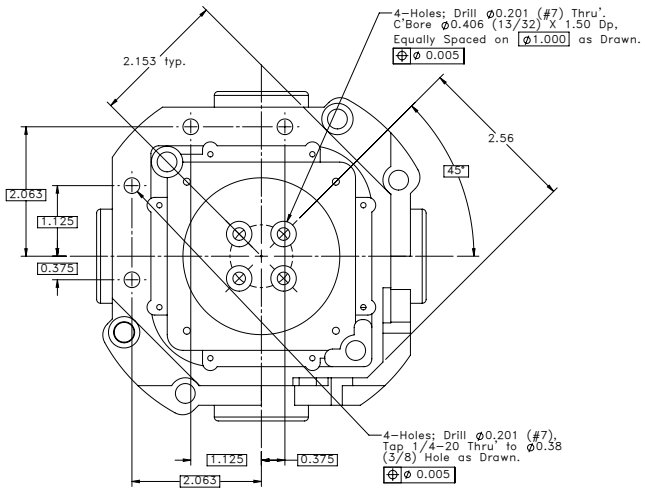

Bottom View

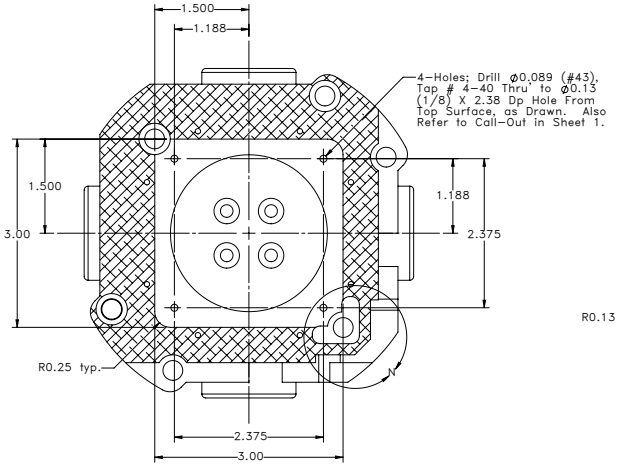

SECTION M–M

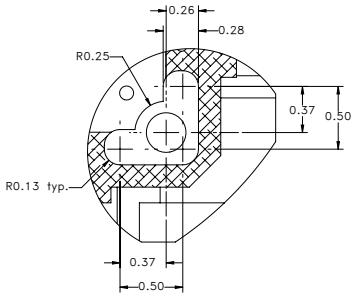

DETAIL N
SCALE 2 : 1

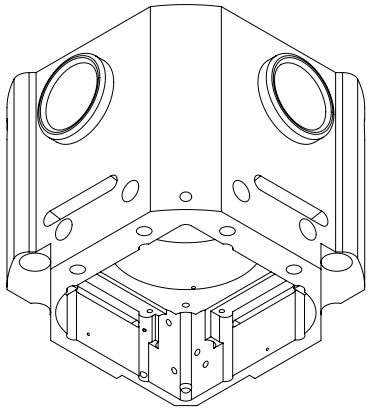

Reverse Isometric View

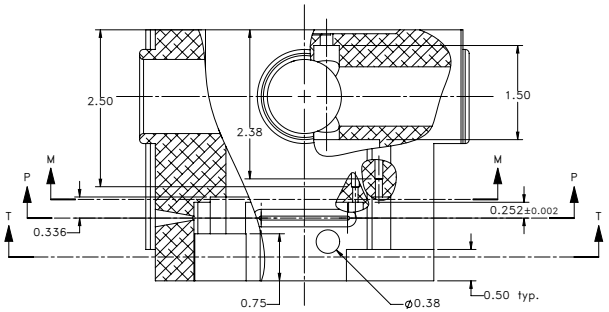

Front View
(Removed & Repeated)

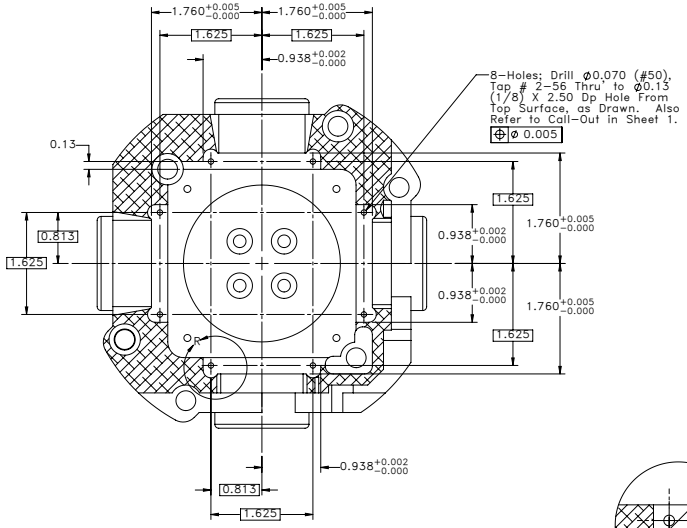

SECTION P–P

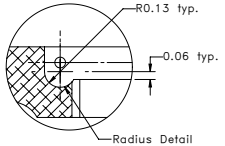

DETAIL R
SCALE 2 : 1

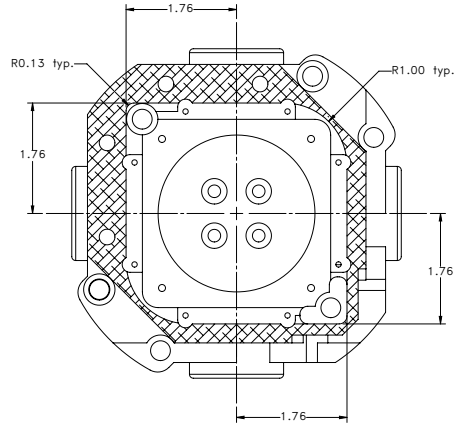

SECTION T–T

TRIUMF	4004 WESBROOK MALL VANCOUVER, BRITISH COLUMBIA CANADA V6T–2A3	CANADA'S NATIONAL LABORATORY FOR PARTICLE AND NUCLEAR PHYSICS				
SCALE 1:1		DWG NO.	SIZE	SHEET 3	REV	
USE IN CONJUNCTION WITH SHEET No. 1	THIRD–ANGLE PROJECTION	IEX1865	D	OF 3	A	

ITEM	DESCRIPTION	MATERIAL	QTY.
1	0.375 OD X 0.250 ID Tubing X 1.813 Lg	Unglazed Alumina	1

DIMENSIONS QUOTED ARE FINISHED DIMENSIONS, NO ALLOWANCE HAS BEEN MADE FOR MANUFACTURE.

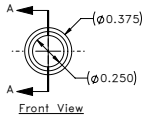

Front View

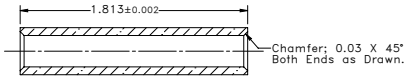

SECTION A–A
(Replaces Right Side View)

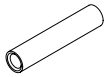
Isometric View
Scale: Full Size.

Notes: 1.) Break All Corners.
2.) Dimensions Listed in BOM Do NOT Include Machining Allowances.
3.) Maximum Inside Radius 0.020" Unless Noted.

REMOVE ALL BURRS AND SHARP EDGES

TOLERANCES UNLESS OTHERWISE SPECIFIED		
DECIMALS	.X	± 0.1
	.XX	± 0.01
	.XXX	± 0.005
ANGULAR		± 1.0°
SURFACE FINISH		63 µ inch

ALL DIMS IN INCHES

REV	DATE	REVISION DESCRIPTION	BY	APPD
A	6/15/2015	ECO–3707 – Change Control Applies.	Mel Good	Jens Dilling

DESIGNED	TRIMF/MSG
DRAWN	Mel Good
CHECKED	Renee Klawitter
REA/WPN #	3060
TRACKING #	0–068

SUB–ASSY IEX1864
ASSEMBLY IEX1860

TRIUMF
4004 WESBROOK MALL
VANCOUVER, BRITISH COLUMBIA
CANADA V6T–2A3

CANADA'S NATIONAL LABORATORY FOR PARTICLE AND NUCLEAR PHYSICS

AD2–W Insulative Sleeve
TITAN Switch Yard Emittance Station
ISAC 1 – TITAN

SCALE	DWG NO.	SIZE	SHEET	REV
2:1	IEX1866	B	1 OF 1	A
DATE Feb. 2015				

THIRD–ANGLE PROJECTION

ITEM	DESCRIPTION	MATERIAL	QTY.
1	Dia. 0.375 X 5.000 Lg Round Bar	BeCu	1

DIMENSIONS QUOTED ARE FINISHED DIMENSIONS, NO ALLOWANCE HAS BEEN MADE FOR MANUFACTURE.

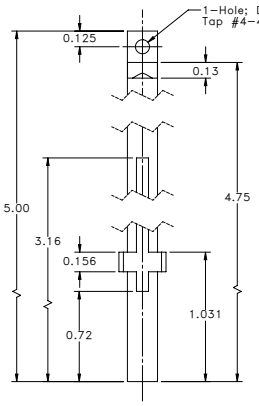

Top View

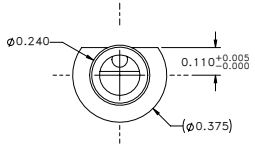

Front View
(Repeated)
Scale: 4 X Full Size.

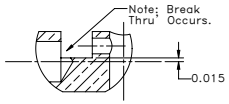

DETAIL B
SCALE 4 : 1

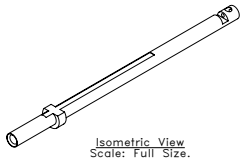

Isometric View
Scale: Full Size.

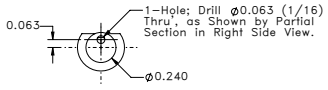

Back View
(Removed)

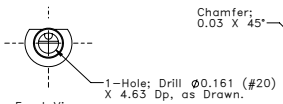

Front View

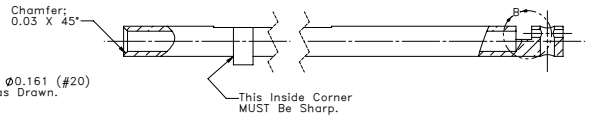

Right Side View

REMOVE ALL BURRS AND SHARP EDGES

Notes: 1.) Break All Corners.
2.) Dimensions Listed in BOM Do NOT Include Machining Allowances.
3.) Maximum Inside Radius 0.020" Unless Noted.

REV	DATE	REVISION DESCRIPTION	BY	APPD
A	6/15/2015	ECO-3707 – Change Control Applies.	Mel Good	Jens Dilling

TOLERANCES UNLESS OTHERWISE SPECIFIED
DECIMALS .X ± 0.1
.XX ± 0.01
.XXX ± 0.005
ANGULAR ± 1.0°
SURFACE FINISH 63 µ inch
ALL DIMS IN INCHES

DESIGNED TRIUMF/MSG
DRAWN Mel Good
CHECKED Renee Klawitter
REA/WPN # 3060
TRACKING # 0-068

SUB-ASSY IEX1864
ASSEMBLY IEX1860

TRIUMF
4004 WESBROOK MALL
VANCOUVER, BRITISH COLUMBIA
CANADA V6T-2A3
CANADA'S NATIONAL LABORATORY FOR PARTICLE AND NUCLEAR PHYSICS

AD2-W Contact Recepticle
TITAN Switch Yard Emittance Station
ISAC 1 – TITAN

SCALE 2:1
DATE Feb. 2015
THIRD-ANGLE PROJECTION
DWG NO. IEX1867
SIZE C
SHEET 1 OF 1
REV A

ITEM	DESCRIPTION	MATERIAL	QTY.
1	4.000 W X 4.563 Lg X 0.125 Thk Sheet	Macor	1

DIMENSIONS QUOTED ARE FINISHED DIMENSIONS, NO ALLOWANCE HAS BEEN MADE FOR MANUFACTURE.

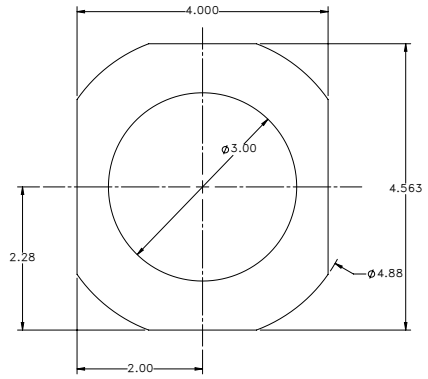

Top View

Front View
(Removed)

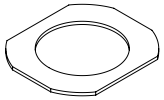

Isometric View
Scale: 1/2 X Full Size.

Notes: 1.) Break All Corners.
2.) Dimensions Listed in BOM Do NOT Include Machining Allowances.
3.) Maximum inside Radius 0.020" Unless Noted.

REMOVE ALL BURRS AND SHARP EDGES

TOLERANCES UNLESS OTHERWISE SPECIFIED	
DECIMALS .X	± 0.1
.XX	± 0.01
.XXX	± 0.005
ANGULAR	± 1.0°
SURFACE FINISH	63 µ inch

ALL DIMS IN INCHES

REV	DATE	REVISION DESCRIPTION	BY	APPD
A	6/15/2015	ECO-3707 – Change Control Applies.	Mel Good	Jens Dilling

TRIUMF
4004 WESBROOK MALL
VANCOUVER, BRITISH COLUMBIA
CANADA V6T-2A3

CANADA'S NATIONAL LABORATORY FOR PARTICLE AND NUCLEAR PHYSICS

DESIGNED TRIUMF/MSG
DRAWN Mel Good
CHECKED Renee Klawitter
REA/WPN # 3060
TRACKING # 0-068

SUB-ASSY IEX1864
ASSEMBLY IEX1860

AD2-W Anti-Rotation Plate
TITAN Switch Yard Emittance Station
ISAC 1 – TITAN

SCALE 1:1
DATE April 2015
THIRD-ANGLE PROJECTION
DWG NO. IEX1868
SIZE B
SHEET 1 OF 1
REV A

ITEM	DESCRIPTION	MATERIAL	QTY.
1	2.750 Square X 0.188 Thk Plate	Oxygen Free Copper	1

DIMENSIONS QUOTED ARE FINISHED DIMENSIONS, NO ALLOWANCE HAS BEEN MADE FOR MANUFACTURE.

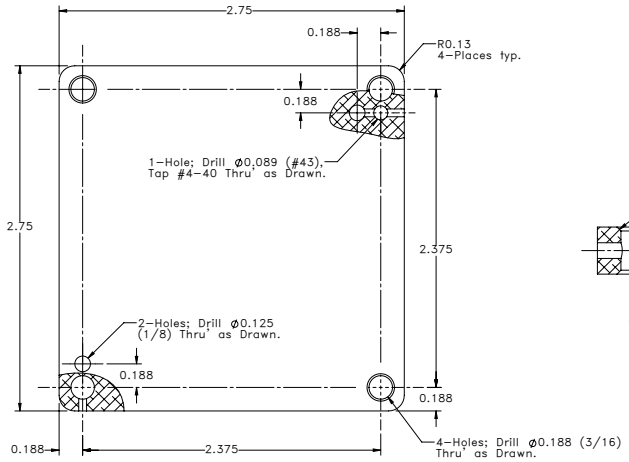

Top View

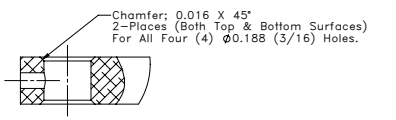

DETAIL A
SCALE 4 : 1

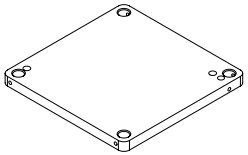

Isometric View
Scale: Full Size.

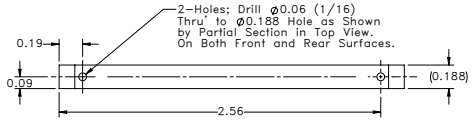

Front View

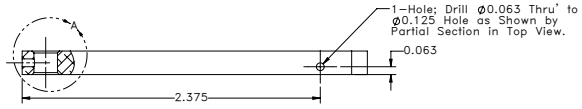

Right Side View

Notes: 1.) Break All Corners.
2.) Dimensions Listed in BOM Do NOT Include Machining Allowances.
3.) Maximum Inside Radius 0.020" Unless Noted.

REMOVE ALL BURRS AND SHARP EDGES

REV	DATE	REVISION DESCRIPTION	BY	APPD.
A	6/15/2015	ECO–3707 – Change Control Applies.	Mel Good	Jens Dilling

TOLERANCES UNLESS OTHERWISE SPECIFIED
DECIMALS .X ± 0.1, .XX ± 0.01, .XXX ± 0.005
ANGULAR ± 1.0°
SURFACE FINISH 63 μ inch
ALL DIMS IN INCHES

DESIGNED TRIUMF/MSG
DRAWN Mel Good
CHECKED Renee Klawitter
REA/WPN # 3060
TRACKING # 0-068

SUB–ASSY IEX1864
ASSEMBLY IEX1860

TRIUMF
4004 WESBROOK MALL
VANCOUVER, BRITISH COLUMBIA
CANADA V6T–2A3
CANADA'S NATIONAL LABORATORY FOR PARTICLE AND NUCLEAR PHYSICS

AD2–W Deflection Plate
TITAN Switch Yard Emittance Station
ISAC 1 – TITAN

SCALE 2:1
DATE Feb. 2015
THIRD–ANGLE PROJECTION
DWG NO. IEX1869
SIZE C
SHEET 1 OF 1
REV A

ITEM	DESCRIPTION	MATERIAL	QTY.
1	Dia. 0.250 X 0.217 Lg Round Bar	Macor	1

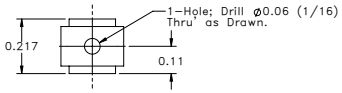

Top View

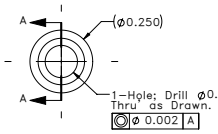

Front View

DIMENSIONS QUOTED ARE FINISHED DIMENSIONS, NO ALLOWANCE HAS BEEN MADE FOR MANUFACTURE.

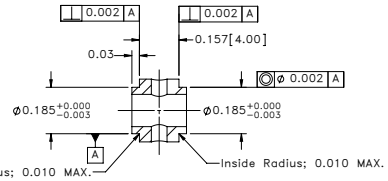

SECTION A–A
(Replaces Right Side View)


Isometric View

Notes: 1.) Break All Corners.
2.) Dimensions Listed in BOM Do NOT Include Machining Allowances.
3.) Maximum Inside Radius 0.020" Unless Noted.

REMOVE ALL BURRS AND SHARP EDGES

REV	DATE	REVISION DESCRIPTION	BY	APPD
A	6/15/2015	ECO–3707 – Change Control Applies.	Mel Good	Jens Dilling

TOLERANCES UNLESS OTHERWISE SPECIFIED
DECIMALS .X ± 0.1
.XX ± 0.01
.XXX ± 0.005
ANGULAR ± 1.0°
SURFACE FINISH 63 μ inch

ALL DIMS IN INCHES

DESIGNED TRIUMF/MSG
DRAWN Mel Good
CHECKED Renee Klawitter
REA/WPN # 3060
TRACKING # 0–068

SUB–ASSY IEX1864
ASSEMBLY IEX1860

TRIUMF
4004 WESBROOK MALL
VANCOUVER, BRITISH COLUMBIA
CANADA V6T–2A3

CANADA'S NATIONAL LABORATORY FOR PARTICLE AND NUCLEAR PHYSICS

AD2–W 4mm Plate Spacer
TITAN Switch Yard Emittance Station
ISAC 1 – TITAN

SCALE 4:1
DATE Feb. 2015
THIRD–ANGLE PROJECTION
DWG NO. IEX1870
SIZE B
SHEET 1 OF 1
REV A

ITEM	DESCRIPTION	MATERIAL	QTY.
1	0.250 Square Bar X 1.865 Lg	Oxygen Free Copper	1

DIMENSIONS QUOTED ARE FINISHED DIMENSIONS, NO ALLOWANCE HAS BEEN MADE FOR MANUFACTURE.

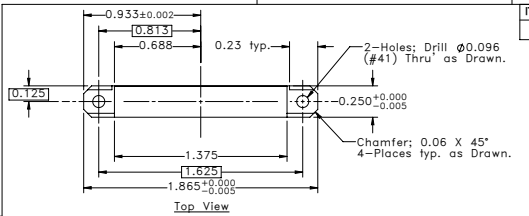

Top View

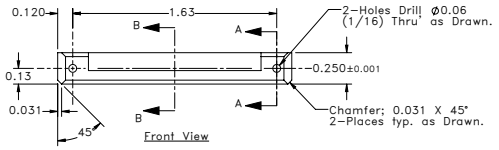

Front View

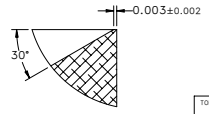

DETAIL C
SCALE 16 : 1

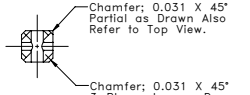

SECTION A–A
(Replaces Right
Side View)

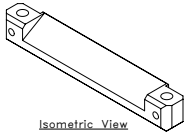
Isometric View

SECTION B–B

REV	DATE	REVISION DESCRIPTION	BY	APPD
A	6/15/2015	ECO–3707 – Change Control Applies.	Mel Good	Jens Dilling

TOLERANCES UNLESS OTHERWISE SPECIFIED
DECIMALS .X ± 0.1
.XX ± 0.01
.XXX ± 0.005
ANGULAR ± 1.0°
SURFACE FINISH 63 μ inch

ALL DIMS IN INCHES

REMOVE ALL BURRS AND SHARP EDGES

Notes: 1.) Break All Corners.
2.) Dimensions Listed in BOM Do NOT Include Machining Allowances.
3.) Maximum Inside Radius 0.020" Unless Noted.

DESIGNED TRIUMF/MSG
DRAWN Mel Good
CHECKED Renee Klawitter
REA/WPN # 3060
TRACKING # 0–068

SUB–ASSY IEX1864
ASSEMBLY IEX1860

TRIUMF
4004 WESBROOK MALL
VANCOUVER, BRITISH COLUMBIA
CANADA V6T–2A3

CANADA'S NATIONAL LABORATORY FOR PARTICLE AND NUCLEAR PHYSICS

AD2–W Entrance/Exit Skimmer Half
TITAN Switch Yard Emittance Station
ISAC 1 – TITAN

SCALE 2:1
DATE Feb. 2015
THIRD–ANGLE PROJECTION
DWG NO. IEX1871
SIZE B
SHEET 1 OF 1
REV A

ITEM	DESCRIPTION	MATERIAL	QTY.
1	0.200 W X 0.357 Lg X 0.004 Thk Sheet	AISI 304	1

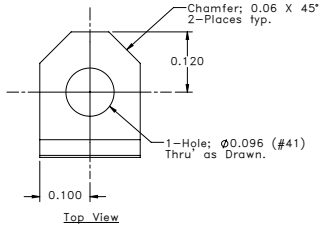

Top View

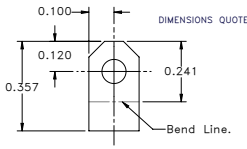

Top View
(Flattened)
Scale: 4 X Full Size.

DIMENSIONS QUOTED ARE FINISHED DIMENSIONS, NO ALLOWANCE HAS BEEN MADE FOR MANUFACTURE.

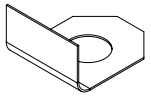
Isometric View

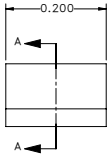

Front View

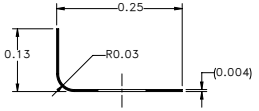

SECTION A–A
(Replaces Right Side View)

Notes: 1.) Break All Corners.
2.) Dimensions Listed in BOM Do NOT Include Machining Allowances.
3.) Maximum Inside Radius 0.020" Unless Noted.

REMOVE ALL BURRS AND SHARP EDGES

REV	DATE	REVISION DESCRIPTION	BY	APPD
A	6/15/2015	ECO–3707 – Change Control Applies.	Mel Good	Jens Dilling

TOLERANCES UNLESS OTHERWISE SPECIFIED
DECIMALS .X ± 0.1
.XX ± 0.01
.XXX ± 0.005
ANGULAR ± 1.0°
SURFACE FINISH 63 μ inch

ALL DIMS IN INCHES

DESIGNED TRIUMF/MSG
DRAWN Mel Good
CHECKED Renee Klawitter
REA/WPN # 3060
TRACKING # 0-068

SUB-ASSY IEX1864
ASSEMBLY IEX1860

TRIUMF
4004 WESBROOK MALL
VANCOUVER, BRITISH COLUMBIA
CANADA V6T-2A3

CANADA'S NATIONAL LABORATORY FOR PARTICLE AND NUCLEAR PHYSICS

AD2–W Entrance/Exit Skimmer Shim
TITAN Switch Yard Emittance Station
ISAC 1 – TITAN

SCALE 8:1
DATE Feb. 2015
THIRD-ANGLE PROJECTION
DWG NO. IEX1872
SIZE B
SHEET 1 OF 1
REV A

ITEM	DESCRIPTION	MATERIAL	QTY.
1	0.250 W X 0.156 Thk X 1.000 Lg Block	Oxygen Free Copper	1

DIMENSIONS QUOTED ARE FINISHED DIMENSIONS, NO ALLOWANCE HAS BEEN MADE FOR MANUFACTURE.

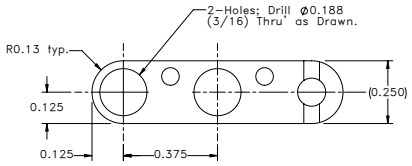

Top View
(Of Type 1)

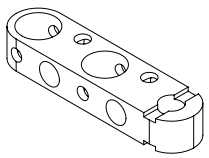

Isometric View
(Of Type 1)

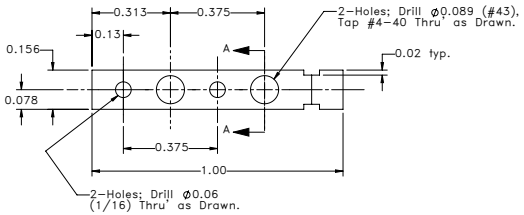

Front View
(Of Type 1)

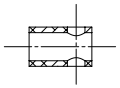

SECTION A–A
(Replaces Right Side View
Of Type 1)

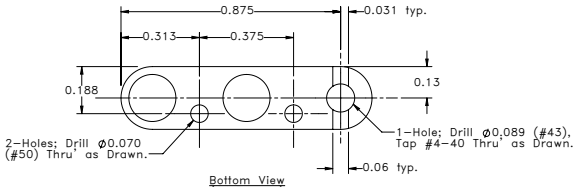

Bottom View
(Of Type 1)

Notes: 1.) Break All Corners.
2.) Dimensions Listed in BOM Do NOT Include Machining Allowances.
3.) Maximum Inside Radius 0.020" Unless Noted.

ITEM	DESCRIPTION	MATERIAL	QTY.
1	0.250 W X 0.156 Thk X 1.000 Lg Block	Oxygen Free Copper	1

DIMENSIONS QUOTED ARE FINISHED DIMENSIONS, NO ALLOWANCE HAS BEEN MADE FOR MANUFACTURE.

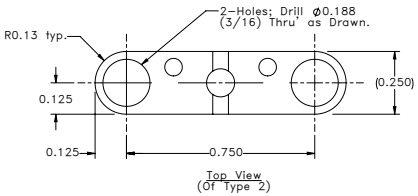

Top View
(Of Type 2)

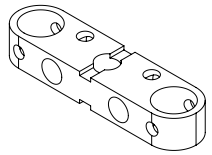

Isometric View
(Of Type 2)

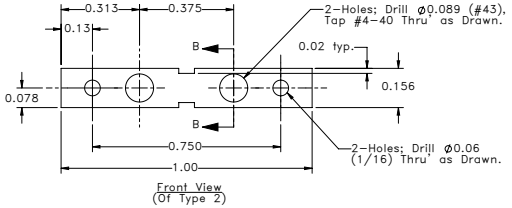

Front View
(Of Type 2)

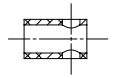

SECTION B–B
(Replaces Right Side View
Of Type 2)

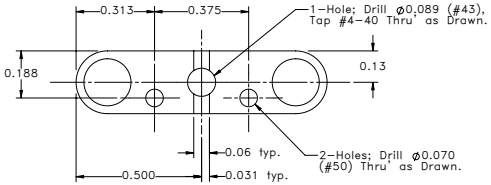

Bottom View
(Of Type 2)

REMOVE ALL BURRS AND SHARP EDGES

TOLERANCES UNLESS OTHERWISE SPECIFIED
DECIMALS .X ± 0.1, .XX ± 0.01, .XXX ± 0.005
ANGULAR ± 1.0°
SURFACE FINISH 63 μ Inch
ALL DIMS IN INCHES

REV	DATE	REVISION DESCRIPTION	BY	APPD
A	6/15/2015	ECO–3707 – Change Control Applies.	Mel Good	Jens Dilling

DESIGNED TRIUMF/MSG
DRAWN Mel Good
CHECKED Renee Klawitter
REA/WPN # 3060
TRACKING # 0–068

SUB–ASSY: IEX1864
ASSEMBLY: IEX1860

TRIUMF
4004 WESBROOK MALL
VANCOUVER, BRITISH COLUMBIA
CANADA V6T–2A3
CANADA'S NATIONAL LABORATORY FOR PARTICLE AND NUCLEAR PHYSICS

AD2–W Conductor Block Type 1 & 2
TITAN Switch Yard Emittance Station
ISAC 1 – TITAN

SCALE 4:1
THIRD–ANGLE PROJECTION
DATE Feb. 2015
DWG NO. IEX1873
SIZE D
SHEET 1 OF 1
REV A

ITEM	DESCRIPTION	MATERIAL	QTY.
1	Dia. 5.625 X 0.188 Thk Disk	6061–T6	1

DIMENSIONS QUOTED ARE FINISHED DIMENSIONS, NO ALLOWANCE HAS BEEN MADE FOR MANUFACTURE.

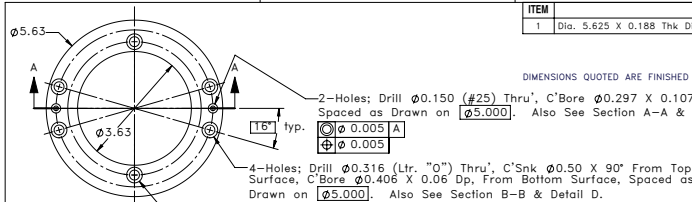

2–Holes; Drill ø0.150 (#25) Thru', C'Bore ø0.297 X 0.107 Dp, Equally Spaced as Drawn on ø5.000. Also See Section A–A & Detail C.

⌾ ø 0.005 A
⌖ ø 0.005

4–Holes; Drill ø0.316 (Ltr. "O") Thru', C'Snk ø0.50 X 90° From Top Surface, C'Bore ø0.406 X 0.06 Dp, From Bottom Surface, Spaced as Drawn on ø5.000. Also See Section B–B & Detail D.

⌾ ø 0.005 A
⌖ ø 0.005

2–Holes; Drill ø0.316 (Ltr. "O") Thru', C'Snk ø0.50 X 90° From Top Surface, C'Bore ø0.406 X 0.06 Dp, From Bottom Surface, Equally Spaced as Drawn on ø4.250. Also See Section B–B & Detail D.

⌾ ø 0.005 A
⌖ ø 0.005

Isometric View

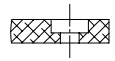

DETAIL C
SCALE 2 : 1

Chamfer; 0.010 X 45°
6–Places typ.

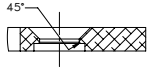

DETAIL D
SCALE 2 : 1

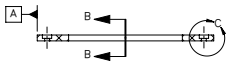

SECTION A–A
(Replaces Front View)

SECTION B–B
(Replaces Right Side View)

Notes: 1.) Break All Corners.
2.) Dimensions Listed in BOM Do NOT Include Machining Allowances.
3.) Maximum Inside Radius 0.020" Unless Noted.

REMOVE ALL BURRS AND SHARP EDGES

REV	DATE	REVISION DESCRIPTION	BY	APPD
A	6/15/2015	ECO–3707 – Change Control Applies.	Mel Good	Jens Dilling

TOLERANCES UNLESS OTHERWISE SPECIFIED
DECIMALS .X ± 0.1
.XX ± 0.01
.XXX ± 0.005
ANGULAR ± 1.0°
SURFACE FINISH 63 µ inch

ALL DIMS IN INCHES

DESIGNED TRIUMF/MSG
DRAWN Mel Good
CHECKED Renee Klawitter
REA/WPN # 3060
TRACKING # 0–068

SUB–ASSY IEX1864
ASSEMBLY IEX1860

TRIUMF
4004 WESBROOK MALL
VANCOUVER, BRITISH COLUMBIA
CANADA V6T–2A3

CANADA'S NATIONAL LABORATORY FOR PARTICLE AND NUCLEAR PHYSICS

AD2–W Top Fixture Plate
TITAN Switch Yard Emittance Station
ISAC 1 – TITAN

SCALE 1:2
DATE Feb. 2015
THIRD–ANGLE PROJECTION
DWG NO. IEX1874
SIZE B
SHEET 1 OF 1
REV A

ITEM	DESCRIPTION	MATERIAL	QTY.
1	Dia. 0.045 X 1.816 Lg Wire	AISI 304	1

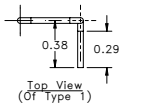

Top View
(Of Type 1)

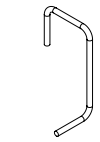
Isometric View
(Of Type 1)

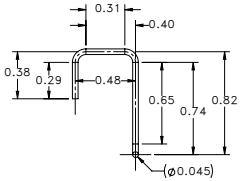

Front View
(Of Type 1)

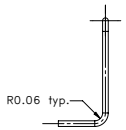

Right Side View
(Of Type 1)


Top View
(Of Type 1)
Scale: Full Size.


Front View
(Of Type 1)
Scale: Full Size.


Right Side View
(Of Type 1)
Scale: Full Size.

ITEM	DESCRIPTION	MATERIAL	QTY.
1	Dia. 0.045 X 2.176 Lg Wire	AISI 304	1

DIMENSIONS QUOTED ARE FINISHED DIMENSIONS, NO ALLOWANCE HAS BEEN MADE FOR MANUFACTURE.

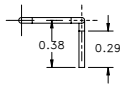

Top View
(Of Type 2)

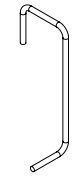
Isometric View
(Of Type 2)

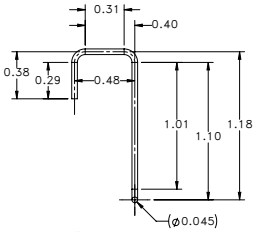

Front View
(Of Type 2)

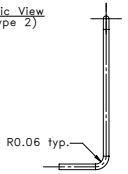

Right Side View
(Of Type 2)


Top View
(Of Type 2)
Scale: Full Size.


Front View
(Of Type 2)
Scale: Full Size.


Right Side View
(Of Type 2)
Scale: Full Size.

REMOVE ALL BURRS AND SHARP EDGES

Notes: 1.) Break All Corners.
2.) Dimensions Listed in BOM Do NOT Include Machining Allowances.
3.) Maximum Inside Radius 0.020" Unless Noted.

TOLERANCES UNLESS OTHERWISE SPECIFIED
DECIMALS .X ± 0.1
.XX ± 0.01
.XXX ± 0.005
ANGULAR ± 1.0°
SURFACE FINISH 63 µ inch
ALL DIMS IN INCHES

DESIGNED TRIUMF/MSG
DRAWN Mel Good
CHECKED Renee Klawitter
REA/WPN # 3060
TRACKING # 0-068

SUB-ASSY IEX1864
ASSEMBLY IEX1860

REV	DATE	REVISION DESCRIPTION	BY	APPD
A	6/15/2015	ECO-3707 – Change Control Applies.	Mel Good	Jens Dilling

TRIUMF
4004 WESBROOK MALL
VANCOUVER, BRITISH COLUMBIA
CANADA V6T-2A3
CANADA'S NATIONAL LABORATORY FOR PARTICLE AND NUCLEAR PHYSICS

AD2–W Defl. Plate Cond. Wire Type 1 & 2
TITAN Switch Yard Emittance Station
ISAC 1 – TITAN

SCALE 2:1
THIRD-ANGLE PROJECTION
DWG NO. IEX1875
SIZE C
SHEET 1 OF 1
REV A
DATE Feb. 2015

ITEM	DESCRIPTION	MATERIAL	QTY.
1	Dia. 0.045 X 2.192 Lg Wire	AISI 304	1

DIMENSIONS QUOTED ARE FINISHED DIMENSIONS, NO ALLOWANCE HAS BEEN MADE FOR MANUFACTURE.

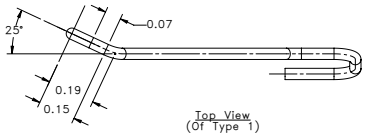

Top View
(Of Type 1)

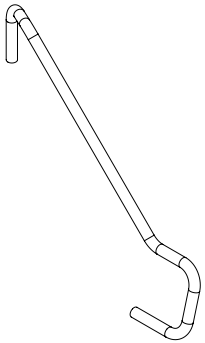

Isometric View
(Of Type 1)

Top View
(Of Type 1)
Scale: Full Size.

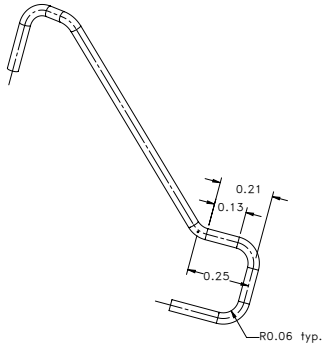

VIEW A–A

Front View
(Of Type 1)
Scale: Full Size.

Right Side View
(Of Type 1)
Scale: Full Size.

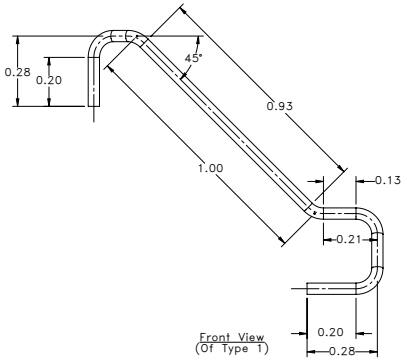

Front View
(Of Type 1)

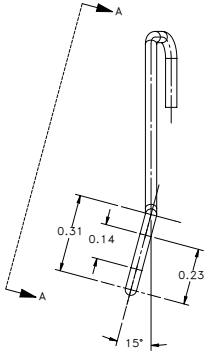

Right Side View
(Of Type 1)

Bottom View
(Of Type 1)
Scale: Full Size.

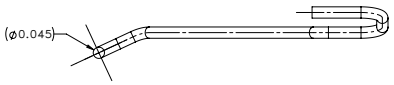

Bottom View
(Of Type 1)

Notes: 1.) Break All Corners.
2.) Dimensions Listed in BOM Do NOT Include Machining Allowances.
3.) Maximum Inside Radius 0.020" Unless Noted.

REMOVE ALL BURRS AND SHARP EDGES

REV	DATE	REVISION DESCRIPTION	BY	APPD
A	6/15/2015	ECO-3707 – Change Control Applies.	Mel Good	Jens Dilling

TOLERANCES UNLESS OTHERWISE SPECIFIED
DECIMALS .X ± 0.1, .XX ± 0.01, .XXX ± 0.005
ANGULAR ± 1.0°
SURFACE FINISH 63 μ Inch
ALL DIMS IN INCHES

TRIUMF
4004 WESBROOK MALL
VANCOUVER, BRITISH COLUMBIA
CANADA V6T-2A3
CANADA'S NATIONAL LABORATORY FOR PARTICLE AND NUCLEAR PHYSICS

DESIGNED TRIUMF/MSG
DRAWN Mel Good
CHECKED Renee Klawitter
REA/WPN # 3060
TRACKING # 0-068

SUB-ASSY: IEX1864
ASSEMBLY: IEX1860

AD2-W Inter-Con. Cond. Wire Type 1 & 2
TITAN Switch Yard Emittance Station
ISAC 1 – TITAN

SCALE 4:1
DATE Feb. 2015
THIRD-ANGLE PROJECTION
DWG NO. IEX1876
SIZE D
SHEET 1 OF 2
REV A

ITEM	DESCRIPTION	MATERIAL	QTY.
1	Dia. 0.045 X 3.699 Lg Wire	AISI 304	1

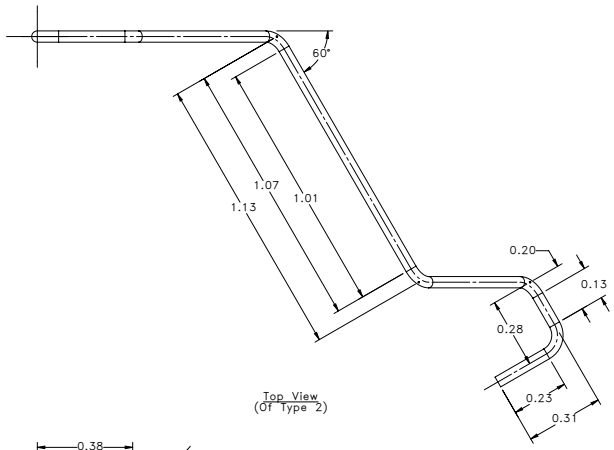

Top View
(Of Type 2)

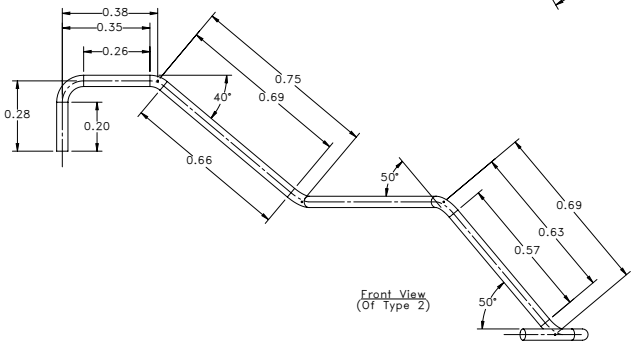

Front View
(Of Type 2)

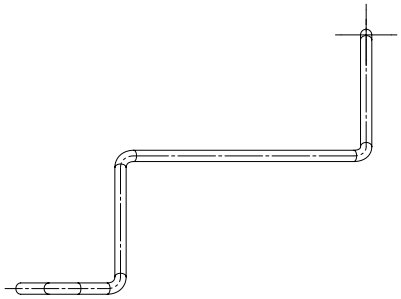

Right Side View
(Of Type 2)

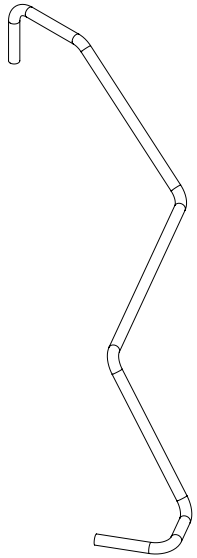

Isometric View
(Of Type 2)
Scale: Full Size.

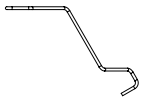

Top View
(Of Type 2)
Scale: Full Size.

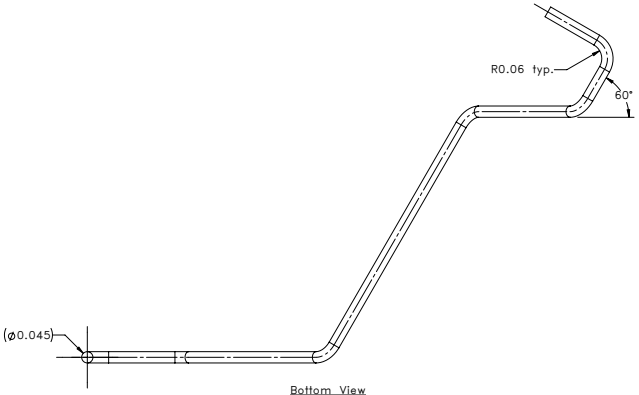

Bottom View
(Of Type 2)

Front View
(Of Type 2)
Scale: Full Size.

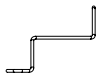

Right Side View
(Of Type 2)
Scale: Full Size.

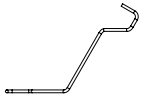

Bottom View
(Of Type 2)
Scale: Full Size.

TRIUMF	4004 WESBROOK MALL VANCOUVER, BRITISH COLUMBIA CANADA V6T-2A3	CANADA'S NATIONAL LABORATORY FOR PARTICLE AND NUCLEAR PHYSICS				
SCALE 4:1		DWG NO.	SIZE	SHEET 2	REV
USE IN CONJUNCTION WITH SHEET No. 1	THIRD-ANGLE PROJECTION	IEX1876	D	OF 2	A

ITEM	DESCRIPTION	MATERIAL	QTY.
1	Dia. 0.045 X 6.388 Lg Wire	AISI 304	1

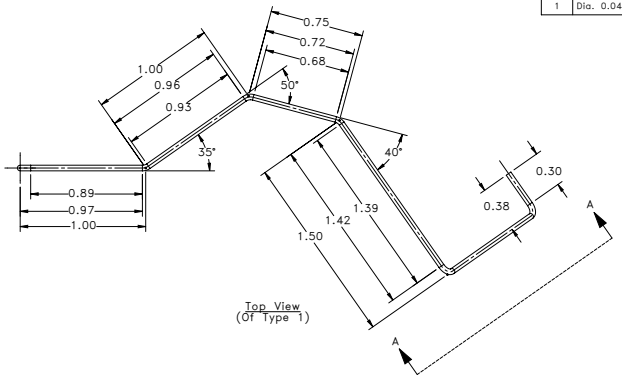

Top View
(Of Type 1)

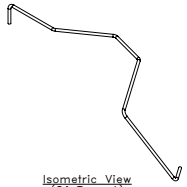

Isometric View
(Of Type 1)
Scale: Full Size.

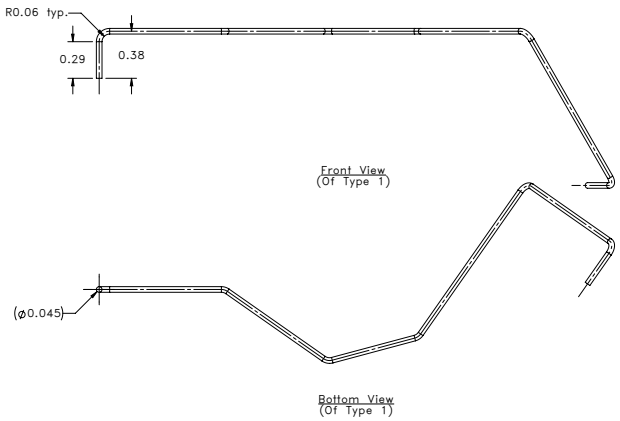

Front View
(Of Type 1)

Bottom View
(Of Type 1)

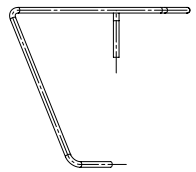

Right Side View
(Of Type 1)

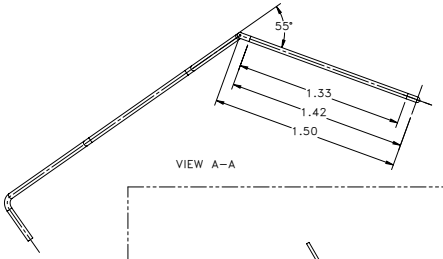

VIEW A–A

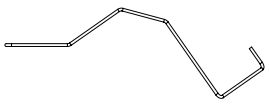

Top View
(Of Type 1)
Scale: Full Size.

Front View
(Of Type 1)
Scale: Full Size.

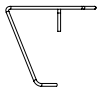

Right Side View
(Of Type 1)
Scale: Full Size.

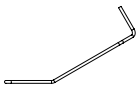

Top View
(Of Type 2)
Scale: Full Size.

Front View
(Of Type 2)
Scale: Full Size.

Right Side View
(Of Type 2)
Scale: Full Size.

Notes: 1.) Break All Corners.
2.) Dimensions Listed in BOM Do NOT Include Machining Allowances.
3.) Maximum Inside Radius 0.020" Unless Noted.

ITEM	DESCRIPTION	MATERIAL	QTY.
1	Dia. 0.045 X 3.182 Lg Wire	AISI 304	1

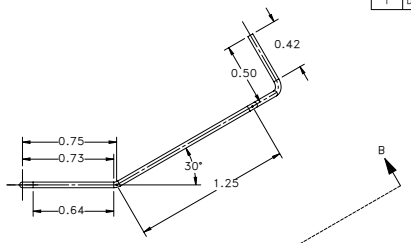

Top View
(Of Type 2)

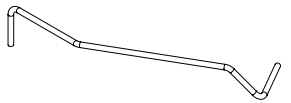

Isometric View
(Of Type 2)

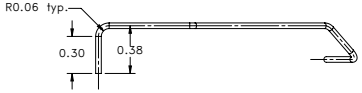

Front View
(Of Type 2)

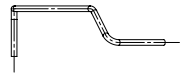

Right Side View
(Of Type 2)

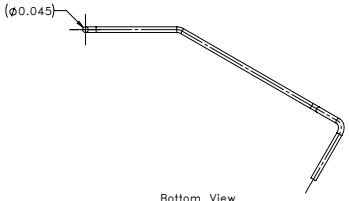

Bottom View
(Of Type 2)

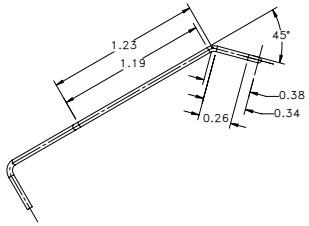

VIEW B–B

DIMENSIONS QUOTED ARE FINISHED DIMENSIONS, NO ALLOWANCE HAS BEEN MADE FOR MANUFACTURE.

REMOVE ALL BURRS AND SHARP EDGES

TOLERANCES UNLESS OTHERWISE SPECIFIED
DECIMALS .X ± 0.1, .XX ± 0.01, .XXX ± 0.005
ANGULAR ± 1.0°
SURFACE FINISH 63 μ Inch
ALL DIMS IN INCHES

DESIGNED TRIUMF/MSG
DRAWN Mel Good
CHECKED Renee Klawitter
REA/WPN # 3060
TRACKING # 0-068

SUB-ASSY: IEX1864
ASSEMBLY: IEX1860

REV	DATE	REVISION DESCRIPTION	BY	APPD
A	6/15/2015	ECO-3707 – Change Control Applies.	Mel Good	Jens Dilling

TRIUMF
4004 WESBROOK MALL
VANCOUVER, BRITISH COLUMBIA
CANADA V6T-2A3

CANADA'S NATIONAL LABORATORY FOR PARTICLE AND NUCLEAR PHYSICS

AD2–W MCP Cond. Wire Type 1–4
TITAN Switch Yard Emittance Station
ISAC 1 – TITAN

SCALE 2:1
DATE Feb. 2015
THIRD-ANGLE PROJECTION
DWG NO. IEX1877
SIZE D
SHEET 1 OF 2
REV A

ITEM	DESCRIPTION	MATERIAL	QTY.
1	Dia. 0.045 X 6.540 Lg Wire	AISI 304	1

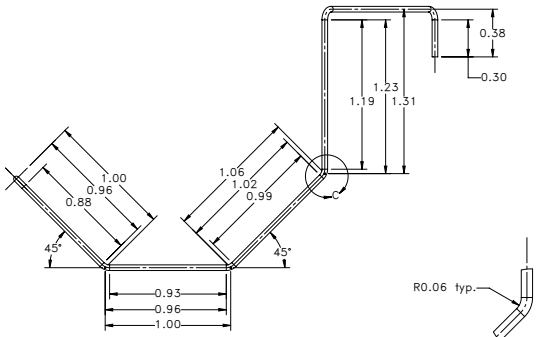

Top View
(Of Type 3)

DETAIL C
SCALE 4 : 1

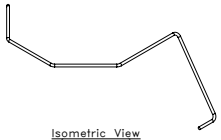

Isometric View
(Of Type 3)
Scale: Full Size.

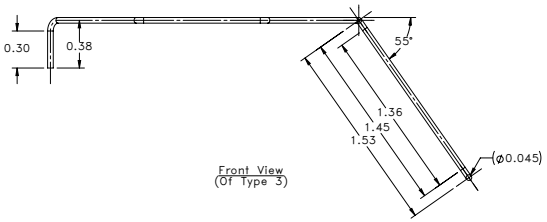

Front View
(Of Type 3)

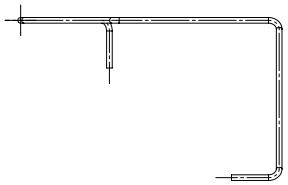

Right Side View
(Of Type 3)

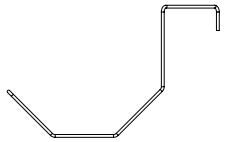

Top View
(Of Type 3)
Scale: Full Size.

Front View
(Of Type 3)
Scale: Full Size.

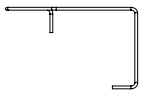

Right Side View
(Of Type 3)
Scale: Full Size.

ITEM	DESCRIPTION	MATERIAL	QTY.
1	Dia. 0.04500 X 3.392 Lg Wire	AISI 304	1

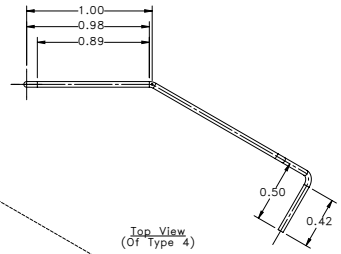

Top View
(Of Type 4)

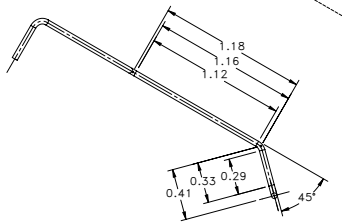

VIEW D–D

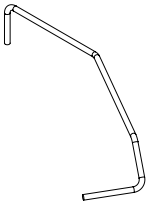

Isometric View
(Of Type 4)

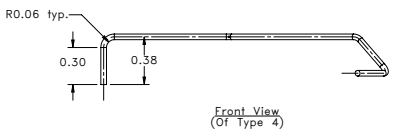

Front View
(Of Type 4)

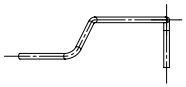

Right Side View
(Of Type 4)

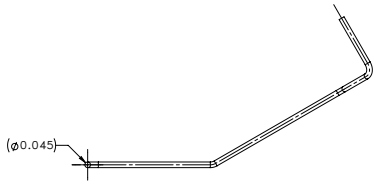

Bottom View
(Of Type 4)

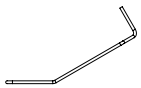

Top View
(Of Type 4)
Scale: Full Size.

Front View
(Of Type 4)
Scale: Full Size.

Right Side View
(Of Type 4)
Scale: Full Size.

TRIUMF
4004 WESBROOK MALL
VANCOUVER, BRITISH COLUMBIA
CANADA V6T-2A3

CANADA'S NATIONAL LABORATORY FOR
PARTICLE AND NUCLEAR PHYSICS

SCALE	DWG NO.	SIZE	SHEET	REV
2:1	IEX1877	D	2 OF 2	A

USE IN CONJUNCTION WITH SHEET No. 1

THIRD-ANGLE PROJECTION

ITEM	REF No.	DESCRIPTION	MATERIAL	QTY.
1	IEX1879	AD2–W Male Conductor Bar	BeCu	1
2	IEX1880	AD2–W Chowdhury Contact Spring	BeCu	1
100		#0–80 X 1/16 Lg Cup Piont Hex Drive Set Screw	SS	1
101	Stores # 1–2/5051	#4–40 X 1/8 Lg Cup Piont Hex Drive Set Screw	SS	1
200	9232000	1 1/3 CF 5kV SHV Recessed Insulator Feed Thru" (MDC Vacuum Products LLC. Part # Quoted or Equiv.)	SS & Ceramic	1

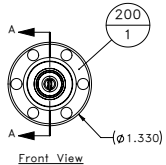

Front View

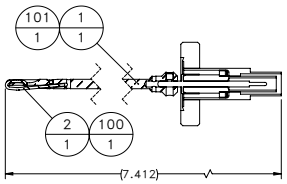

SECTION A–A
(Replaces Right Side View)

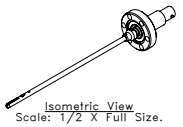
Isometric View
Scale: 1/2 X Full Size.

Note: UHV Cleanliness Standards MUST Be Followed and Maintained During the Complete Assembly.
Also Refer to Document 44430; "TRIUMF UHV Cleaning and Assembly Procedures"

Notes:
1.) Quantities Listed in BOM are Required to Assemble and/or Install One (1) Assembly as Drawn.
2.) All Vacuum Surfaces in this Assembly and/or Installation MUST be Cleaned to Ultra High Vacuum (UHV) Standards. Refer to Document 44430; "TRIUMF UHV Cleaning and Assembling Procedures" Located on DocuShare.
3.) UHV Cleanliness Standards MUST be Followed and Maintained During the Complete Installation or Assembly.

REV	DATE	REVISION DESCRIPTION	BY	APPD
A	6/15/2015	ECO–3707 – Change Control Applies.	Mel Good	Jens Dilling

TOLERANCES UNLESS OTHERWISE SPECIFIED
DECIMALS .X ± 0.1
.XX ± 0.01
.XXX ± 0.005
ANGULAR ± 1.0°
SURFACE FINISH 63 µ inch
ALL DIMS IN INCHES

TRIUMF
4004 WESBROOK MALL
VANCOUVER, BRITISH COLUMBIA
CANADA V6T–2A3
CANADA'S NATIONAL LABORATORY FOR PARTICLE AND NUCLEAR PHYSICS

DESIGNED TRIUMF/MSG
DRAWN Mel Good
CHECKED Renne Klawitter
REA/WPN # 3060
TRACKING # 0–068

SUB–ASSY IEX1862
ASSEMBLY IEX1860

AD2–W Cond. Bar Assembly
TITAN Switch Yard Emittance Station
ISAC 1 – TITAN

SCALE 1:1
DATE Feb. 2015
THIRD–ANGLE PROJECTION
DWG NO. IEX1878
SIZE B
SHEET 1 OF 1
REV A

ITEM	DESCRIPTION	MATERIAL	QTY.
1	Dia. 0.375 X 5.750 Lg Round Bar	BeCu	1

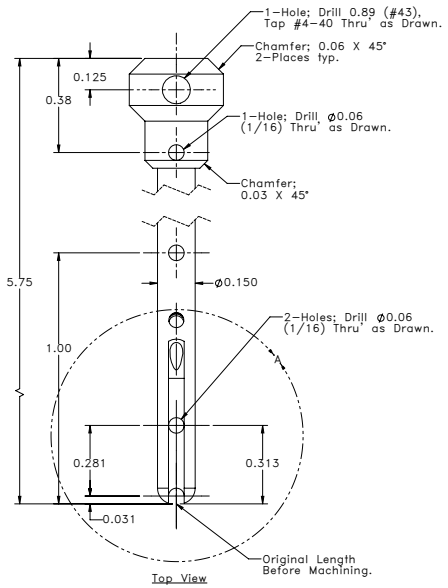

Top View

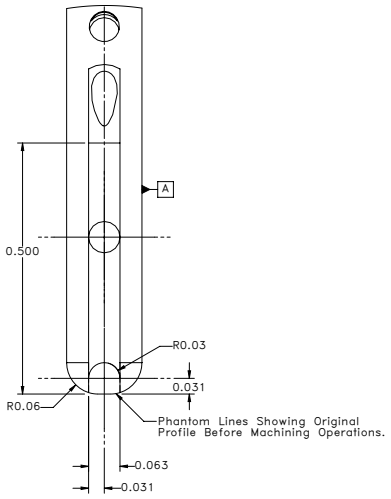

DETAIL A
SCALE 8 : 1

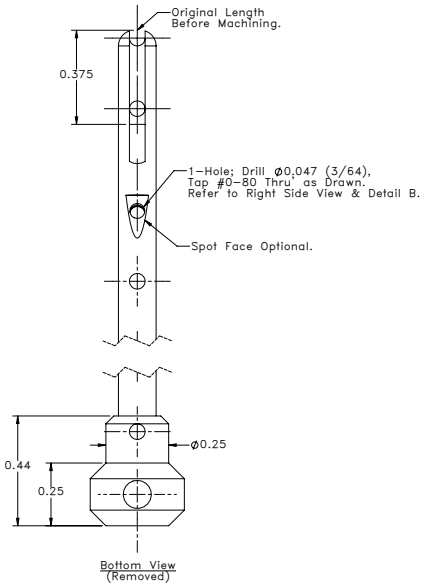

Bottom View
(Removed)

DIMENSIONS QUOTED ARE FINISHED DIMENSIONS, NO ALLOWANCE HAS BEEN MADE FOR MANUFACTURE.

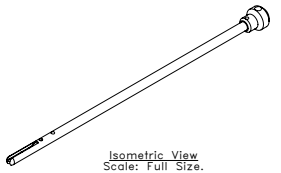

Isometric View
Scale: Full Size.

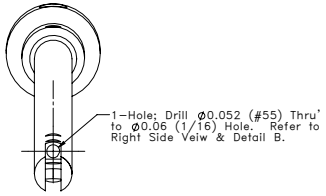

VIEW C–C
⌒5.0°
(Removed)

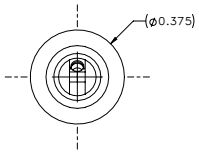

Front View

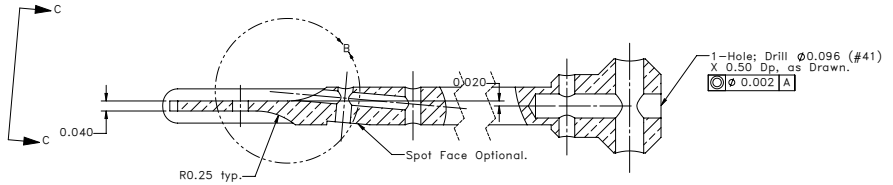

Right Side View

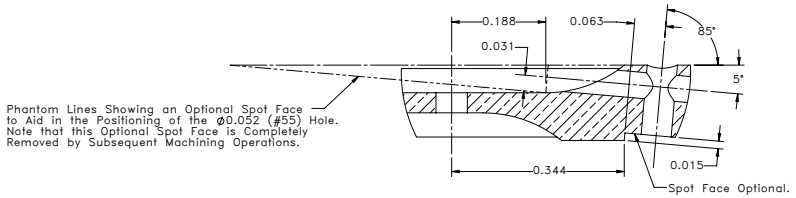

DETAIL B
SCALE 8 : 1

Notes: 1.) Break All Corners.
2.) Dimensions Listed in BOM Do NOT Include Machining Allowances.
3.) Maximum Inside Radius 0.020" Unless Noted.

REMOVE ALL BURRS AND SHARP EDGES

TOLERANCES UNLESS OTHERWISE SPECIFIED
DECIMALS .X ± 0.1, .XX ± 0.01, .XXX ± 0.005
ANGULAR ± 1.0°
SURFACE FINISH 63 μ Inch

ALL DIMS IN INCHES

DESIGNED	TRIUMF/MSG
DRAWN	Mel Good
CHECKED	Renee Klawitter
REA/WPN #	3060
TRACKING #	0–068
SUB–ASSY:	IEX1878
ASSEMBLY:	IEX1860

REV	DATE	REVISION DESCRIPTION	BY	APPD
A	6/15/2015	ECO–3707 – Change Control Applies.	Mel Good	Jens Dilling

TRIUMF
4004 WESBROOK MALL
VANCOUVER, BRITISH COLUMBIA
CANADA V6T–2A3

CANADA'S NATIONAL LABORATORY FOR PARTICLE AND NUCLEAR PHYSICS

AD2–W Male Conductor Bar
TITAN Switch Yard Emittance Station
ISAC 1 – TITAN

SCALE	DWG NO.	SIZE	SHEET	REV
4:1	IEX1879	D	1 OF 1	A

THIRD–ANGLE PROJECTION

DATE Feb. 2015

ITEM	DESCRIPTION	MATERIAL	QTY.
1	Dia. 0.039 X 1.35 Lg Wire	BeCu	1

DIMENSIONS QUOTED ARE FINISHED DIMENSIONS, NO ALLOWANCE HAS BEEN MADE FOR MANUFACTURE.

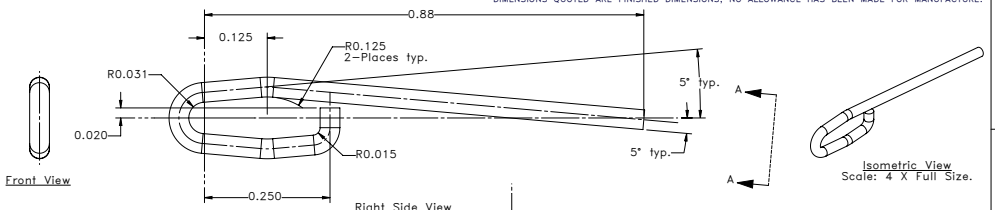

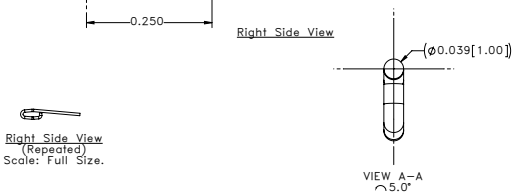

Right Side View
(Repeated)
Scale: Full Size.

Notes: 1.) Break All Corners.
2.) Dimensions Listed in BOM Do NOT Include Machining Allowances.
3.) Maximum Inside Radius 0.020" Unless Noted.

REMOVE ALL BURRS AND SHARP EDGES

REV	DATE	REVISION DESCRIPTION	BY	APPD
A	6/15/2015	ECO–3707 – Change Control Applies.	Mel Good	Jens Dilling

TOLERANCES UNLESS OTHERWISE SPECIFIED
DECIMALS .X ± 0.1
.XX ± 0.01
.XXX ± 0.005
ANGULAR ± 1.0°
SURFACE FINISH 63 µ inch

ALL DIMS IN INCHES

DESIGNED TRIUMF/MSG
DRAWN Mel Good
CHECKED Renee Klawitter
REA/WPN # 3060
TRACKING # 0–068

SUB–ASSY IEX1878
ASSEMBLY IEx1860

TRIUMF
4004 WESBROOK MALL
VANCOUVER, BRITISH COLUMBIA
CANADA V6T–2A3

CANADA'S NATIONAL LABORATORY FOR PARTICLE AND NUCLEAR PHYSICS

AD2–W Chowdhury Contact Spring
TITAN Switch Yard Emittance Station
ISAC 1 – TITAN

SCALE 8:1
DATE Feb. 2015
THIRD–ANGLE PROJECTION
DWG NO. IEX1880
SIZE B
SHEET 1 OF 1
REV A

B Drawings of the RFA detector

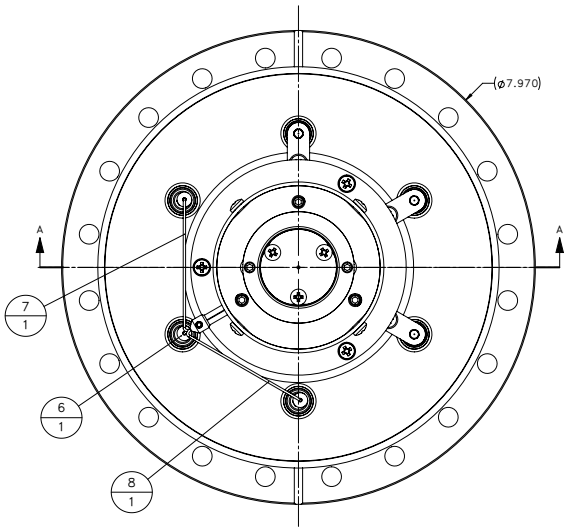

Top View

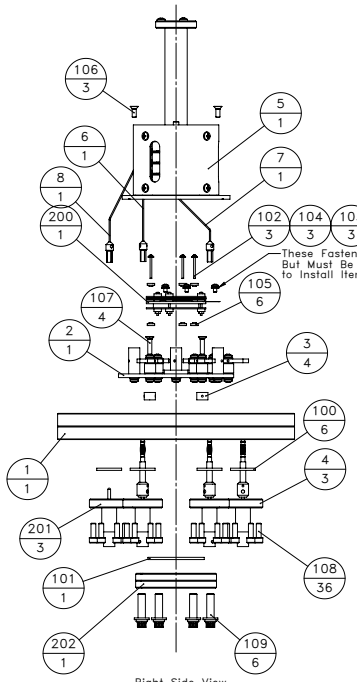

These Fasteners Belong to Item 2, But Must Be Temporarily Removed to Install Item 200.

Right Side View
Scale: 1/2 X Full Size.
(Exploded)

Refer to Note #2 Concerning the BOM Quantities Column.

ITEM	REF No.	DESCRIPTION	MATERIAL	QTY.
1	IEX1882	RFA Main Mounting Flange	AISI 304	1
2	IEX1883	RFA Mounting Plate Ass'y	Varies	1
3	IEX1887	RFA Mounting Plate Stand-Off	6061-T6	4
4	IEX1888	RFA Conductive Rod Assembly	Varies	3
5	IEX1890	RFA Unit Assembly	SS & Ceramic	1
6	IEX1902	RFA Wire Conductor Ass'y Type 1	SS & Cu	1
7	IEX1902	RFA Wire Conductor Ass'y Type 2	SS & Cu	1
8	IEX1902	RFA Wire Conductor Ass'y Type 3	SS & Cu	1
100	G-133	1 1/3 CF Non-Plated, Copper Gasket (Duniway Stock Room Corp. Part # Quoted or Equiv. (Pkg of 10))	Oxygen Free Cu	6
101	G-275	2 3/4 CF Non-Plated, Standard I.D. Copper Gasket (Duniway Stock Room Corp. Part # Quoted or Equiv. (Pkg of 10))	Oxygen Free Cu	1
102		#0-80 X 3/4 Lg Phillips Drive Pan Hd Machine Screw	SS	3
103		#0 Helical Lock Washer	SS	3
104		#0 Flat Washer Regular Series	SS	3
105	31602	#0 Advanced Performance Detector (APD) Mounting Washer (PHOTONIS USA Inc. Part # Quoted or Equiv.)	Ceramic	6
106		#6-32 X 3/8 Lg Phillips Drive Flat Hd Machine Screw	SS	3
107	F-610-EP	#6-32 X 5/8 Lg Phillips Drive Flat Hd Electropolished Vented Machine Screw (U-C Components Inc. Part # Quoted or Equiv.)	SS	4
108	SAX-32-050	#8-32 X 1/2 Lg Soc Hd Cap Screw c/w Washer (Pkg. of 25 Cap Screws & 25 Washers) (Duniway Stockroom Corp. Part # Quoted or Equiv.)	Ag Plated SS	36
109	SBX-28-087	1/4-28 X 7/8 Lg 12 Point Cap Screw c/w Washer (Pkg. of 25 Cap Screws & 25 Washers) (Duniway Stockroom Corp. Part # Quoted or Equiv.)	Ag Plated SS	6
200	APD 2 PS 25/12/10/ 12 D 60:1 P20	Microchannel Plate Detector c/w Phosphor Screen (PHOTONIS USA Inc. Part # Quoted or Equiv.)	SS & Ceramic	1
201	9232000	1 1/3 CF 5kV SHV Recessed Insulator Feed Thru (MDC Vacuum Products LLC. Part # Quoted or Equiv.)	SS & Ceramic	3
202	VPZL-275	2 3/4" CF Kodial Glass Viewport (Kurt J Lesker Co. Part # Quoted or Equiv.)	SS & Glass	1

Note: UHV Cleanliness Standards MUST Be Followed and Maintained During the Complete Assembly.
Also Refer to Document 44430; "TRIUMF UHV Cleaning and Assembly Procedures"

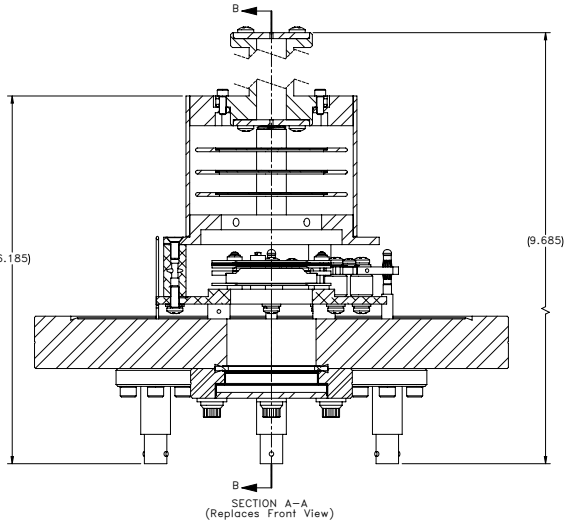

SECTION A-A
(Replaces Front View)

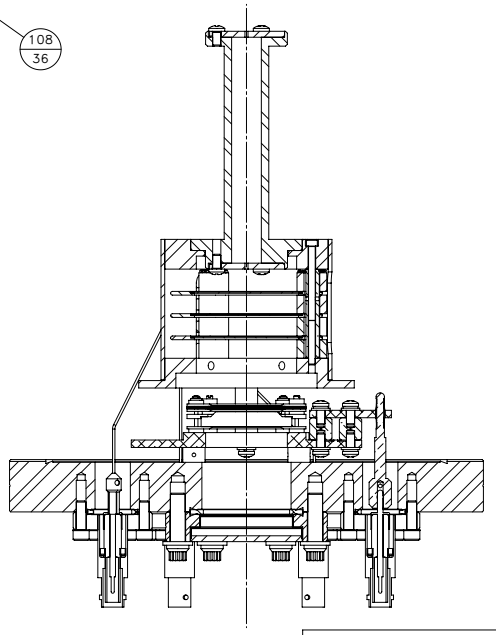

SECTION B-B
(Replaces Right Side View)

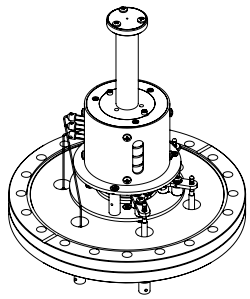

Isometric View
Scale: 1/2 X Full Size.

Notes:
1.) Quantities Listed in BOM are Required to Assemble and/or Install One (1) Assembly as Drawn.
2.) When Sets and/or Packages are Described in the BOM, the Number of Individual or Least Used Part is Listed in the Quantities Column. (Ex. Bolt, Washer & Platenut Sets; the Quantity of Platenuts is Listed as it is Understood that Two (2) Bolts & Two (2) Washers are Required for Each Platenut.)
3.) All Vacuum Surfaces in this Assembly and/or Installation MUST be Cleaned to Ultra High Vacuum (UHV) Standards. Refer to Document 44430; "TRIUMF UHV Cleaning and Assembling Procedures" Located on DocuShare.
4.) UHV Cleanliness Standards MUST be Followed and Maintained During the Complete Installation or Assembly.

REV	DATE	REVISION DESCRIPTION	BY	APPD
A	6/18/2015	ECO-3707 - Change Control Applies.	Mel Good	Jens Dilling

TOLERANCES UNLESS OTHERWISE SPECIFIED
DECIMALS .X ± 0.1, .XX ± 0.01, .XXX ± 0.005
ANGULAR ± 1.0°
SURFACE FINISH 63 µ inch
ALL DIMS IN INCHES

DESIGNED TRIUMF/MSG
DRAWN Mel Good
CHECKED Renee Klawitter
REA/WPN # 3060
TRACKING # 0-068
SUB-ASSY:
ASSEMBLY: IEX1860

TRIUMF
4004 WESBROOK MALL
VANCOUVER, BRITISH COLUMBIA
CANADA V6T-2A3
CANADA'S NATIONAL LABORATORY FOR PARTICLE AND NUCLEAR PHYSICS

Ass'y (Retarding Field Analyzer (RFA)) TITAN Switch Yard Emittance Station ISAC 1 - TITAN

SCALE 1:1
DATE Feb. 2015
THIRD-ANGLE PROJECTION
DWG NO. IEX1881
SIZE D
SHEET 1 OF 1
REV A

ITEM	DESCRIPTION	MATERIAL	QTY.
1	8 CF to 2 3/4 CF Reducing Flange (Kurt J. Lesker Co. Part # RF800X275 or Equiv.)	AISI 304	1

DIMENSIONS QUOTED ARE FINISHED DIMENSIONS, NO ALLOWANCE HAS BEEN MADE FOR MANUFACTURE.

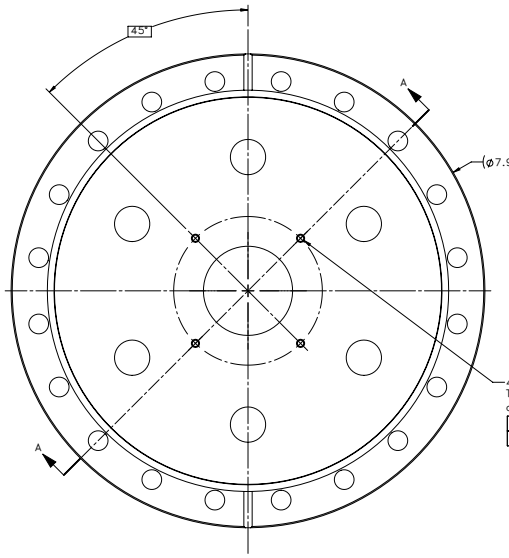

Top View

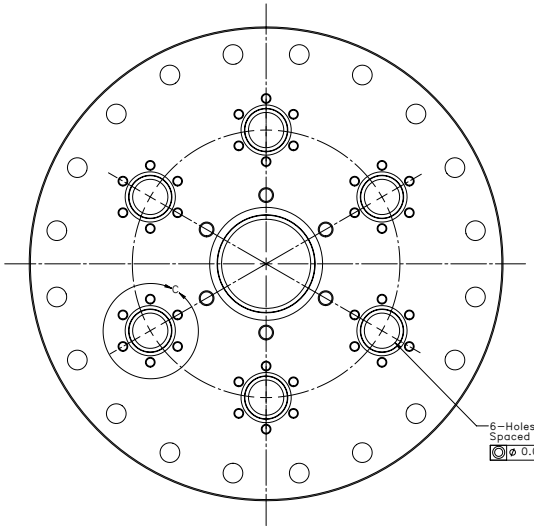

Bottom View
(Removed)

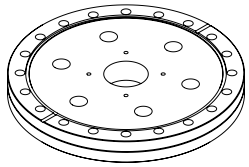

Isometric View
Scale: 1/2 X Full Size.

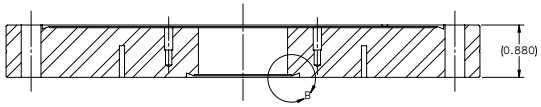

SECTION A–A
(Replaces Front View)

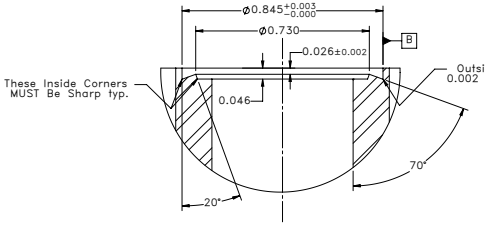

DETAIL E
SCALE 4 : 1
(Details Represented Here
typ. for all Six (6) Instances)

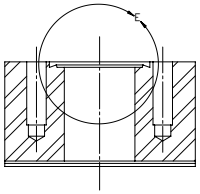

SECTION D–D
SCALE 2 : 1

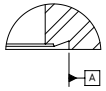

DETAIL B
SCALE 2 : 1

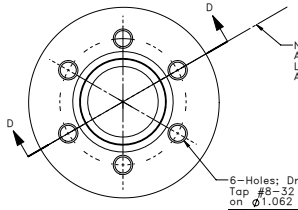

DETAIL C
SCALE 2 : 1

Notes: 1.) Break All Corners.
2.) Dimensions Listed in BOM Do NOT Include Machining Allowances.
3.) Maximum Inside Radius 0.020" Unless Noted.

REMOVE ALL BURRS AND SHARP EDGES

TOLERANCES UNLESS OTHERWISE SPECIFIED
DECIMALS .X ± 0.1
.XX ± 0.01
.XXX ± 0.005
ANGULAR ± 1.0°
SURFACE FINISH 63 μ inch

ALL DIMS IN INCHES

DESIGNED	TRIUMF/MSG
DRAWN	Mel Good
CHECKED	Renee Klawitter
REA/WPN #	3060
TRACKING #	0-068
SUB-ASSY:	IEX1881
ASSEMBLY:	IEX1860

REV	DATE	REVISION DESCRIPTION	BY	APPD
A	6/9/2015	ECO–3707 – Change Control Applies.	Mel Good	Jens Dilling

TRIUMF
4004 WESBROOK MALL
VANCOUVER, BRITISH COLUMBIA
CANADA V6T–2A3

CANADA'S NATIONAL LABORATORY FOR PARTICLE AND NUCLEAR PHYSICS

RFA Main Mounting Flange
TITAN Switch Yard Emittance Station
ISAC 1 – TITAN

SCALE	DWG NO.	SIZE	SHEET	REV
1:1	IEX1882	D	1 OF 1	A

DATE Feb. 2015

THIRD ANGLE PROJECTION

ITEM	REF No.	DESCRIPTION	MATERIAL	QTY.
1	IEX1884	RFA Mounting Plate	6061-T6	1
2	IEX1885	RFA Conductor Bar	Oxygen Free Copper	3
3	IEX1886	RFA Stand-Off	6061-T6	3
100	7712	3/8 Dia. X 3/8 Lg Threaded Commercial Grade Ceramic Standoff (KEYSTONE Electronics Corp Cat. # Quoted or Equiv.)	Ceramic	6
102	Stores # 1-2/2015	#4-40 X 3/16 Lg Phillips Drive Pan Hd Machine Screw	SS	3
103	Stores # 1-2/3007	#4 Helical Lock Washer	SS	3
104		#4 Flat Washer Narrow Series	SS	3
105	P-605-EP	#6-32 X 5/16 Lg Phillips Drive Pan Hd Electropolished Vented Machine Screw (U-C Components Inc. Part # Quoted or Equiv.)	SS	12
106	Stores # 1-2/2047	#6-32 X 3/8 Lg Phillips Drive Pan Hd Machine Screw	SS	3
107	Stores # 1-2/3013	#6 Helical Lock Washer	SS	15
108		#6 Flat Washer Narrow Series	SS	15

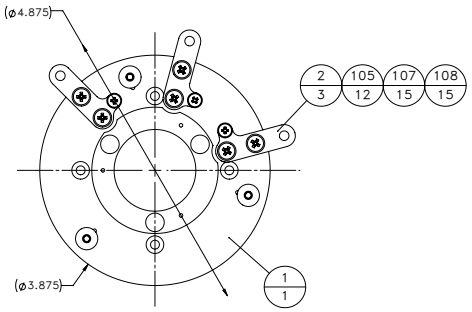

Top View

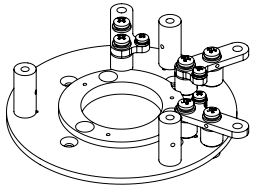
Isometric View

Note: UHV Cleanliness Standards MUST Be Followed and Maintained During the Complete Assembly.
Also Refer to Document 44430; "TRIUMF UHV Cleaning and Assembly Procedures"

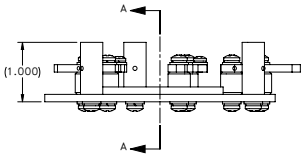

Front View

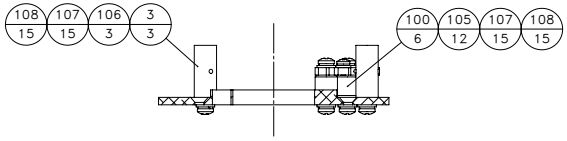

SECTION A-A
(Replaces Right Side View)

Notes:
1.) Quantities Listed in BOM are Required to Assemble and/or Install One (1) Assembly as Drawn.
2.) All Vacuum Surfaces in this Assembly and/or Installation MUST be Cleaned to Ultra High Vacuum (UHV) Standards. Refer to Document 44430; "TRIUMF UHV Cleaning and Assembling Procedures" Located on DocuShare.
3.) UHV Cleanliness Standards MUST be Followed and Maintained During the Complete Installation or Assembly.

REV	DATE	REVISION DESCRIPTION	BY	APPD
A	6/9/2015	ECO-3707 - Change Control Applies.	Mel Good	Jens Dilling

TOLERANCES UNLESS OTHERWISE SPECIFIED
DECIMALS .X ± 0.1
.XX ± 0.01
.XXX ± 0.005
ANGULAR ± 1.0°
SURFACE FINISH 63 µ inch
ALL DIMS IN INCHES

TRIUMF
4004 WESBROOK MALL
VANCOUVER, BRITISH COLUMBIA
CANADA V6T-2A3
CANADA'S NATIONAL LABORATORY FOR PARTICLE AND NUCLEAR PHYSICS

DESIGNED TRIUMF/MSG	SUB-ASSY IEX1881
DRAWN Mel Good	
CHECKED Renee Klawitter	ASSEMBLY IEX1860
REA/WPN # 3060	
TRACKING # 0-068	

RFA Mounting Plate Ass'y
TITAN Switch Yard Emittance Station
ISAC 1 - TITAN

SCALE	DWG NO.	SIZE	SHEET	REV
1:1	IEX1883	C	1 OF 1	A
DATE Feb. 2015				

THIRD-ANGLE PROJECTION

ITEM	DESCRIPTION	MATERIAL	QTY.
1	Dia. 3.875 X 0.250 Thk Disk	6061-T6	1

DIMENSIONS QUOTED ARE FINISHED DIMENSIONS, NO ALLOWANCE HAS BEEN MADE FOR MANUFACTURE.

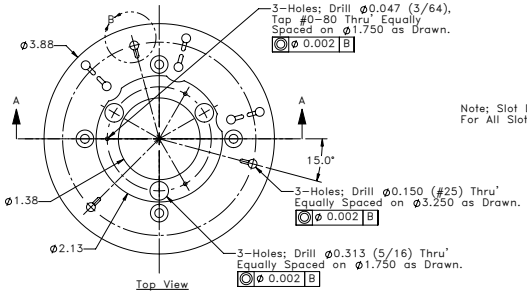

Top View

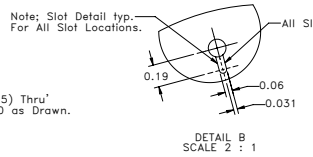

DETAIL B
SCALE 2 : 1

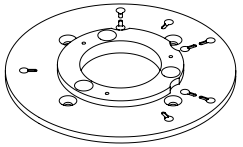

Isometric View
Scale: 1/4 X Full Size.

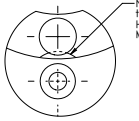

DETAIL C
SCALE 2 : 1

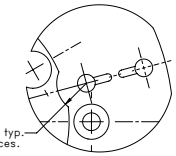

DETAIL D
SCALE 2 : 1

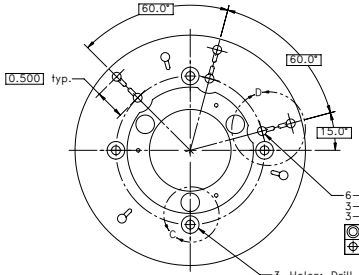

Top View
(Repeated)

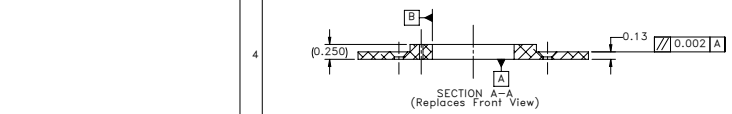

SECTION A-A
(Replaces Front View)

REMOVE ALL BURRS AND SHARP EDGES

Notes: 1.) Break All Corners.
2.) Dimensions Listed in BOM Do NOT Include Machining Allowances.
3.) Maximum Inside Radius 0.020" Unless Noted.

REV	DATE	REVISION DESCRIPTION	BY	APPD
A	6/9/2015	ECO-3707 – Change Control Applies.	Mel Good	Jens Dilling

TOLERANCES UNLESS OTHERWISE SPECIFIED
DECIMALS .X ± 0.1
.XX ± 0.01
.XXX ± 0.005
ANGULAR ± 1.0°
SURFACE FINISH 63 μ inch
ALL DIMS IN INCHES

DESIGNED TRIUMF/MSG
DRAWN Mel Good
CHECKED Renee Klawitter
REA/WPN # 3060
TRACKING # 0-068

SUB-ASSY IEX1883
ASSEMBLY IEX1860

TRIUMF
4004 WESBROOK MALL
VANCOUVER, BRITISH COLUMBIA
CANADA V6T-2A3

CANADA'S NATIONAL LABORATORY FOR PARTICLE AND NUCLEAR PHYSICS

RFA Mounting Plate
TITAN Switch Yard Emittance Station
ISAC 1 – TITAN

SCALE 1:1
DATE Feb. 2015
THIRD-ANGLE PROJECTION
DWG NO. IEX1884
SIZE C
SHEET 1 OF 1
REV A

ITEM	DESCRIPTION	MATERIAL	QTY.
1	1.375 Lg X 0.656 W X 0.125 Thk Sheet	Oxygen Free Copper	1

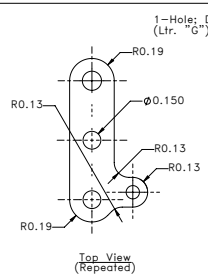

Top View
(Repeated)

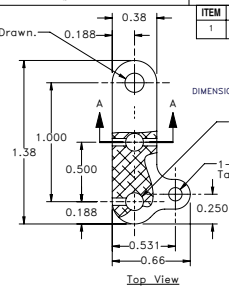

Top View

DIMENSIONS QUOTED ARE FINISHED DIMENSIONS, NO ALLOWANCE HAS BEEN MADE FOR MANUFACTURE.

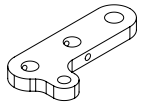
Isometric View


Right Side View
(Removed)

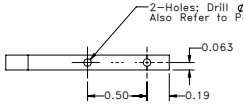

Left Side View

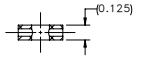

SECTION A–A
(Replaces Front View)

Notes: 1.) Break All Corners.
2.) Dimensions Listed in BOM Do NOT Include Machining Allowances.
3.) Maximum Inside Radius 0.020" Unless Noted.

REMOVE ALL BURRS AND SHARP EDGES

REV	DATE	REVISION DESCRIPTION	BY	APPD
A	6/9/2015	ECO–3707 – Change Control Applies.	Mel Good	Jens Dilling

TOLERANCES UNLESS OTHERWISE SPECIFIED
DECIMALS .X ± 0.1
.XX ± 0.01
.XXX ± 0.005
ANGULAR ± 1.0°
SURFACE FINISH 63 μ inch
ALL DIMS IN INCHES

DESIGNED TRIUMF/MSG
DRAWN Mel Good
CHECKED Renee Klawitter
REA/WPN # 3060
TRACKING # 0-068
SUB-ASSY IEX1883
ASSEMBLY IEX1860

TRIUMF
4004 WESBROOK MALL
VANCOUVER, BRITISH COLUMBIA
CANADA V6T–2A3
CANADA'S NATIONAL LABORATORY FOR PARTICLE AND NUCLEAR PHYSICS

RFA Conductor Bar
TITAN Switch Yard Emittance Station
ISAC 1 – TITAN

SCALE 2:1
DATE Feb. 2015
THIRD-ANGLE PROJECTION
DWG NO. IEX1885
SIZE B
SHEET 1 OF 1
REV A

ITEM	DESCRIPTION	MATERIAL	QTY.
1	Dia. 0.375 X 0.875 Lg Round Bar	6061-T6	1

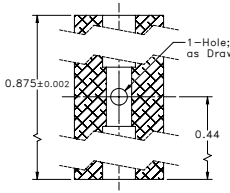

SECTION A-A
(Replaces Top View)

DIMENSIONS QUOTED ARE FINISHED DIMENSIONS, NO ALLOWANCE HAS BEEN MADE FOR MANUFACTURE.

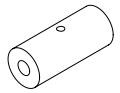

Isometric View
Scale: 2 X Full Size.

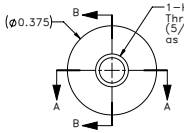

Front View

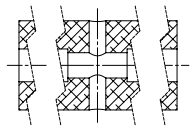

SECTION B-B
(Replaces Right
Side View)

Notes: 1.) Break All Corners.
2.) Dimensions Listed in BOM Do NOT Include Machining Allowances.
3.) Maximum Inside Radius 0.020" Unless Noted.

REMOVE ALL BURRS AND SHARP EDGES

REV	DATE	REVISION DESCRIPTION	BY	APPD
A	6/9/2015	ECO-3707 - Change Control Applies.	Mel Good	Jens Dilling

TOLERANCES UNLESS OTHERWISE SPECIFIED
DECIMALS .X ± 0.1
.XX ± 0.01
.XXX ± 0.005
ANGULAR ± 1.0°
SURFACE FINISH 63 µ inch
ALL DIMS IN INCHES

TRIUMF
4004 WESBROOK MALL
VANCOUVER, BRITISH COLUMBIA
CANADA V6T-2A3

CANADA'S NATIONAL LABORATORY FOR PARTICLE AND NUCLEAR PHYSICS

DESIGNED TRIUMF/MSG
DRAWN Mel Good
CHECKED Renee Klawitter
REA/WPN # 3060
TRACKING # 0-068

SUB-ASSY IEX1883
ASSEMBLY IEX1860

RFA Stand-Off
TITAN Switch Yard Emittance Station
ISAC 1 - TITAN

SCALE 4:1
DATE Feb. 2015
THIRD-ANGLE PROJECTION
DWG NO. IEX1886
SIZE B
SHEET 1 OF 1
REV A

ITEM	DESCRIPTION	MATERIAL	QTY.
1	Dia. 0.375 X 0.250 Lg Round Bar	6061-T6	1

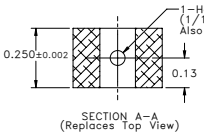

SECTION A-A
(Replaces Top View)

DIMENSIONS QUOTED ARE FINISHED DIMENSIONS, NO ALLOWANCE HAS BEEN MADE FOR MANUFACTURE.

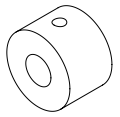

Isometric View

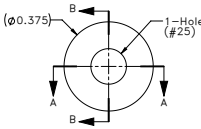

Front View

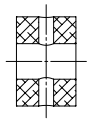

SECTION B-B
(Replaces Right
Side View)

Notes: 1.) Break All Corners.
2.) Dimensions Listed in BOM Do NOT Include Machining Allowances.
3.) Maximum Inside Radius 0.020" Unless Noted.

REMOVE ALL BURRS AND SHARP EDGES

REV	DATE	REVISION DESCRIPTION	BY	APPD
A	6/9/2015	ECO-3707 - Change Control Applies.	Mel Good	Jens Dilling

TOLERANCES UNLESS OTHERWISE SPECIFIED
DECIMALS .X ± 0.1
.XX ± 0.01
.XXX ± 0.005
ANGULAR ± 1.0°
SURFACE FINISH 63 µ inch
ALL DIMS IN INCHES

TRIUMF
4004 WESBROOK MALL
VANCOUVER, BRITISH COLUMBIA
CANADA V6T-2A3

CANADA'S NATIONAL LABORATORY FOR PARTICLE AND NUCLEAR PHYSICS

DESIGNED TRIUMF/MSG
DRAWN Mel Good
CHECKED Renee Klawitter
REA/WPN # 3060
TRACKING # 0-068

SUB-ASSY IEX1881
ASSEMBLY IEX1860

RFA Mounting Plate Stand-Off
TITAN Switch Yard Emittance Station
ISAC 1 - TITAN

SCALE 4:1
DATE Feb. 2015
THIRD-ANGLE PROJECTION
DWG NO. IEX1887
SIZE B
SHEET 1 OF 1
REV A

ITEM	REF No.	DESCRIPTION	MATERIAL	QTY.
1	IEX1889	Conductor Rod	BeCu	1
100	Stores # 1-2/5051	#4-40 X 1/8 Lg Cup Piont Hex Drive Set Screw	SS	1
101	TL-331CS	Banana Plug Spring (Mueller Electric Part No. Quoted) (Purchase from Radar Inc.)	BeCu	1
200	9232000	1 1/3 CF 5kV SHV Recessed Insulator Feed Thru (MDC Vacuum Products LLC. Part # Quoted or Equiv.)	SS & Ceramic	1

Note: UHV Cleanliness Standards MUST Be Followed and Maintained During the Complete Assembly.
Also Refer to Document 44430; "TRIUMF UHV Cleaning and Assembly Procedures"

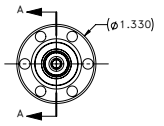

Front View

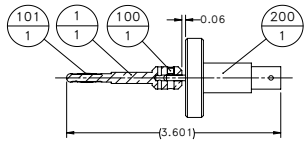

SECTION A-A
(Replaces Right Side View)

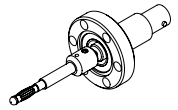

Isometric View

Notes:
1.) Quantities Listed in BOM are Required to Assemble and/or Install One (1) Assembly as Drawn.
2.) All Vacuum Surfaces in this Assembly and/or Installation MUST be Cleaned to Ultra High Vacuum (UHV) Standards. Refer to Document 44430; "TRIUMF UHV Cleaning and Assembling Procedures" Located on DocuShare.
3.) UHV Cleanliness Standards MUST be Followed and Maintained During the Complete Installation or Assembly.

REV	DATE	REVISION DESCRIPTION	BY	APPD
A	6/9/2015	ECO-3707 - Change Control Applies.	Mel Good	Jens Dilling

TOLERANCES UNLESS OTHERWISE SPECIFIED
DECIMALS .X ± 0.1
.XX ± 0.01
.XXX ± 0.005
ANGULAR ± 1.0°
SURFACE FINISH 63 µ inch
ALL DIMS IN INCHES

TRIUMF
4004 WESBROOK MALL
VANCOUVER, BRITISH COLUMBIA
CANADA V6T-2A3

CANADA'S NATIONAL LABORATORY FOR PARTICLE AND NUCLEAR PHYSICS

DESIGNED TRIUMF/MSG
DRAWN Mel Good
CHECKED Renee Kiawitter
REA/WPN # 3060
TRACKING # 0-068

SUB-ASSY IEX1881
ASSEMBLY IEX1860

RFA Conductive Rod Assembly
TITAN Switch Yard Emittance Station
ISAC 1 - TITAN

SCALE 1:1
DATE Feb. 2015
THIRD-ANGLE PROJECTION
DWG NO. IEX1888
SIZE B
SHEET 1 OF 1
REV A

ITEM	DESCRIPTION	MATERIAL	QTY.
1	Dia. 0.375 X 1.938 Lg Round Bar	BeCu	1

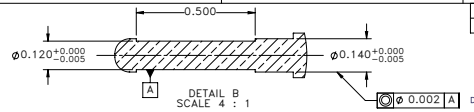

DIMENSIONS QUOTED ARE FINISHED DIMENSIONS, NO ALLOWANCE HAS BEEN MADE FOR MANUFACTURE.

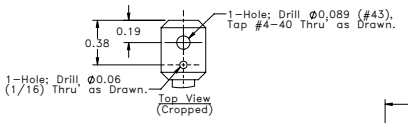

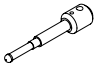

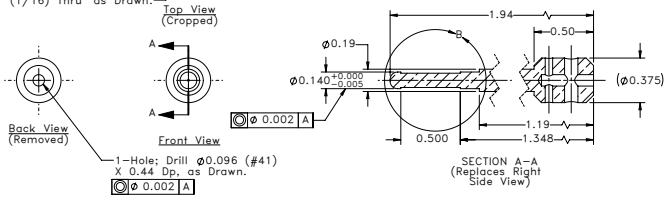

Notes: 1.) Break All Corners.
2.) Dimensions Listed in BOM Do NOT Include Machining Allowances.
3.) Maximum Inside Radius 0.020" Unless Noted.

REMOVE ALL BURRS AND SHARP EDGES

REV	DATE	REVISION DESCRIPTION	BY	APPD
A	6/9/2015	ECO−3707 − Change Control Applies.	Mel Good	Jens Dilling

TOLERANCES UNLESS OTHERWISE SPECIFIED
DECIMALS .X ± 0.1
.XX ± 0.01
.XXX ± 0.005
ANGULAR ± 1.0°
SURFACE FINISH 63 µ inch
ALL DIMS IN INCHES

TRIUMF
4004 WESBROOK MALL
VANCOUVER, BRITISH COLUMBIA
CANADA V6T−2A3
CANADA'S NATIONAL LABORATORY FOR PARTICLE AND NUCLEAR PHYSICS

DESIGNED TRIUMF/MSG
DRAWN Mel Good
CHECKED Renee Kiawitter
REA/WPN # 3060
TRACKING # 0−068

SUB−ASSY IEX1888
ASSEMBLY IEX1860

Conductor Rod
TITAN Switch Yard Emittance Station
ISAC 1 − TITAN

SCALE 2:1
DATE Feb. 2015
THIRD−ANGLE PROJECTION
DWG NO. IEX1889
SIZE B
SHEET 1 OF 1
REV A

ITEM	REF No.	DESCRIPTION	MATERIAL	QTY.
1	IEX1891	RFA Unit Outer Housing	AISI 304	1
2	IEX1892	RFA Unit Internal Assembly	SS & Ceramic	1
3	IEX1899	RFA Orifice Assembly	SS	1
100		#4-40 X 5/16 Lg Soc Hd Cap Screw	SS	2
101	Stores # 1-5/2041	#6-32 X 3/16 Lg Phillips Drive Pan Hd Machine Screw	SS	8

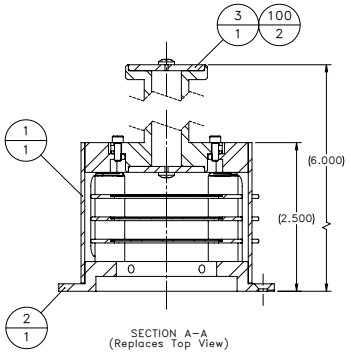

SECTION A–A
(Replaces Top View)

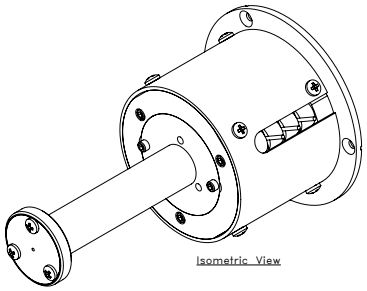

Isometric View

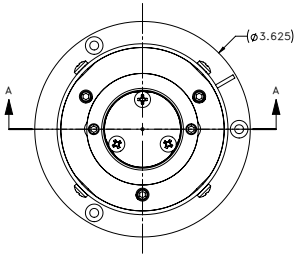

Front View

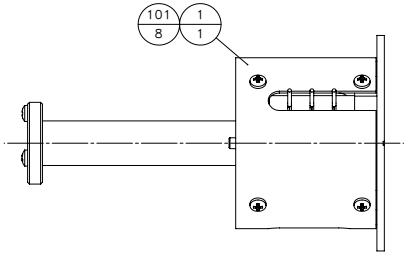

Right Side View

Note: UHV Cleanliness Standards MUST Be Followed and Maintained During the Complete Assembly.
Also Refer to Document 44430; "TRIUMF UHV Cleaning and Assembly Procedures"

Notes:
1.) Quantities Listed in BOM are Required to Assemble and/or Install One (1) Assembly as Drawn.
2.) All Vacuum Surfaces in this Assembly and/or Installation MUST be Cleaned to Ultra High Vacuum (UHV) Standards. Refer to Document 44430; "TRIUMF UHV Cleaning and Assembling Procedures" Located on DocuShare.
3.) UHV Cleanliness Standards MUST be Followed and Maintained During the Complete Installation or Assembly.

REV	DATE	REVISION DESCRIPTION	BY	APPD
A	6/18/2015	ECO-3707 – Change Control Applies.	Mel Good	Jens Dilling

TOLERANCES UNLESS OTHERWISE SPECIFIED
DECIMALS .X ± 0.1
.XX ± 0.01
.XXX ± 0.005
ANGULAR ± 1.0°
SURFACE FINISH 63 μ inch
ALL DIMS IN INCHES

DESIGNED TRIUMF/CC/MSG
DRAWN Mel Good
CHECKED Renee Kiawitter
REA/WPN # 3060
TRACKING # 0-068

SUB-ASSY IEX1881
ASSEMBLY IEX1860

TRIUMF
4004 WESBROOK MALL
VANCOUVER, BRITISH COLUMBIA
CANADA V6T-2A3

CANADA'S NATIONAL LABORATORY FOR PARTICLE AND NUCLEAR PHYSICS

RFA Unit Assembly
TITAN Switch Yard Emittance Station
ISAC 1 – TITAN

SCALE 1:1
THIRD-ANGLE PROJECTION
DWG NO. IEX1890
SIZE C
SHEET 1 OF 1
REV A
DATE Feb. 2015

ITEM	DESCRIPTION	MATERIAL	QTY.
1	2 1/2" Sch 40 Pipe X 2.360 Lg	AISI 304	1

DIMENSIONS QUOTED ARE FINISHED DIMENSIONS, NO ALLOWANCE HAS BEEN MADE FOR MANUFACTURE.

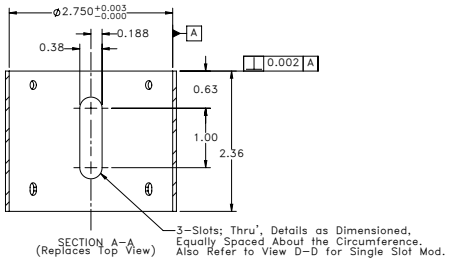

SECTION A–A
(Replaces Top View)

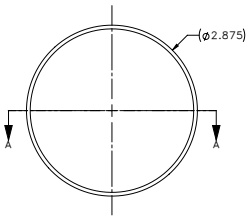

Front View

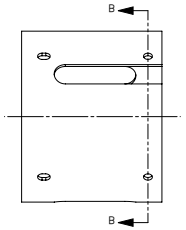

Right Side View

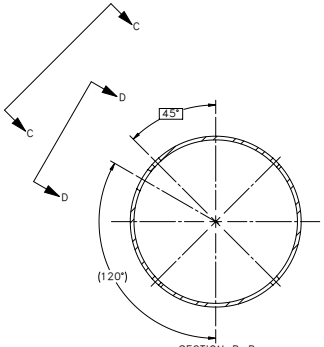

SECTION B–B

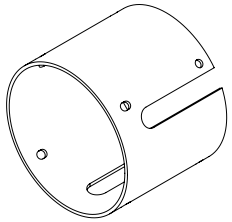

Isometric View

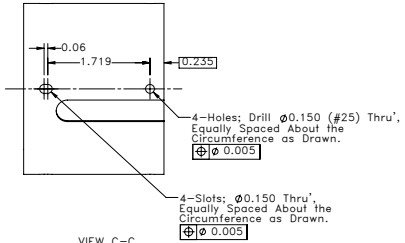

VIEW C–C
(Removed & Rotated 45°
Counter ClockWise)

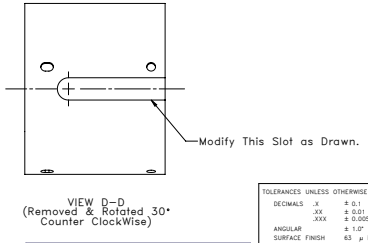

VIEW D–D
(Removed & Rotated 30°
Counter ClockWise)

REMOVE ALL BURRS AND SHARP EDGES

Notes: 1.) Break All Corners.
2.) Dimensions Listed in BOM Do NOT Include Machining Allowances.
3.) Maximum Inside Radius 0.020" Unless Noted.

TOLERANCES UNLESS OTHERWISE SPECIFIED	
DECIMALS .X	± 0.1
.XX	± 0.01
.XXX	± 0.005
ANGULAR	± 1.0°
SURFACE FINISH	63 µ inch

ALL DIMS IN INCHES

DESIGNED TRIUMF/CC/MSG	SUB-ASSY IEX1890
DRAWN Mel Good	
CHECKED Renee Klawitter	ASSEMBLY IEX1860
REA/WPN # 3060	
TRACKING # 0-068	

REV	DATE	REVISION DESCRIPTION	BY	APPD
A	6/9/2015	ECO-3707 – Change Control Applies.	Mel Good	Jens Dilling

TRIUMF
4004 WESBROOK MALL
VANCOUVER, BRITISH COLUMBIA
CANADA V6T-2A3

CANADA'S NATIONAL LABORATORY FOR PARTICLE AND NUCLEAR PHYSICS

RFA Unit Outer Housing
TITAN Switch Yard Emittance Station
ISAC 1 – TITAN

SCALE	DWG NO.	SIZE	SHEET	REV
1:1	IEX1891	C	1 OF 1	A
DATE Feb. 2015	THIRD-ANGLE PROJECTION			

ITEM	REF No.	DESCRIPTION	MATERIAL	QTY.
1	IEX1893	RFA Unit Rear Plate	AISI 304	1
2	IEX1894	RFA Unit Isolation Rod	Unglazed Alumina	3
3	IEX1895	RFA Unit Isolation Ring	Macor	12
4	IEX1896	RFA Unit Front Plate	AISI 304	1
5	IEX1897	RFA Unit Grid Plate Assembly	SS	3
100		#4-40 X 2 Lg Soc Hd Cap Screw	SS	3
101	1692K53	0.48 OD X 0.28 ID X 0.313 Free Length Conical Compression Spring (McMaster-Carr Part # Quoted or Equiv.)	SS	3

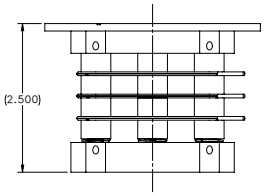

Top View

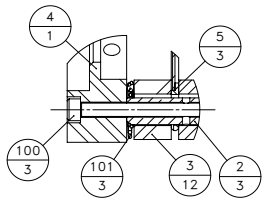

DETAIL B
SCALE 2 : 1

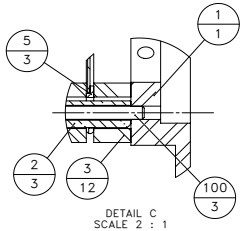

DETAIL C
SCALE 2 : 1

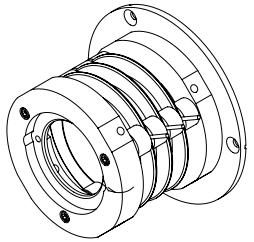

Isometric View

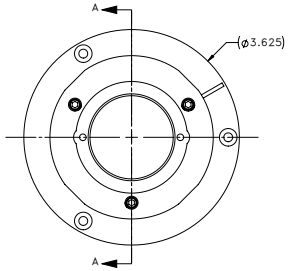

Front View

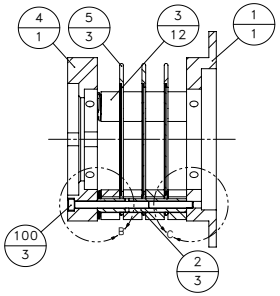

SECTION A-A
(Replaces Right
Side View)

Note: UHV Cleanliness Standards MUST Be Followed and Maintained During the Complete Assembly.
Also Refer to Document 44430; "TRIUMF UHV Cleaning and Assembly Procedures"

Notes:
1.) Quantities Listed in BOM are Required to Assemble and/or Install One (1) Assembly as Drawn.
2.) All Vacuum Surfaces in this Assembly and/or Installation MUST be Cleaned to Ultra High Vacuum (UHV) Standards. Refer to Document 44430; "TRIUMF UHV Cleaning and Assembling Procedures" Located on DocuShare.
3.) UHV Cleanliness Standards MUST be Followed and Maintained During the Complete Installation or Assembly.

REV	DATE	REVISION DESCRIPTION	BY	APPD
A	6/9/2015	ECO-3707 – Change Control Applies.	Mel Good	Jens Dilling

TOLERANCES UNLESS OTHERWISE SPECIFIED
DECIMALS .X ± 0.1
.XX ± 0.01
.XXX ± 0.005
ANGULAR ± 1.0°
SURFACE FINISH 63 μ inch
ALL DIMS IN INCHES

DESIGNED	TRIUMF/CC/MSG
DRAWN	Mel Good
CHECKED	Renee Klawitter
REA/WPN #	3060
TRACKING #	0-068
SUB-ASSY	IEX1890
ASSEMBLY	IEX1860

TRIUMF
4004 WESBROOK MALL
VANCOUVER, BRITISH COLUMBIA
CANADA V6T-2A3

CANADA'S NATIONAL LABORATORY FOR PARTICLE AND NUCLEAR PHYSICS

RFA Unit Internal Assembly
TITAN Switch Yard Emittance Station
ISAC 1 – TITAN

SCALE	DWG NO.	SIZE	SHEET	REV
1:1	IEX1892	C	1 OF 1	A

DATE Feb. 2015

THIRD-ANGLE PROJECTION

ITEM	DESCRIPTION	MATERIAL	QTY.
1	Dia. 3.625 X 0.500 Thk Disk	AISI 304	1

DIMENSIONS QUOTED ARE FINISHED DIMENSIONS, NO ALLOWANCE HAS BEEN MADE FOR MANUFACTURE.

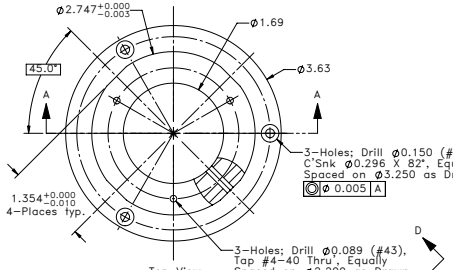

Top View

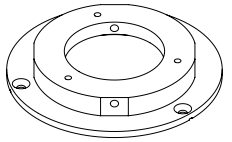

Isometric View

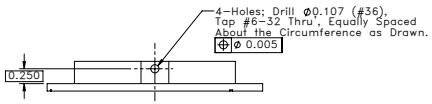

VIEW D–D
(Removed & Rotated 45° ClockWise)

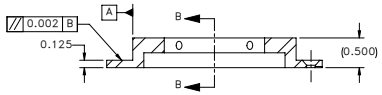

SECTION A–A
(Replaces Front View)

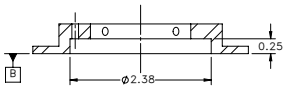

SECTION B–B
(Replaces Right Side View)

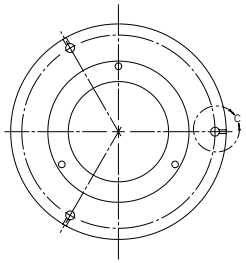

Bottom View

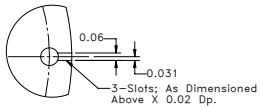

DETAIL C
SCALE 2 : 1

REMOVE ALL BURRS AND SHARP EDGES

Notes: 1.) Break All Corners.
2.) Dimensions Listed in BOM Do NOT Include Machining Allowances.
3.) Maximum Inside Radius 0.020" Unless Noted.

REV	DATE	REVISION DESCRIPTION	BY	APPD
A	6/9/2015	ECO–3707 – Change Control Applies.	Mel Good	Jens Dilling

TOLERANCES UNLESS OTHERWISE SPECIFIED
DECIMALS .X ± 0.1
.XX ± 0.01
.XXX ± 0.005
ANGULAR ± 1.0°
SURFACE FINISH 63 μ inch
ALL DIMS IN INCHES

TRIUMF
4004 WESBROOK MALL
VANCOUVER, BRITISH COLUMBIA
CANADA V6T–2A3

CANADA'S NATIONAL LABORATORY FOR PARTICLE AND NUCLEAR PHYSICS

DESIGNED TRIUMF/WSG	SUB–ASSY IEX1892
DRAWN Mel Good	
CHECKED Renee Klawitter	ASSEMBLY IEX1860
REA/WPN # 3060	
TRACKING # 0–068	

RFA Unit Rear Plate
TITAN Switch Yard Emittance Station
ISAC 1 – TITAN

SCALE	DWG NO.	SIZE	SHEET	REV
1:1	IEX1893	C	1 OF 1	A
DATE Feb. 2015	THIRD–ANGLE PROJECTION			

ITEM	DESCRIPTION	MATERIAL	QTY.
1	0.250 O.D. X 0.125 I.D. Tubing X 1.500 Lg	Unglazed Alumina	1

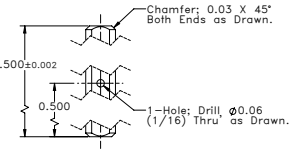

Top View

DIMENSIONS QUOTED ARE FINISHED DIMENSIONS, NO ALLOWANCE HAS BEEN MADE FOR MANUFACTURE.

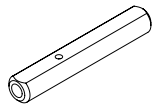

Isometric View
Scale: 1/4 X Full Size.

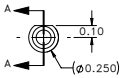

Front View

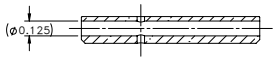

SECTION A–A
(Replaces Right Side View)

Notes: 1.) Break All Corners.
2.) Dimensions Listed in BOM Do NOT Include Machining Allowances.
3.) Maximum Inside Radius 0.020" Unless Noted.

REMOVE ALL BURRS AND SHARP EDGES

REV	DATE	REVISION DESCRIPTION	BY	APPD
A	6/9/2015	ECO–3707 – Change Control Applies.	Mel Good	Jens Dilling

TOLERANCES UNLESS OTHERWISE SPECIFIED
DECIMALS .X ± 0.1
.XX ± 0.01
.XXX ± 0.005
ANGULAR ± 1.0°
SURFACE FINISH 63 µ inch
ALL DIMS IN INCHES

TRIUMF
4004 WESBROOK MALL
VANCOUVER, BRITISH COLUMBIA
CANADA V6T–2A3

CANADA'S NATIONAL LABORATORY FOR PARTICLE AND NUCLEAR PHYSICS

DESIGNED TRIUMF/CC/MSG
DRAWN Mel Good
CHECKED Renee Klawitter
REA/WPN # 3060
TRACKING # 0–068

SUB–ASSY IEX1892
ASSEMBLY IEX1860

RFA Unit Isolation Rod
TITAN Switch Yard Emittance Station
ISAC 1 – TITAN

SCALE 2:1
DATE Feb. 2015
THIRD–ANGLE PROJECTION
DWG NO. IEX1894
SIZE B
SHEET 1 OF 1
REV A

ITEM	DESCRIPTION	MATERIAL	QTY.
1	Dia. 0.500 X 0.313 Lg Rod	Macor	1

DIMENSIONS QUOTED ARE FINISHED DIMENSIONS, NO ALLOWANCE HAS BEEN MADE FOR MANUFACTURE.

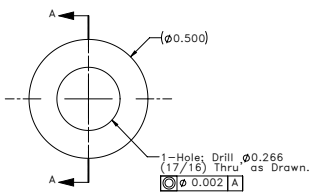

Front View

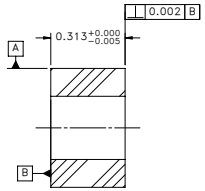

SECTION A–A
(Replaces Right
Side View)

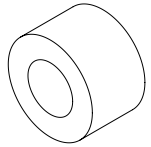

Isometric View

Notes: 1.) Break All Corners.
2.) Dimensions Listed in BOM Do NOT Include Machining Allowances.
3.) Maximum Inside Radius 0.020" Unless Noted.

REMOVE ALL BURRS AND SHARP EDGES

REV	DATE	REVISION DESCRIPTION	BY	APPD
A	6/9/2015	ECO-3707 – Change Control Applies.	Mel Good	Jens Dilling

TOLERANCES UNLESS OTHERWISE SPECIFIED
DECIMALS .X ± 0.1
.XX ± 0.01
.XXX ± 0.005
ANGULAR ± 1.0°
SURFACE FINISH 63 µ inch
ALL DIMS IN INCHES

TRIUMF
4004 WESBROOK MALL
VANCOUVER, BRITISH COLUMBIA
CANADA V6T-2A3

CANADA'S NATIONAL LABORATORY FOR PARTICLE AND NUCLEAR PHYSICS

DESIGNED TRIUMF/CC/MSG
DRAWN Mel Good
CHECKED Renee Klawitter
REA/WPN # 3060
TRACKING # 0-068

SUB-ASSY IEX1892
ASSEMBLY IEX1860

RFA Unit Isolation Ring
TITAN Switch Yard Emittance Station
ISAC 1 – TITAN

SCALE 4:1
DATE Feb. 2015
THIRD-ANGLE PROJECTION
DWG NO. IEX1895
SIZE B
SHEET 1 OF 1
REV A

ITEM	DESCRIPTION	MATERIAL	QTY.
1	Dia. 2.747 X 0.500 Thk Disk	AISI 304	1

DIMENSIONS QUOTED ARE FINISHED DIMENSIONS, NO ALLOWANCE HAS BEEN MADE FOR MANUFACTURE.

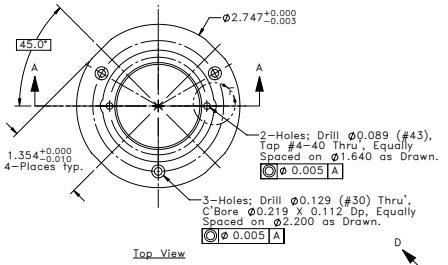

Top View

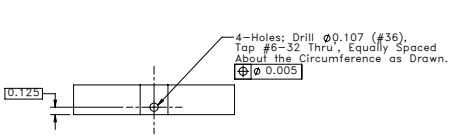

VIEW D–D
(Removed & Rotated 45° ClockWise)

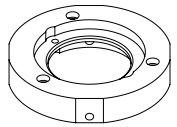

Isometric View

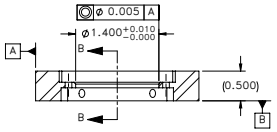

SECTION A–A
(Replaces Front View)

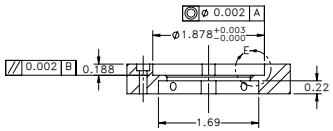

SECTION B–B
(Replaces Right Side View)

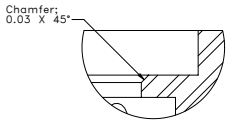

DETAIL E
SCALE 4 : 1

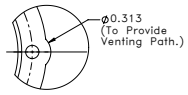

DETAIL F
SCALE 2 : 1

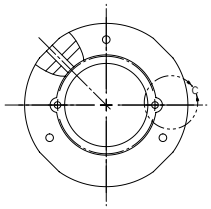

Bottom View

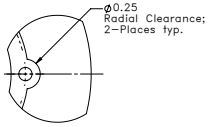

DETAIL C
SCALE 2 : 1

REMOVE ALL BURRS AND SHARP EDGES

Notes: 1.) Break All Corners.
2.) Dimensions Listed in BOM Do NOT Include Machining Allowances.
3.) Maximum Inside Radius 0.020" Unless Noted.

TOLERANCES UNLESS OTHERWISE SPECIFIED
DECIMALS .X ± 0.1
.XX ± 0.01
.XXX ± 0.005
ANGULAR ± 1.0°
SURFACE FINISH 63 µ inch
ALL DIMS IN INCHES

REV	DATE	REVISION DESCRIPTION	BY	APPD
A	6/9/2015	ECO–3707 – Change Control Applies.	Mel Good	Jens Dilling

DESIGNED TRIUMF/CC/MSG
DRAWN Mel Good
CHECKED Renee Klawitter
REA/WPN # 3060
TRACKING # 0–068
SUB–ASSY IEX1892
ASSEMBLY IEX1860

TRIUMF
4004 WESBROOK MALL
VANCOUVER, BRITISH COLUMBIA
CANADA V6T–2A3

CANADA'S NATIONAL LABORATORY FOR PARTICLE AND NUCLEAR PHYSICS

RFA Unit Front Plate
TITAN Switch Yard Emittance Station
ISAC 1 – TITAN

SCALE 1:1
DATE Feb. 2015
THIRD–ANGLE PROJECTION
DWG NO. IEX1896
SIZE C
SHEET 1 OF 1
REV A

ITEM	REF No.	DESCRIPTION	MATERIAL	QTY.
1	IEX1898	RFA Unit Grid Frame	AISI 304	1
2		Dia. 0.06 X 0.50 Lg Wire	SS	1
3		635 Square Mesh Wire Cloth	316 SS	1

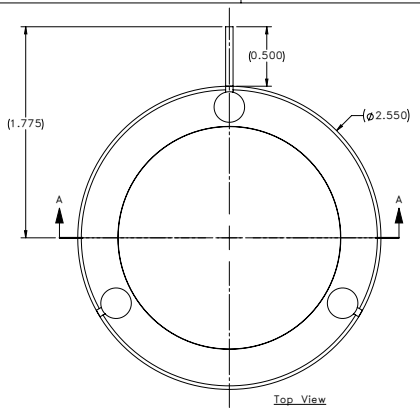

Top View

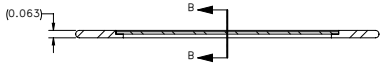

SECTION A–A
(Replaces Front View)

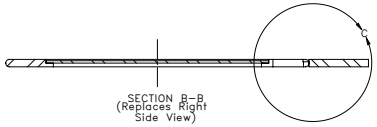

SECTION B–B
(Replaces Right Side View)

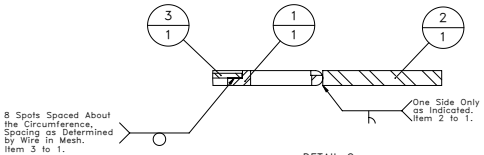

DETAIL C
SCALE 4 : 1

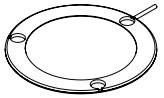

Isometric View
Scale: Full Size.

Note: UHV Cleanliness Standards MUST Be Followed and Maintained During the Complete Assembly.
Also Refer to Document 44430; "TRIUMF UHV Cleaning and Assembly Procedures"

Notes: 1.) Quantities Listed in BOM are Required to Assemble and/or Install One (1) Assembly as Drawn.
2.) All Vacuum Surfaces in this Assembly and/or Installation MUST be Cleaned to Ultra High Vacuum (UHV) Standards. Refer to Document 44430; "TRIUMF UHV Cleaning and Assembling Procedures" Located on DocuShare.
3.) UHV Cleanliness Standards MUST be Followed and Maintained During the Complete Installation or Assembly.

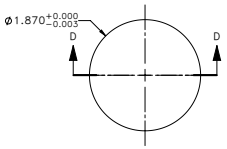

Top View
(Of Item 3)
Scale: Full Size.

635 Square Mesh Wire Cloth
Wire Diameter: 0.00085"
Width of Opening: 0.00065"
% of Open Area: 38.0%
Phoenix Wire Cloth Inc.

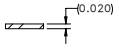

DETAIL E
SCALE 4 : 1

Isometric View
(Of Item 3)
Scale: Full Size.

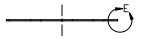

SECTION D–D
SCALE 1 : 1
(Replaces Front View
Of Item 3)

Notes: 1.) Break All Corners.
2.) Dimensions Listed in BOM Do NOT Include Machining Allowances.
3.) Maximum Inside Radius 0.020" Unless Noted.

REV	DATE	REVISION DESCRIPTION	BY	APPD
A	6/9/2015	ECO–3707 – Change Control Applies.	Mel Good	Jens Dilling

TOLERANCES UNLESS OTHERWISE SPECIFIED
DECIMALS .X ± 0.1
.XX ± 0.01
.XXX ± 0.005
ANGULAR ± 1.0°
SURFACE FINISH 63 µ inch
ALL DIMS IN INCHES

DESIGNED TRIUMF/CC/MSG	SUB–ASSY IEX1892
DRAWN Mel Good	
CHECKED Renee Klawitter	ASSEMBLY IEX1860
REA/WPN # 3060	
TRACKING # 0–068	

TRIUMF
4004 WESBROOK MALL
VANCOUVER, BRITISH COLUMBIA
CANADA V6T–2A3
CANADA'S NATIONAL LABORATORY FOR PARTICLE AND NUCLEAR PHYSICS

RFA Unit Grid Plate Assembly
TITAN Switch Yard Emittance Station
ISAC 1 – TITAN

SCALE	DWG NO.	SIZE	SHEET	REV
2:1	IEX1897	C	1 OF 1	A

DATE Feb. 2015
THIRD–ANGLE PROJECTION

ITEM	DESCRIPTION	MATERIAL	QTY.
1	Dia.2.550 X 0.063 Thk Disk	AISI 304	1

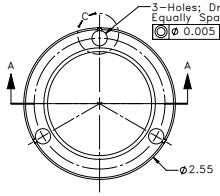

Top View

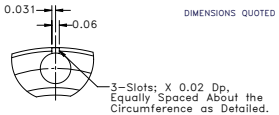

DETAIL C
SCALE 2 : 1

DIMENSIONS QUOTED ARE FINISHED DIMENSIONS, NO ALLOWANCE HAS BEEN MADE FOR MANUFACTURE.


Isometric View
Scale: 1/2 X Full Size.

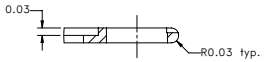

DETAIL D
SCALE 4 : 1

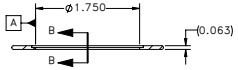

SECTION A-A
(Replaces Front View)

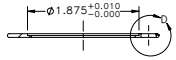

SECTION B-B
(Replaces Right Side View)

Notes: 1.) Break All Corners.
2.) Dimensions Listed in BOM Do NOT Include Machining Allowances.
3.) Maximum Inside Radius 0.020" Unless Noted.

REMOVE ALL BURRS AND SHARP EDGES

REV	DATE	REVISION DESCRIPTION	BY	APPD
A	6/9/2015	ECO-3707 – Change Control Applies.	Mel Good	Jens Dilling

TOLERANCES UNLESS OTHERWISE SPECIFIED
DECIMALS .X ± 0.1
.XX ± 0.01
.XXX ± 0.005
ANGULAR ± 1.0°
SURFACE FINISH 63 μ inch
ALL DIMS IN INCHES

DESIGNED TRIUMF/CC/MSG
DRAWN Mel Good
CHECKED Renee Klawitter
REA/WPN # 3060
TRACKING # 0-068
SUB-ASSY IEX1897
ASSEMBLY IEX1860

TRIUMF
4004 WESBROOK MALL
VANCOUVER, BRITISH COLUMBIA
CANADA V6T-2A3
CANADA'S NATIONAL LABORATORY FOR PARTICLE AND NUCLEAR PHYSICS

RFA Unit Grid Frame
TITAN Switch Yard Emittance Station
ISAC 1 – TITAN

SCALE 1:1
DATE Feb. 2015
THIRD-ANGLE PROJECTION
DWG NO. IEX1898
SIZE B
SHEET 1 OF 1
REV A

ITEM	REF No.	DESCRIPTION	MATERIAL	QTY.
1	IEX1900	RFA Removable Orifice Holder	AISI 304	1
2	IEX1901	RFA Pin Hole Insert	AISI 304	2
100	Stores # 1-2/2044	#6-32 X 1/4 Lg Phillips Drive Pan Hd Machine Screw	SS	6

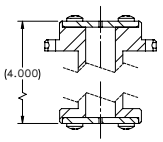

SECTION A-A
(Replaces Top View)

Note: UHV Cleanliness Standards MUST Be Followed and Maintained During the Complete Assembly.
Also Refer to Document 44430; "TRIUMF UHV Cleaning and Assembly Procedures"

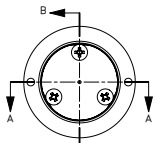

Front View

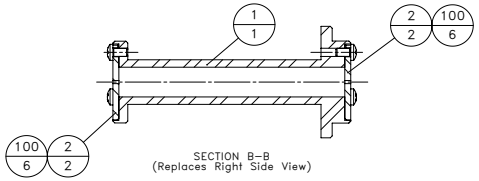

SECTION B-B
(Replaces Right Side View)

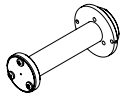

Isometric View
Scale: 1/2 X Full Size.

Notes:
1.) Quantities Listed in BOM are Required to Assemble and/or Install One (1) Assembly as Drawn.
2.) All Vacuum Surfaces in this Assembly and/or Installation MUST be Cleaned to Ultra High Vacuum (UHV) Standards. Refer to Document 44430; "TRIUMF UHV Cleaning and Assembling Procedures" Located on DocuShare.
UHV Cleanliness Standards MUST be Followed and Maintained During the Complete Installation or Assembly.
3.)
4.)
5.)

REV	DATE	REVISION DESCRIPTION	BY	APPD
A	6/18/2015	ECO-3707 – Change Control Applies.	Mel Good	Jens Dilling

TOLERANCES UNLESS OTHERWISE SPECIFIED
DECIMALS .X ± 0.1
.XX ± 0.01
.XXX ± 0.005
ANGULAR ± 1.0°
SURFACE FINISH 63 μ inch
ALL DIMS IN INCHES

TRIUMF
4004 WESBROOK MALL
VANCOUVER, BRITISH COLUMBIA
CANADA V6T-2A3

CANADA'S NATIONAL LABORATORY FOR PARTICLE AND NUCLEAR PHYSICS

DESIGNED TRIUMF/CC/MSG
DRAWN Mel Good
CHECKED Renee Kiawitter
REA/WPN # 3060
TRACKING # 0-068

SUB-ASSY IEX1890
ASSEMBLY IEX1860

RFA Orifice Assembly
TITAN Switch Yard Emittance Station
ISAC 1 – TITAN

SCALE 1:1
DATE Feb. 2015
THIRD-ANGLE PROJECTION
DWG NO. IEX1899
SIZE B
SHEET 1 OF 1
REV A

ITEM	DESCRIPTION	MATERIAL	QTY.
1	Dia. 1.875 X 4.000 Thk Disk	AISI 304	1

DIMENSIONS QUOTED ARE FINISHED DIMENSIONS, NO ALLOWANCE HAS BEEN MADE FOR MANUFACTURE.

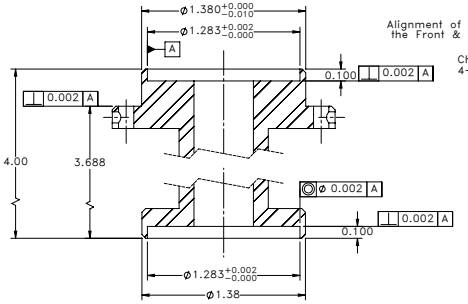

SECTION A–A
(Replaces Top View)

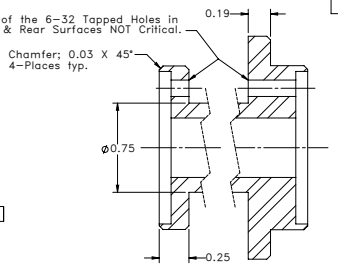

SECTION B–B
(Removed)

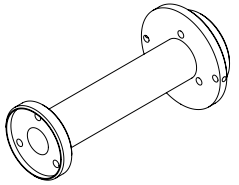

Isometric View
Scale: Full Size.

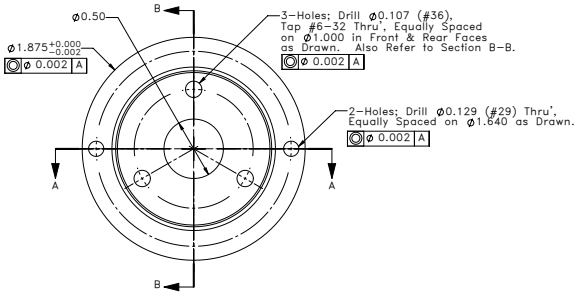

Front View

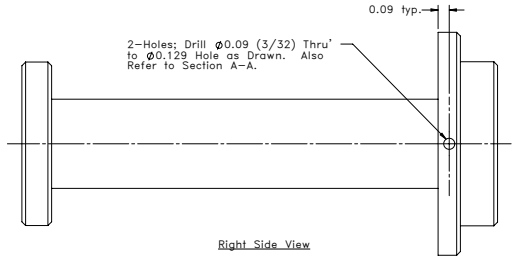

Right Side View

Notes: 1.) Break All Corners.
2.) Dimensions Listed in BOM Do NOT Include Machining Allowances.
3.) Maximum Inside Radius 0.020" Unless Noted.

REMOVE ALL BURRS AND SHARP EDGES

TOLERANCES UNLESS OTHERWISE SPECIFIED	
DECIMALS .X	± 0.1
.XX	± 0.01
.XXX	± 0.005
ANGULAR	± 1.0°
SURFACE FINISH	63 μ inch
ALL DIMS IN INCHES	

DESIGNED TRIUMF/CC/MSG	SUB–ASSY IEX1899
DRAWN Mel Good	
CHECKED Renee Klawitter	ASSEMBLY IEX1860
REA/WPN # 3060	
TRACKING # 0–068	

REV	DATE	REVISION DESCRIPTION	BY	APPD
A	6/18/2015	ECO–3707 – Change Control Applies.	Mel Good	Jens Dilling

TRIUMF
4004 WESBROOK MALL
VANCOUVER, BRITISH COLUMBIA
CANADA V6T–2A3

CANADA'S NATIONAL LABORATORY FOR PARTICLE AND NUCLEAR PHYSICS

RFA Removable Orifice Holder
TITAN Switch Yard Emittance Station
ISAC 1 – TITAN

SCALE	DWG NO.	SIZE	SHEET	REV
2:1	IEX1900	C	1 OF 1	A

THIRD–ANGLE PROJECTION

DATE Feb. 2015

ITEM	DESCRIPTION	MATERIAL	QTY.
1	Dia. 1.280 X 0.100 Thk Disk	AISI 304	1

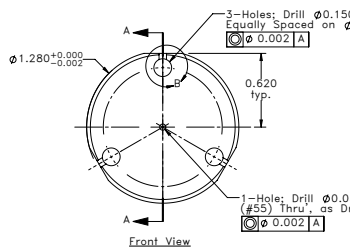

Front View

DIMENSIONS QUOTED ARE FINISHED DIMENSIONS, NO ALLOWANCE HAS BEEN MADE FOR MANUFACTURE.

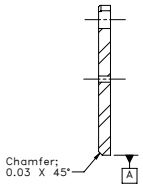

SECTION A–A
(Replace Right Side View)

Isometric View
Scale: Full Size.

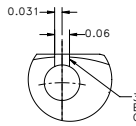

DETAIL B
SCALE 4 : 1

Notes: 1.) Break All Corners.
2.) Dimensions Listed in BOM Do NOT Include Machining Allowances.
3.) Maximum Inside Radius 0.020" Unless Noted.

REMOVE ALL BURRS AND SHARP EDGES

REV	DATE	REVISION DESCRIPTION	BY	APPD
A	6/9/2015	ECO–3707 – Change Control Applies.	Mel Good	Jens Dilling

TOLERANCES UNLESS OTHERWISE SPECIFIED
DECIMALS .X ± 0.1
.XX ± 0.01
.XXX ± 0.005
ANGULAR ± 1.0°
SURFACE FINISH 63 μ inch
ALL DIMS IN INCHES

TRIUMF
4004 WESBROOK MALL
VANCOUVER, BRITISH COLUMBIA
CANADA V6T–2A3

CANADA'S NATIONAL LABORATORY FOR PARTICLE AND NUCLEAR PHYSICS

DESIGNED TRIUMF/CC/MSG
DRAWN Mel Good
CHECKED Renee Klawitter
REA/WPN # 3060
TRACKING # 0–068

SUB–ASSY IEX1899
ASSEMBLY IEX1860

RFA Pin Hole Insert
TITAN Switch Yard Emittance Station
ISAC 1 – TITAN

SCALE 2:1
DATE Feb. 2015
THIRD–ANGLE PROJECTION
DWG NO. IEX1901
SIZE B
SHEET 1 OF 1
REV A

ITEM	REF No.	DESCRIPTION	MATERIAL	QTY.
1	IEX1903	RFA Conductor Wire Type 1	SS	1
200	110102	Set Screw Connector Mod. # POC60-5 (Accu-Glass Products Inc. Part # Quoted or Equiv.) (Pkg of 5)	Copper	1
201	110103	Set Screw Connector Mod. # POC94-5 (Accu-Glass Products Inc. Part # Quoted or Equiv.) (Pkg of 5)	Copper	1

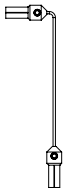

Top View
(Of Type 1)

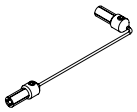

Isometric View
(Of Type 1)

Front View
(Of Type 1)

Right Side View
(Of Type 1)

ITEM	REF No.	DESCRIPTION	MATERIAL	QTY.
1	IEX1903	RFA Conductor Wire Type 2	SS	1
200	110102	Set Screw Connector Mod. # POC60-5 (Accu-Glass Products Inc. Part # Quoted or Equiv.) (Pkg of 5)	Copper	1
201	110103	Set Screw Connector Mod. # POC94-5 (Accu-Glass Products Inc. Part # Quoted or Equiv.) (Pkg of 5)	Copper	1

Top View
(Of Type 2)

Front View
(Of Type 2)

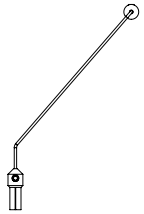

Right Side View
(Of Type 2)

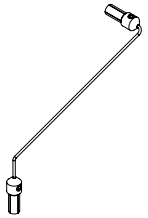

Isometric View
(Of Type 2)

Notes: 1.) Quantities Listed in BOM are Required to Assemble and/or Install One (1) Assembly as Drawn.
2.) All Vacuum Surfaces in this Assembly and/or Installation MUST be Cleaned to Ultra High Vacuum (UHV) Standards. Refer to Document 44430; "TRIUMF UHV Cleaning and Assembling Procedures" Located on DocuShare.
3.) UHV Cleanliness Standards MUST be Followed and Maintained During the Complete Installation or Assembly.

ITEM	REF No.	DESCRIPTION	MATERIAL	QTY.
1	IEX1903	RFA Conductor Wire Type 3	SS	1
200	110102	Set Screw Connector Mod. # POC60-5 (Accu-Glass Products Inc. Part # Quoted or Equiv.) (Pkg of 5)	Copper	1
201	110103	Set Screw Connector Mod. # POC94-5 (Accu-Glass Products Inc. Part # Quoted or Equiv.) (Pkg of 5)	Copper	1

Top View
(Of Type 3)

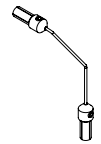

Isometric View
(Of Type 3)

Front View
(Of Type 3)

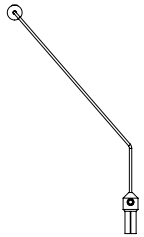

Right Side View
(Of Type 3)

Note: UHV Cleanliness Standards MUST Be Followed and Maintained During the Complete Assembly.
Also Refer to Document 44430; "TRIUMF UHV Cleaning and Assembly Procedures"

REV	DATE	REVISION DESCRIPTION	BY	APPD
A	6/9/2015	ECO-3707 – Change Control Applies.	Mel Good	Jens Dilling

TOLERANCES UNLESS OTHERWISE SPECIFIED
DECIMALS .X ± 0.1
.XX ± 0.01
.XXX ± 0.005
ANGULAR ± 1.0°
SURFACE FINISH 63 μ inch
ALL DIMS IN INCHES

DESIGNED TRIUMF/MSG
DRAWN Mel Good
CHECKED Renee Klawitter
REA/WPN # 3060
TRACKING # 0-068

SUB-ASSY: IEX1881
ASSEMBLY: IEX1860

TRIUMF
4004 WESBROOK MALL
VANCOUVER, BRITISH COLUMBIA
CANADA V6T-2A3
CANADA'S NATIONAL LABORATORY FOR PARTICLE AND NUCLEAR PHYSICS

RFA Wire Conductor Ass'y Type 1 – 3
TITAN Switch Yard Emittance Station
ISAC 1 – TITAN

SCALE 1:1
DATE Feb. 2015
THIRD-ANGLE PROJECTION
DWG NO. IEX1902
SIZE D
SHEET 1 OF 1
REV A

ITEM	DESCRIPTION	MATERIAL	QTY.
1	Dia. 0.040 X 2.965 Lg Wire	SS	1

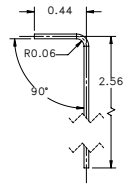

Top View
(Of Type 1)

Top View
(Of Type 1 Repeated)
Scale: Full Size.

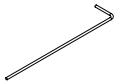

Isometric View
(Of Type 1)
Scale: Full Size.

Front View
(Of Type 1)

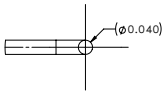

DETAIL A
SCALE 6 : 1

Top View
(Of Type 2 Repeated)
Scale: Full Size.

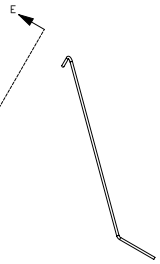

VIEW E–E
SCALE 1 : 1

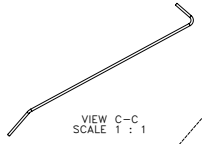

VIEW C–C
SCALE 1 : 1

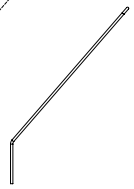

Right Side View
(Of Type 2 Repeated)
Scale: Full Size.

Notes: 1.) Break All Corners.
2.) Dimensions Listed in BOM Do NOT Include Machining Allowances.
3.) Maximum Inside Radius 0.020" Unless Noted.

ITEM	DESCRIPTION	MATERIAL	QTY.
1	Dia. 0.040 X 4.32 Lg Wire	SS	1

DIMENSIONS QUOTED ARE FINISHED DIMENSIONS, NO ALLOWANCE HAS BEEN MADE FOR MANUFACTURE.

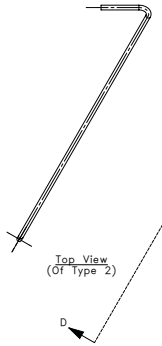

Top View
(Of Type 2)

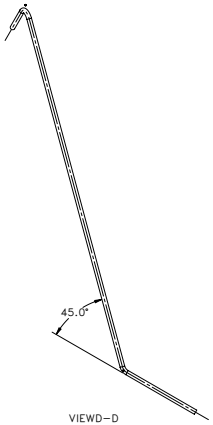

VIEWD–D

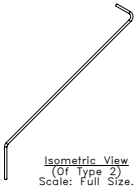

Isometric View
(Of Type 2)
Scale: Full Size.

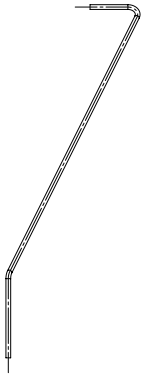

Front View
(Of Type 2)

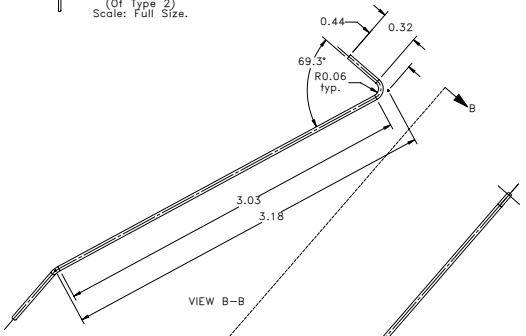

VIEW B–B

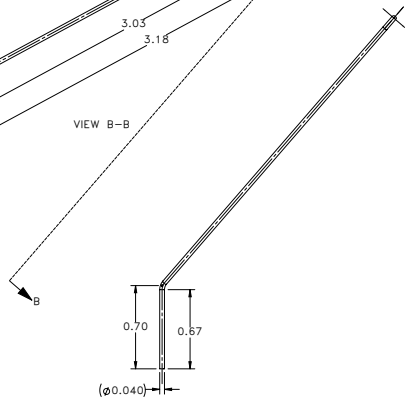

Right Side View
(Of Type 2)

REMOVE ALL BURRS AND SHARP EDGES

TOLERANCES UNLESS OTHERWISE SPECIFIED
DECIMALS .X ± 0.1
.XX ± 0.01
.XXX ± 0.005
ANGULAR ± 1.0°
SURFACE FINISH 63 µ inch

ALL DIMS IN INCHES

REV	DATE	REVISION DESCRIPTION	BY	APPD
A	6/9/2015	ECO–3707 – Change Control Applies.	Mel Good	Jens Dilling

DESIGNED TRIUMF/MSG
DRAWN Mel Good
CHECKED Renee Klawitter
REA/WPN # 3060
TRACKING # 0–068

SUB–ASSY: IEX1902
ASSEMBLY: IEX1860

TRIUMF
4004 WESBROOK MALL
VANCOUVER, BRITISH COLUMBIA
CANADA V6T–2A3

CANADA'S NATIONAL LABORATORY FOR PARTICLE AND NUCLEAR PHYSICS

RFA Conductor Wire Type 1 – 3
TITAN Switch Yard Emittance Station
ISAC 1 – TITAN

SCALE 2:1
DATE Feb. 2015
THIRD–ANGLE PROJECTION
DWG NO. IEX1903
SIZE D
SHEET 1 OF 2
REV A

ITEM	DESCRIPTION	MATERIAL	QTY.
1	Dia. 0.040 X 4.63 Lg Wire	SS	1

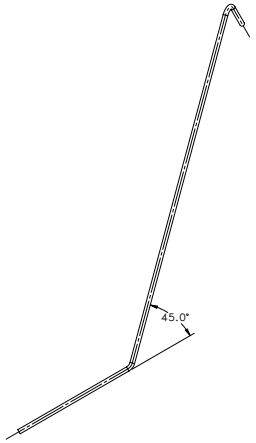

VIEW H–H

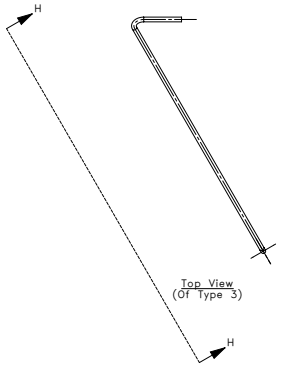

Top View
(Of Type 3)

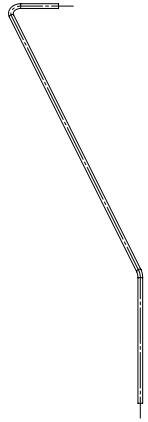

Front View
(Of Type 3)

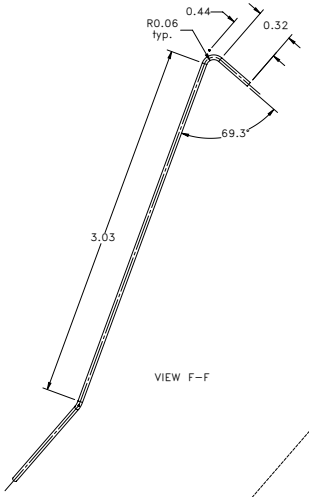

VIEW F–F

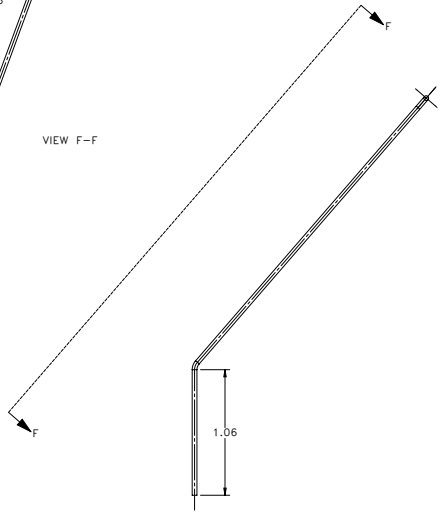

Right Side View
(Of Type 3)

Isometric View
(Of Type 3)
Scale: Full Size.

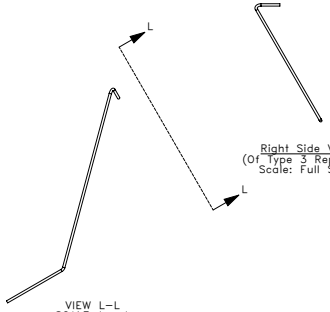

Right Side View
(Of Type 3 Repeated)
Scale: Full Size.

VIEW L–L
SCALE 1 : 1

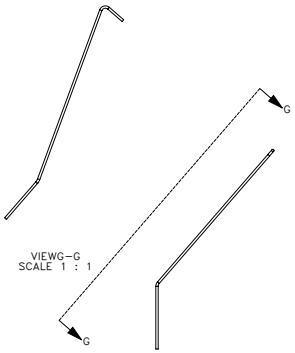

VIEWG–G
SCALE 1 : 1

Right Side View
(Of Type 3 Repeated)
Scale: Full Size.

Notes: 1.) Break All Corners.
2.) Dimensions Listed in BOM Do NOT Include Machining Allowances.
3.) Maximum Inside Radius 0.020" Unless Noted.

TRIUMF	4004 WESBROOK MALL VANCOUVER, BRITISH COLUMBIA CANADA V6T-2A3	CANADA'S NATIONAL LABORATORY FOR PARTICLE AND NUCLEAR PHYSICS				
SCALE 2:1	THIRD-ANGLE PROJECTION	DWG NO. IEX1903	SIZE D	SHEET 2 OF 2	REV A
USE IN CONJUNCTION WITH SHEET No.:					

Declaration of authorship:

I, Ruben Schupp, declare that this thesis and the work presented in it is entirely my own. Where I have consulted the work of others, it is always clearly stated.

Heidelberg, February 10, 2016 .....